Diss. ETH No. 19679

In silico bone biology in a murine model of bone adaptation

A dissertation submitted to

ETH ZURICH

for the degree of

Doctor of Sciences

presented by

Friederike A. Schulte

Dipl. Inf, Universität Erlangen-Nürnberg, Germany

born 4^{th} July, 1981

citizen of Germany

accepted on the recommendation of

Prof. Dr. Ralph Müller, examiner

Dr. Bert van Rietbergen, co-examiner

2011

Table of Contents

Acknowledgements

The work presented in this thesis would not have been possible without the help of a number of people. I would like to express my profound gratitude to them.

First of all, I would like to thank Prof. Dr. Ralph Müller who made it possible for me to carry out this work at his institute. His incredible enthusiasm for research and his ability to recognize the big potential in the small results has always been highly motivating for me. Second, I would like to acknowledge Dr. Bert van Rietbergen. Being someone who is not only experienced in one of the fields this thesis is dedicated to but in the entity of them, I am very glad that he agreed to be my co-referee.

Special thanks also to Dr. Gisela Kuhn for her kind way of supervision and for giving me a better understanding of bone biology. In particular, I would like to say thank you to Floor Lambers. It was a pleasure to work with her that closely together every day these four years. It's all about the small things that we shared, the cups of tea (you might not believe it, but it really was all scientific discussion that we had...), the conferences we went to together, the dinners from time to time at home with our husbands, and much more.

Furthermore, I would like to acknowledge the past and present members of the Institute for Biomechanics. Such kind of work is not raised by a single person. It requires discussion, ideas, technical (and moral) support which I have always found in our group. In particular, I would like to mention Dr. Davide Ruffoni, Dr. Duncan Webster, Claudia Weigt, Dr. Andy Wirth, Dr. Tom Müller, Dr. Samuela Rigozzi, Dr. Kathryn Stok, Dr. Martin Stauber, Dr. Thomas Kohler and David Christen. All the same, I am grateful to Christoph Schröter, Sandro Badilatti, Alex Zwahlen, Tarun Kumar and Abhay Kapoor who have helped me completing this work with their student projects. It was a pleasure for me to work together with them. Also, thank you to all members of the Institute for providing such a nice and motivating work atmosphere. And an extra thanks to our secretary Catherine Palmer who proof-read almost my full thesis.

Likewise, my time in Zurich would not have been the same without the friends I found here over the years. They made my life complete and colorful. I am very

grateful to my parents and sisters who always believed in me during all these years and whose support and advice, especially in the last phase of this thesis, were invaluable for me. And lastly, I would like to thank my own small family, Jens and Lara. Lara has enriched the last one and a half years of my PhD enourmously with her happiness and smile. Jens' love, encouragement and faithful support throughout all stages of this PhD is so appreciated. I count myself very lucky to have him on my side.

Finally, financial support by the European Union for the osteoporotic virtual physiological human project (VPHOP FP7-ICT2008-223865), the Swiss National Foundation (SNF) and ETH Zurich is gratefully acknowledged.

March 2011

Friederike A. Schulte

Summary

Bone is an organ able to adapt to changing mechanical requirements. Its most common disease is osteoporosis which is a major research topic these days. Here, *in silico* modeling provides a powerful tool to assist in experimental research where questions unrealizable by experiment to date can be tested. However, in the past decade the lack of appropriate validation data has led to an abundance of remodeling theories without the availability of tools to prove or disprove them. It is only with the advent of *in vivo* micro-computed tomography that the gap between computational modeling and experimental validation can be closed. Especially the possibility of identifying separately regions of bone formation and resorption in the experiment is considered a big step forward in validating *in silico* simulations. For this reason, the present thesis was divided into three aims: (i) To quantify three-dimensional bone formation and resorption rates from time-lapsed *in vivo* micro-CT measurements, (ii) to investigate the existence of a local mechanical regulation mechanism of bone remodeling and (iii) to implement and validate a computational *in silico* model of bone adaptation using the underlying experimental *in vivo* data.

In a first step, a technique to extract dynamic bone formation and resorption rates from follow-up *in vivo* micro-computed tomography scans was developed. Since bone formation indices are well-established measures in histomorphometry, the proposed method was validated by means of the histomorphometric gold standard which resulted in a good agreement between the two methods. Furthermore, the newly developed technique was shown to be highly reproducible and sensitive to detect changes in different experimental groups. Compared to histomorphometry, the assessment via *in vivo* micro-computed tomography has the advantage of being three-dimensional, non-invasive, non-destructive, and fully-automated.

Furthermore, the new technique was applied to identify both local bone formation and resorption sites and to compare them to the underlying local mechanical milieu. A number of computational models are based on the assumption that local bone formation and resorption are a direct result of the mechanical strain environment.

The proposed experimental *in vivo* setup allowed this question to be investigated on an experimental basis. Results showed that mean strain-energy-density (SED) at formation sites was significantly higher than mean SED at constant sites while mean SED at resorption sites was significantly lower than mean SED at constant sites. Furthermore, a strong correlation between increasing strain-energy-density-values and subsequent probability for bone formation was found as well as a strong reciprocal correlation between increasing SED-values and subsequent probability for bone resorption. These findings show quantitative evidence of a local mechano-regulatory mechanism at the cellular level.

The knowledge gained from the first two aims was in a third step used to implement and validate a predictive computational model of bone adaptation. First, a validation setup using experimental *in vivo* data was developed to determine the prediction error of a computational model. In this section, a simple thickening algorithm was implemented to simulate the bone response to increased mechanical loading. While morphometric indices were accurately predicted after four weeks of experiment, spatial patterns of formation and resorption could not be replicated by the *in silico* model. This finding underlined the importance of using a local feedback mechanism, deciding on-site whether bone should be formed or resorbed. Thus, in a second step, a mechanical feedback loop was implemented in the *in silico* model. Results showed that after four weeks of mechanical loading, an agreement between morphometric as well as dynamic remodeling rates was achieved. Bone loss after ovariectomy was as well successfully simulated, including the prediction of a saturation level at a lower bone mass after a few weeks, however still showing discrepancies in spatial patterns of bone remodeling. With these results, it was underlined that continued validation by means of experimental *in vivo* data is able to guide the development of the *in silico* model and simultaneously gain novel insights into the biological interrelationships involved during bone adaptation.

In conclusion, this thesis revealed that experimental *in vivo* micro-CT, combined with computational modeling, builds a powerful unit for addressing questions which to date were reserved for the field of *in silico* modeling. It is expected that the insight gained from such findings may have far-reaching consequences for the global understanding of bone remodeling and related osteoporosis research.

Zusammenfassung

Knochen ist ein Organ mit der Fähigkeit, sich selbst zu verändern. Die am weitesten verbreitete Knochenkrankheit ist Osteoporose, die heutzutage von grossem Forschungsinteresse ist. Computergestützte Simulationsmodelle stellen hier ein leistungsstarkes Werkzeug zur Unterstützung experimenteller Forschung dar, da sie Hypothesen überprüfen können, die für experimentelle Studien noch nicht zugänglich sind. Das Fehlen von geeigneten Validierungsdaten hat jedoch in den letzten zehn Jahren zu einer hohen Anzahl von Simulationsmodellen geführt, ohne dass entsprechende Werkzeuge verfügbar waren, um diese zu bestätigen oder zu entkräften. Erst die Einführung der *in-vivo*-Mikrocomputertomografie hat es möglich gemacht, die Lücke zwischen Simulationsmodellen und experimentellen Validierungsdaten zu schliessen. Speziell die Möglichkeit, Knochenauf- und -abbauraten im Experiment zu erfassen, wird als ein grosser Fortschritt für die Validierung von computergestützten Simulationsmodellen angesehen. In dieser Arbeit wurden daher drei Ziele verfolgt: (i) dreidimensionale Knochenformations- und -resorptionsraten anhand von *in-vivo*-Mikrocomputertomografie-Daten zu quantifizieren, (ii) das Vorhandensein eines lokalen belastungsbasierten Regulationsmechanismus zur Knochenremodellierung zu untersuchen und (iii) ein Simulationsmodell der Knochenadaption zu implementieren sowie mittels der vorhandenen *in-vivo*-Mikrocomputertomografie-Daten zu validieren.

In einem ersten Schritt wurde eine Technik zum Extrahieren von dreidimensionalen Knochenformations- und -resorptionsraten mittels *in-vivo*-Mikrocomputertomografie entwickelt. Knochenaufbauraten sind gängige Masseinheiten in der Histomorphometrie. Daher wurde die vorgeschlagene Analysetechnik erfolgreich mit dem Goldstandard verglichen. Ausserdem wurde nachgewiesen, dass die neue Methode reproduzierbar sowie sensitiv in der Erfassung von Unterschieden zwischen verschiedenen experimentellen Gruppen ist. Der Vorteil im Vergleich zu herkömmlicher Histomorphometrie ist, dass die neue Analysetechnik dreidimensional, nicht-invasiv, nicht-destruktiv und vollautomatisiert ist.

Die neue Methode wurde ausserdem angewendet, um lokale Knochenformations- und -resorptionsstellen zu identifizieren und die darin vorherrschenden Belastungsbedingungen zu untersuchen. Eine Anzahl von computergestützten Simulationsmodellen basiert auf der Annahme, dass lokaler Knochenauf- und -abbau ein direktes Resultat der mechanischen Belastungsumgebung sind. Der vorgeschlagene experimentelle *in-vivo*-Versuchsaufbau ermöglichte es, diese Fragestellung auf experimenteller Ebene zu untersuchen. Die Ergebnisse zeigten, dass die mittleren Belastungsdichte-(SED)-Werte an Aufbaustellen signifikant höher als an konstanten Stellen, sowie an Abbaustellen signifikant niedriger als an konstanten Stellen waren. Weiter wurde eine hohe Korrelation zwischen ansteigender SED und nachfolgender Aufbauwahrscheinlichkeit und eine reziproke Korrelation zwischen ansteigender SED und der Wahrscheinlichkeit für Knochenresorption gefunden. Diese Resultate belegen das Vorhandensein eines mechano-regulatorischen Mechanismus‘ auf zellulärem Niveau.

In einem letzten Schritt wurden die gewonnenen Erkenntnisse aus den ersten zwei Teilschritten benutzt, um ein voraussagendes Simulationsmodell der Knochenadaption zu entwickeln und zu validieren. Zuerst wurde mittels der experimentellen *in-vivo*-Daten ein Validierungssetup erarbeitet, mit Hilfe dessen der Vorhersagefehler eines computergestützten Modells bestimmt werden kann. In diesem Abschnitt wurde ein einfacher Verdickungsalgorithmus implementiert, um die Knochenantwort auf erhöhte mechanische Belastung zu simulieren. Während die morphometrischen Parameter nach vier Wochen im Experiment genau vorhergesagt wurden, konnten die räumlichen Muster von Knochenformation und -resorption nicht nachgebildet werden. Dieses Resultat unterstreicht die Notwendigkeit eines Kontroll-Mechanismus‘, der lokal über Knochenauf- oder -abbau entscheidet. Daher wurde in einem zweiten Schritt eine belastungsbasierte Kontrollschleife in das *in-silico*-Modell implementiert. Die Ergebnisse zeigten, dass nach vier Wochen simulierter mechanischer Belastung sowohl morphometrische Parameter als auch dynamische Knochenumbauraten mit dem Experiment übereinstimmten. Knochenverlust nach einer Ovarektomie wurde ebenfalls erfolgreich simuliert, inklusive des Eintretens eines Sättigungsniveaus bei einer niedrigeren Knochenmasse nach einigen Wochen. Mit diesen Ergebnissen wurde aufgezeigt, dass wiederholte Validierung anhand der experimentellen *in-vivo*-Daten die Entwicklung eines Modells leiten und gleichzeitig zu neuen Einblicken in die biologischen Zusammenhänge von Knochenanpassung

führen kann.

Zusammenfassend macht diese Arbeit deutlich, dass experimentelle *in-vivo*-Daten in Kombination mit computergestützter Simulation eine leistungsstarke Einheit bilden. Mit diesem Werkzeug können Fragen geklärt werden, die bis jetzt dem Feld der Computersimulation vorbehalten waren. Es wird erwartet, dass die Beantwortung solcher Fragestellungen weitreichende Konsequenzen für das generelle Verständnis von Knochenremodellierung und die damit verknüpfte Osteoporoseforschung haben wird.

Chapter 1

Introduction

1.1 Thesis motivation

New advances in biomedical research often go hand in hand with the development of enhanced imaging technologies. The visualization of larger volumes or more details usually enables a better understanding of the physiological processes of the human body.

Bone research benefitted from the invention of micro-computed tomography (micro-CT) a few decades ago [1]. Micro-CT permits non-destructive data acquisition, three-dimensional imaging and larger volumes of interest to be evaluated compared to conventional imaging methods such as two-dimensional dual energy X-ray absorptiometry (DXA) or histomorphometry. Along with the advent of micro-CT, three-dimensional quantification techniques for the characterization of the trabecular bone structure were developed allowing a fully-automated analysis and thus higher throughput of bone samples [2–5].

A better understanding of the trabecular bone microstructure is of special interest since the bone of elderly people becomes more susceptible to osteoporosis, which is one of the most common bone diseases. Osteoporosis is characterized by a deterioration of the bone microstructure and an increased fracture risk. It affects more than 40% of women and 13% of men after the age of 50 [6]. Counting over 2.3 million fractures annually in Europe and the USA alone, osteoporosis has become a major health problem, reflected in the higher morbidity and mortality of patients as well as in increased health care costs [7].

To understand the biological processes underlying osteoporosis, a better comprehension of the mechanisms involved at the cellular level in the bone microstructure

is essential. It is known that the pathological mechanism in osteoporosis causes an imbalance between bone formation and bone resorption. A choreographed balance between these two processes, also called bone remodeling, typically ensures that bone material can be renewed constantly over time. It is well established that a key regulator of bone remodeling is mechanical loading since prolonged bed rest leads to massive bone loss while mechanical overloading results in a net gain in bone mass, i.e. a shift in the remodeling balance towards more bone formation. How the mechanical stimulus is translated into biochemical signals triggering bone formation and resorption is still poorly understood. Lacking access to experimental measures of dynamic bone formation and resorption rates *in vivo*, the investigation of the interplay between bone forming and resorbing cells and a potential mechanical signal has to date mostly been reserved for *in silico* simulation models.

With the recent advent of high-resolution *in vivo* micro-CT for rodents [8], it has become feasible to monitor the same bone structure over a period of time. Beyond that, by re-alignment of follow-up measurements, the changes at a particular location in the bone can be tracked [9]. Thus, there is hope that high-resolution *in vivo* micro-CT will allow the investigation of questions regarding bone adaptation that have to date been reserved for *in silico* simulation models. Those have, however, often been lacking concise validation due to the previous non-existence of suitable experimental data. In particular, this concerns the transient changes in the bone microstructure over time, and the exploration of different remodeling theories related to a - so far only hypothesized - local mechano-regulatory mechanism of bone adaptation [10–13].

Furthermore, it is assumed that computer simulations validated by means of experimental *in vivo* data can make a better prediction on the course of bone adaptation or disease, accompanying fracture risk and potential treatments. Although high-resolution *in vivo* micro-CT is so far only available for rodents, the validation of *in silico* models is presumed to be a first step towards a precise prediction of bone changes and the successful future use of computer models in clinics to assist diagnosis and to monitor therapy.

Another added value of experimental *in vivo* micro-CT data for the validation of *in silico* models is that they will potentially provide access to experimental measures of dynamic bone remodeling rates *in vivo*. Such information is to date not available since bone formation rates can only be measured by conventional two-dimensional histomorphometry. Histomorphometric assessment of dynamic bone morphometry

requires a laborious and operator-dependent analysis including the destruction of the bone samples. Bone resorption suffers from a lack of an equivalent time-dependent quantity to be measured and is typically estimated by biochemical markers. Thus there is a need for a three-dimensional, non-invasive and fully-automated assessment of bone formation and resorption rates. Especially, the quantification of experimental bone resorption rates is assumed to have a high potential for improving our understanding of the cellular mechanisms involved during bone remodeling in healthy and diseased states. It is anticipated that the insight gained from experimental bone formation and resorption rates will additionally contribute to the development of more sophisticated computational models.

1.2 Specific aims

The global aim of this thesis was to develop a predictive *in silico* model for bone adaptation which uses new insights gained from experimental *in vivo* micro-CT data, including newly developed bone formation and resorption rates. Furthermore, the computational model should be validated by means of the underlying *in vivo* data. Here, the advantage of the adjacency to the experiment is that the predictive value of the *in silico* model can be determined, sensitive and precise validation results can be ensured, and discrepancies between the model and experiment may give new insights into biological processes. Thus these discrepancies have the potential to guide the development of the *in silico* model accordingly.

Specifically, the following three aims were defined:

Aim I: Quantify three-dimensional bone formation and resorption rates from time-lapsed *in vivo* micro-CT measurements.

Aim II: Investigate the existence of a local mechanical regulation mechanism of bone remodeling.

Aim III: Implement and validate a computational *in silico* model of bone adaptation using the underlying experimental *in vivo* data.

1.3 Outline of the thesis

Chapter 2 provides a background about bone biology. Furthermore, possible factors that influence bone remodeling are outlined. This concerns bone loss related to osteoporosis as well as bone changes in response to varying mechanical loading. Moreover, an overview of current measuring techniques for static and dynamic bone morphometry is presented. The last section of this chapter is concerned with state-of-the-art computer simulations of bone adaptation.

Chapter 3 describes the development and validation of a technique to extract three-dimensional dynamic bone formation and resorption rates. This technique is based on rigid image registration of follow-up *in vivo* micro-CT measurements. Since image registration may introduce interpolation errors, the effect of different interpolators on the subsequent bone morphometric indices is investigated in the first section. The second section deals with the three-dimensional extraction of dynamic bone formation and resorption rates from *in vivo* micro-CT scans. These rates are established similarly to corresponding two-dimensional indices in dynamic histomorphometry. For this reason, the introduction of three-dimensional quantification requires investigating reproducibility, accuracy and sensitivity of the new technique. Here, reproducibility is assessed by repeated *ex vivo* measurements of the last measurement time point and determination of precision errors and intra-class correlation coefficients of the newly introduced dynamic bone morphometry parameters. Accuracy is investigated by comparing the new dynamic morphometry rates to the conventionally determined histomorphometric values (gold standard). Sensitivity is explored by application of the new parameters to an experimental *in vivo* loading study.

Chapter 4 deals with the comparison of bone formation and resorption sites and the corresponding mechanical milieu associated with these sites. The theory of mechano-regulation, also referred as Wolff's law, states that cellular bone remodeling is governed by the prevailing local mechanical environment. By using dynamic morphometry combined with finite element analysis to determine local stresses and strains, it became possible, for the first time, to test whether such local mechano-regulation exists.

Chapter 5 is concerned with the development and validation of a computational

simulation model for bone adaptation. The first section focuses on a new validation technique of *in silico* models, making use of the fact that *in vivo* micro-CT data allow determining the prediction error of a computational algorithm. Here, the validation data result from a mouse tail loading model developed in our group [14, 15]. In this section, the computational algorithm uses an open-loop control disregarding local mechanical feedback in the bone. In the second section, an algorithm based on a mechanical feedback-loop is implemented and the resulting strain-adaptive *in silico* model is validated by means of an animal loading and an animal ovariectomy experiment.

Chapter 6 contains the synthesis of the presented work including the major findings of this thesis, its additional value for the community, as well as its limitations and an outlook on future work.

References

[1] L. A. Feldkamp, S. A. Goldstein, A. M. Parfitt, G. Jesion, and M. Kleerekoper. The direct examination of three-dimensional bone architecture in vitro by computed tomography. *J Bone Miner Res*, 4(1):3–11, 1989.

[2] T. Hildebrand and P Rüegsegger. A new method for the model-independent assessment of thickness in three-dimensional images. *J Microsc*, 185:67–75, 1997.

[3] T. Hildebrand and P. Rüegsegger. Quantification of bone microarchitecture with the structure model index. *Comput Methods Biomech Biomed Engin*, 1(1):15–23, 1997.

[4] R. Müller and P. Rüegsegger. Micro-tomographic imaging for the nondestructive evaluation of trabecular bone architecture. *Stud Health Technol Inform*, 40:61–79, 1997.

[5] A. Odgaard. Three-dimensional methods for quantification of cancellous bone architecture. *Bone*, 20(4):315–328, 1997.

[6] S. Khosla, B. L. Riggs, E. J. Atkinson, A. L. Oberg, L. J. McDaniel, M. Holets, J. M. Peterson, and L. J. Melton 3rd. Effects of sex and age on bone mi-

crostructure at the ultradistal radius: a population-based noninvasive in vivo assessment. *J Bone Miner Res*, 21(1):124–131, 2006.

[7] World Health Organization. Prevention and Management of Osteoporosis. *Report of a WHO Scientific Group. WHO Technical Report Series*, 921:1–164, 2003.

[8] J.A. Gasser and J. Yam. In vivo non-invasive monitoring of changes in structural cancellous bone parameters with a novel prototype microct in rats. *J Bone Miner Res*, 17(Suppl. 2), 2002.

[9] J. H. Waarsing, J. S. Day, J. C. van der Linden, A. G. Ederveen, C. Spanjers, N. De Clerck, A. Sasov, J. A. N. Verhaar, and H. Weinans. Detecting and tracking local changes in the tibiae of individual rats: a novel method to analyse longitudinal in vivo micro-ct data. *Bone*, 34(1):163–169, 2004.

[10] J. Wolff. *Das Gesetz der Transformation der Knochen (The Law of Bone Remodelling)*. Springer-Verlag, Berlin, Germany, 1892.

[11] H. M. Frost. The mechanostat: a proposed pathogenic mechanism of osteoporoses and the bone mass effects of mechanical and nonmechanical agents. *Bone Miner*, 2(2):73–85, 1987.

[12] R. Huiskes, R. Ruimerman, G. H. van Lenthe, and J. D. Janssen. Effects of mechanical forces on maintenance and adaptation of form in trabecular bone. *Nature*, 405(6787):704–706, 2000.

[13] D. P. Fyhrie and D. R. Carter. A unifying principle relating stress to trabecular bone morphology. *J Orthop Res*, 4(3):304–17, 1986.

[14] D. J. Webster, P. L. Morley, G. H. van Lenthe, and R. Müller. A novel in vivo mouse model for mechanically stimulated bone adaptation - a combined experimental and computational validation study. *Comput Methods Biomech Biomed Engin*, 11(5):435–441, 2008.

[15] F. M. Lambers, G. Kuhn, F. A. Gerhard, and R. Müller. In vivo micro computed tomography allows monitoring of load induced microstructural bone adaptation. *Bone*, 44(S2):300, 2009.

Chapter 2

Background

2.1 Bone

Bone is one of the major organs in the human body. It builds up the skeletal system, together with cartilage, ligaments and tendons. The skeleton as such forms the framework of the body, protects the inner soft-tissue organs, and provides points of attachment for locomotion. Besides structure-related functions, bone also serves as a calcium and phosphate storage and is able to release minerals into the blood when required. Furthermore, it has a hematopoietic function in that blood cells are produced in the red bone marrow.

Bone consists of about 62% inorganic minerals, 13% H_2O and 25% organic collagen. The high degree of mineralization is responsible for its stiff structure. Nonetheless, bone material is relatively light per unit volume due to its unique composition. Load bearing bones typically consist of two main parts: the cortical shell and the trabecular compartment (see Figure 2.1). The cortex gives shape to the bone; it surrounds the inner spongy structure of trabeculae in the end pieces or the inside and is thick in the middle to protect the bone from large deformation. The spaces between the trabecular structures and devoid of trabecular bone are filled with bone marrow. This design ensures very high stability at a comparatively low bone mass.

Bone itself is a living tissue. A number of cell types can be found within it amongst which are four types of specific bone cells: osteoblasts, osteoclasts, osteocytes, and bone lining cells. Osteoblasts are responsible for bone formation. Osteoclasts resorb bone. Osteocytes are assumed to have the task of communication throughout the bone matrix, and bone lining cells are quiescent osteoblasts covering the bone surface. This biological cell machinery enables bone to adapt its internal structure to

its specific needs. Such needs include the constant renewal of old bone with newer material including the repair of everyday micro-fractures as well as the adaptation to changes in mechanical requirements. This remodeling process takes place by a sensitive interplay between bone forming and resorbing cells orchestered by osteocytes. A pathological disturbance of this balance, e.g. a systemic lack of estrogen as it occurs in post-menopausal osteoporosis, will lead to a shift towards an increase in either of these processes, e.g. to increased bone resorption in the case of osteoporosis.

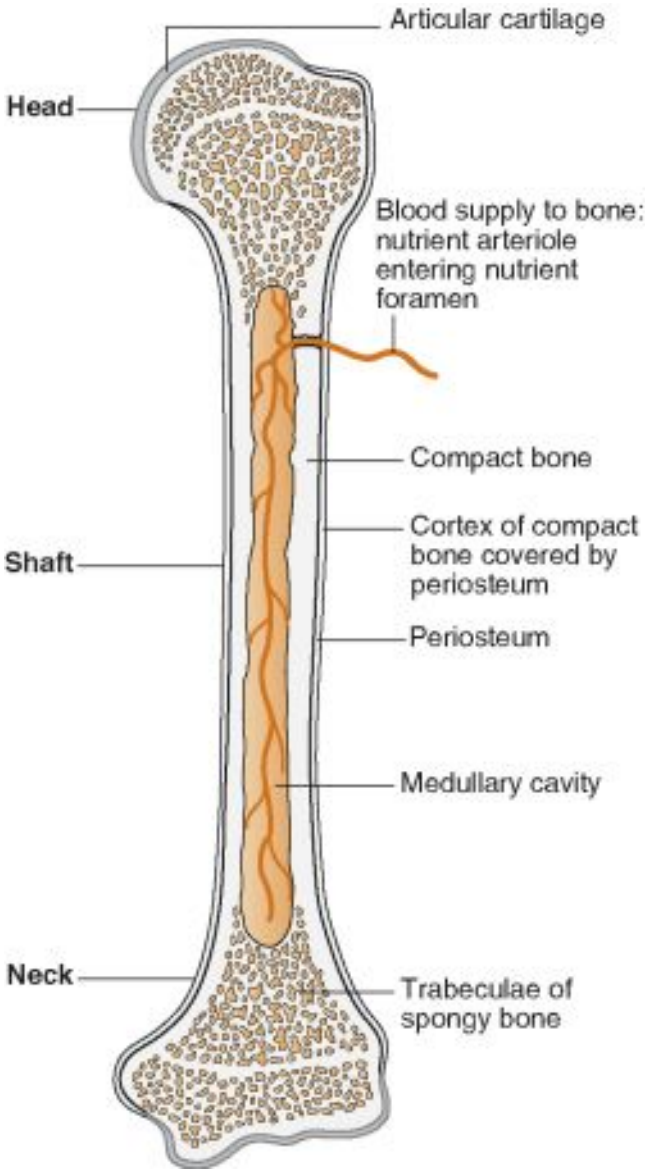

Figure 2.1: Schematic drawing of a longitudinal section through a typical long bone. (Source: Aspinall & O'Reilly [1])

2.2 Osteoporosis and bone adaptation

Osteoporosis is the most common bone disease in the aging population. It is characterized by a reduction in bone density, a deterioration of bone architecture and an increased fracture risk [2]. This disease is most prevalent in women after menopause, and in this context is called post-menopausal osteoporosis. Osteoporosis affects more than 75 million people in Europe, Japan and the USA, and causes over 2.3 million fractures annually in Europe and the USA alone [2]. In osteoporosis, the morbidity of the disease arises from the associated fractures with the most serious osteoporotic fracture being that of the hip. An estimated 1.3-1.7 million hip fractures occurred worldwide in 1990 [3] and by 2025, this number is expected to increase to almost 3 million. These numbers indicate that osteoporosis presents a global socio-economic health care problem [2]. There exist pharmaceutical treatments such as bisphosphonate or parathyroid hormone therapies. The exact pathological mechanism causing osteoporosis, however, is not clear to date.

To be able to retrace the pathological mechanism of osteoporosis, it is essential to understand the laws to which bone complies under physiological conditions. There are several phenomena which strongly indicate a mechanical influence on the bone structure. After prolonged bed rest, the bone mass of patients is drastically reduced [4–6]. The first space flights in the late 1960s repatriated their pilots with severe symptoms of osteoporosis most probably because of the decreased gravitational forces in space [7–10]. In later flights these symptoms could at least be partly prevented by an extensive training program during the space journeys [11, 12]. A phenomenon being observed in some professional sportsmen, e.g. tennis players, is a thickened bone in the extremity exposed to exorbitant training as some sports can induce extreme loads on a particular part of the body [13–17].

In addition to such observed phenomena in humans, animal models are commonly used in bone research. An established model for post-menopausal osteoporosis is the ovariectomized rat [18, 19]. Following estrogen depletion, ovariectomy induces an increase in bone turnover and an acceleration of bone loss [18, 20]. In contrast to humans, ovariectomized animal models do not show a more fragile phenotype. For this reason, they are usually referred to as osteopenia models [21]. A classical mouse model of mechanical unloading (bedrest, space flights) is tail suspension [22, 23]. An anabolic bone response could successfully be established by mechanical loading of particular bones in the body. Several approaches for applying load to a specific bone

exist [24–27]. A model developed at the Institute for Biomechanics is the loading of the caudal vertebra in the mouse tail [28].

2.3 Quantitative bone morphometry

Bone research requires techniques to describe the inner bone structure in a quantitative fashion. Such techniques enable statements on the effect of a disease, the success of a treatment or the changes in bone morphology over time.

Micro-computed tomography (micro-CT) represents a common, non-invasive, and three-dimensional device to image the trabecular bone microstructure at image resolutions ranging from millimeters down to nanometers. Today, *in vivo* measurements are constrained to about 10 μm resolution for small animals scanned in an *in vivo* micro-CT system and to about 80 μm resolution for humans using clinical high-resolution peripheral quantitative CT (HR-pQCT) systems. The evaluation of the acquired micro-CT measurements can be performed by the quantification of structural and other properties. In the trabecular compartment, this includes the extraction of morphometric parameters such as bone volume fraction (BV/TV in %), specific bone surface (BS/BV in mm^2/mm^3), trabecular thickness (Tb.Th, in mm), trabecular separation (Tb.Sp, in mm), trabecular number (Tb.N, in 1/mm), the degree of anisotropy (DA), the structure model index (SMI) and many more. A disadvantage to be considered in *in vivo* micro-computed tomography is the emerging X-ray radiation. A second drawback is that it is not possible to directly image cell activity in the bone with micro-computed tomography as is the case in other imaging techniques, i.e. in histology-based light microscopy.

Histomorphometry is a two-dimensional method which is based on the analysis of small bone sections gained from human or animal biopsies or autopsies. In order to quantify dynamic bone formation rates, the bone is stained *in vivo* with a substance able to incorporate into an actively mineralizing osteoid, e.g., calcein or tetracyclin. A short time period between a first and a second labeling injection allows time-dependent assessment of the mineralization fronts, visible as epifluorescent lines. From these lines, a number of bone formation parameters including bone formation rate (BFR), mineral apposition rate (MAR), and mineralizing surface (MS) can be determined [29]. Histomorphometric assessment of bone resorption suffers from the lack of an equivalent dynamic marker. Alternatively, resorption cavities are studied

in terms of their relative and absolute extent [30]. Eroded surface (ES) is measured as the percentage of crenated surfaces per total surface; furthermore, markers exist that are able to visualize the osteoclast number and activity (Oc.N) [31]. The disadvantage of histomorphometric assessment of dynamic bone remodeling rates is the destructive, laborious and operator-dependent nature of the underlying imaging technique. Alternatively, biochemical markers are currently being used to assess both bone formation and resorption from samples of blood or urine. Nevertheless, these markers fail to depict local changes in the bone as they can only reflect systematic changes in the body.

References

[1] V. Aspinall and M. O'Reilly. *Introduction to Veterinary Anatomy and Physiology*. Butterworth-Heinemann, 1st edition, 2004.

[2] World Health Organization. Prevention and Management of Osteoporosis. *Report of a WHO Scientific Group. WHO Technical Report Series*, 921:1–164, 2003.

[3] B. Gullberg, O. Johnell, and J. A. Kanis. World-wide projections for hip fracture. *Osteoporos Int*, 7(5):407–13, 1997.

[4] A. D. Leblanc, V. S. Schneider, H. J. Evans, D. A. Engelbretson, and J. M. Krebs. Bone-mineral loss and recovery after 17 weeks of bed rest. *Journal of Bone and Mineral Research*, 5(8):843–850, 1990.

[5] B. Krolner and B. Toft. Vertebral bone loss: an unheeded side effect of therapeutic bed rest. *Clin Sci (Lond)*, 64(5):537–40, 1983.

[6] C. L. Donaldson, S. B. Hulley, J. M. Vogel, R. S. Hattner, J. H. Bayers, and D. E. McMillan. Effect of prolonged bed rest on bone mineral. *Metabolism*, 19(12):1071–84, 1970.

[7] S. C. White, C. A. Berry, and R. R. Hessberg. Effects of weightlessness on astronauts–a summary. *Life Sci Space Res*, 10:47–55, 1972.

[8] G. D. Whedon, L. Lutwak, P. Rambaut, M. Whittle, C. Leach, J. Reid, and M. Smith. Mineral and nitrogen metabolic studies on skylab flights and compar-

ison with effects of earth long-term recumbency. *Life Sci Space Res*, 14:119–27, 1976.

[9] G. D. Whedon, L. Lutwak, P. C. Rambaut, M. W. Whittle, J. Reid, M. C. Smith, C. Leach, C. R. Stadler, and D. D. Sanford. Mineral and nitrogen balance study observations: the second manned skylab mission. *Aviat Space Environ Med*, 47(4):391–6, 1976.

[10] P. C. Rambaut and R. S. Johnston. Prolonged weightlessness and calcium loss in man. *Acta Astronaut*, 6(9):1113–22, 1979.

[11] Victor A. Convertino and Konstantin Tsiolkovsky. Physiological adaptations to weightlessness: Effects on exercise and work performance, 1990.

[12] Charles M. Tipton. Considerations for exercise prescriptions in future space flights, 1983.

[13] S. C. Tsai, C. H. Kao, and S. J. Wang. Comparison of bone mineral density between athletic and non-athletic chinese male adolescents. *Kaohsiung J Med Sci*, 12(10):573–80, 1996.

[14] H. Resch, P. Pietschmann, K. Kromer, E. Krexner, P. Bernecker, and R. Willvonseder. Peripheral and axial bone mass in austrian free climbers. *Klin Wochenschr*, 69(7):303–6, 1991.

[15] B. Cohen, P. J. Millett, B. Mist, M. A. Laskey, and N. Rushton. Effect of exercise training programme on bone mineral density in novice college rowers. *Br J Sports Med*, 29(2):85–8, 1995.

[16] E. Ozcivici, Y. K. Luu, B. Adler, Y. X. Qin, J. Rubin, S. Judex, and C. T. Rubin. Mechanical signals as anabolic agents in bone. *Nat Rev Rheumatol*, 6(1):50–9, 2010.

[17] H. H. Jones, J. D. Priest, W. C. Hayes, C. C. Tichenor, and D. A. Nagel. Humeral hypertrophy in response to exercise. *J Bone Joint Surg Am*, 59(2):204–8, 1977.

[18] D. N. Kalu. The ovariectomized rat model of postmenopausal bone loss. *Bone Miner*, 15(3):175–91, 1991.

[19] J. H. Kinney, N. E. Lane, and D. L. Haupt. In vivo, three-dimensional microscopy of trabecular bone. *J Bone Miner Res*, 10(2):264–70, 1995.

[20] I. Yamazaki and H. Yamaguchi. Characteristics of an ovariectomized osteopenic rat model. *J Bone Miner Res*, 4(1):13–22, 1989.

[21] D. B. Kimmel, Moran E.L., and Bogoch E.R. Animal models of osteopenia or osteoporosis. *An Ya and Friedman RJ (eds), Animal Models in Orthopaedic Research, 1st ed. CRC Press, Boca Raton*, pages 279–305, 1999.

[22] D. Amblard, M. H. Lafage-Proust, A. Laib, T. Thomas, P. Ruegsegger, C. Alexandre, and L. Vico. Tail suspension induces bone loss in skeletally mature mice in the c57bl/6j strain but not in the c3h/hej strain. *Journal of Bone and Mineral Research*, 18(3):561–569, 2003.

[23] T. A. Bateman, C. R. Dunstan, V. L. Ferguson, D. L. Lacey, R. A. Ayers, and S. J. Simske. Osteoprotegerin mitigates tail suspension-induced osteopenia. *Bone*, 26(5):443–9, 2000.

[24] T. S. Gross, S. Srinivasan, C. C. Liu, T. L. Clemens, and S. D. Bain. Noninvasive loading of the murine tibia: an in vivo model for the study of mechanotransduction. *J Bone Miner Res*, 17(3):493–501, 2002.

[25] E. A. Pedersen, M. P. Akhter, D. M. Cullen, D. B. Kimmel, and R. R. Recker. Bone response to in vivo mechanical loading in c3h/hej mice. *Calcif Tissue Int*, 65(1):41–6, 1999.

[26] R. L. De Souza, M. Matsuura, F. Eckstein, S. C. Rawlinson, L. E. Lanyon, and A. A. Pitsillides. Non-invasive axial loading of mouse tibiae increases cortical bone formation and modifies trabecular organization: a new model to study cortical and cancellous compartments in a single loaded element. *Bone*, 37(6):810–8, 2005.

[27] J. C. Fritton, E. R. Myers, T. M. Wright, and M. C. H. van der Meulen. Loading induces site-specific increases in mineral content assessed by microcomputed tomography of the mouse tibia. *Bone*, 36(6):1030–1038, 2005.

[28] D. J. Webster, P. L. Morley, G. H. van Lenthe, and R. Müller. A novel in vivo mouse model for mechanically stimulated bone adaptation - a combined

experimental and computational validation study. *Comput Methods Biomech Biomed Engin*, 11(5):435–441, 2008.

[29] A. M. Parfitt. Trabecular bone architecture in the pathogenesis and prevention of fracture. *Am J Med*, 82(1B):68–72, 1987.

[30] J. P. Roux, M. E. Arlot, E. Gineyts, P. J. Meunier, and P. D. Delmas. Automatic-interactive measurement of resorption cavities in transiliac bone biopsies and correlation with deoxypyridinoline. *Bone*, 17(2):153–6, 1995.

[31] C. Minkin. Bone acid phosphatase: tartrate-resistant acid phosphatase as a marker of osteoclast function. *Calcif Tissue Int*, 34(3):285–90, 1982.

2.4 *In silico* biology of bone modelling and remodelling: adaptation

Friederike A. Gerhard[1], Duncan J. Webster[1], G. Harry van Lenthe[2], and Ralph Müller[1]

[1]Institute for Biomechanics, ETH Zürich, Zürich, Switzerland
[2]Division of Biomechanics and Engineering Design, Katholieke Universiteit Leuven, Celestijnenlaan 300C, PB 2419, 3001 Leuven, Belgium

published in:
Phil. Trans. R. Soc. A
367:2011 - 2030, 2009

Abstract:
Modelling and remodelling are the processes by which bone adapts its shape and internal structure to external influences. However, the cellular mechanisms triggering osteoclastic resorption and osteoblastic formation are still unknown. In order to investigate current biological theories, *in silico* models can be applied. In the past, most of these models were based on the continuum assumption, but some questions related to bone adaptation can be addressed better by models incorporating the trabecular microstructure. In this paper, existing simulation models are reviewed and one of the microstructural models is extended to test the hypothesis that bone adaptation can be simulated without particular knowledge of the local strain distribution in the bone. Validation using an experimental murine loading model showed that this is possible. Furthermore, the experimental model revealed that bone formation cannot be attributed only to an increase in trabecular thickness but also to structural reorganization including the growth of new trabeculae. How these new trabeculae arise is still an unresolved issue and might be better addressed by incorporating other levels of hierarchy, especially the cellular level. The cellular level sheds light on the activity and interplay between the different cell types, leading to the effective change in the whole bone. For

this reason, hierarchical multi-scale simulations might help in the future to better understand the biomathematical laws behind bone adaptation.

Keywords:
bone; remodelling; adaptation; loading; simulation; hierarchical modelling

2.4.1 Introduction

Bone is a material able to adapt to its external mechanical environment. This insight was gained more than a century ago by a German anatomist called Wolff [1] and has been since referred to as Wolff's law. The underlying mechanisms and triggering factors of bone reorganization, however, are not well understood. In the 1970s, new discoveries [2–5] were made when it was realized that astronauts returned from space flights with significant bone loss. Likewise, it was observed that people exposed to prolonged bed rest also suffered from considerable bone atrophy [6–8]. These observations led to the assumption that bone needs everyday physical activity and the gravitational forces on Earth to sustain a structure capable of coping with daily physical demands. This form of bone loss seems to be driven by mechanics and is typically classified as disuse osteoporosis, as opposed to the so-called post-menopausal osteoporosis (hormone driven). These days, this disease is considered one of the major health problems facing middleaged women and elderly people of either sex [9]. In 2000, the total direct costs in Europe were estimated at 32 billion euros, which are expected to increase to 77 billion euros in 2050 based on the expected demographic shift in Europe [10].

To combat post-menopausal osteoporosis, a deeper understanding of the microstructural adaptation mechanisms (called bone modelling and remodelling) is sought. Bone modelling is necessary to prepare the bone for increased or changing loads and is defined as the process of bone formation and resorption on separate surfaces, i.e. uncoupled formation and resorption [11]. Bone remodelling undertakes the replacement of aged and damaged bone tissue with new (and undamaged) bone to prevent the development of fatigue fractures. Here, bone resorption and formation need to take place at the same site, i.e. coupled formation and resorption [12]. These mechanisms occur both in the cortical shell and in the trabecular compartment. However, remodelling is shown to be more sensitive in the trabecular

compartment. For this reason, this paper concentrates on trabecular bone adaptation. Figure 2.2 highlights the difference between cortical and trabecular bone as well as introducing the cells implicated in bone adaptation, respectively. The cellular mechanisms will be described in more detail in Section 2.4.2.

Since the adaptation of trabecular bone due to changing loading conditions or post-menopausal osteoporosis is a process that takes weeks up to years, data acquisition often represents a critical factor in research studies. Computer simulations have therefore gained more and more importance during the last 20 years. A computer simulation tries to describe the complex interdependent biological processes involved using a set of mathematical equations and attempts to mirror the actual biological process *in silico*. The quality of such models is therefore determined by the relevance and accuracy of the underlying assumptions upon which the governing mathematical equations have been formulated. While many of the earlier research questions aimed at a deeper understanding of the macroscopic mechanical properties, the scientific community has started to focus more and more on how these mechanical properties are determined by the underlying cellular processes, a field referred to as mechanobiology. This evolution has improved our understanding of the cellular mechanisms and molecular pathways governing bone adaptation. However, we must be careful not to neglect the global, macroscopic impact of these biological processes when we are interested in determining bone competence. Thus, in order to gain a deeper understanding of the whole process of bone modelling and remodelling, there is a need for hierarchical simulation models investigating different levels of resolution and incorporating these levels in a multi-scale approach. This paper provides an overview of the most important underlying biological principles and reviews the state of the art of hierarchical computational approaches that are used to describe the adaptation of bone due to mechanical loading and disease. Although a number of *in silico* models have been proposed for bone regeneration (see [13] in the same issue), this paper will only focus on adaptation models. To illustrate the power of *in silico* models, we will extend an established microstructural bone loss algorithm to describe bone adaptation due to increased mechanical loading. Its purpose is to investigate the feasibility of modelling bone adaptation without specific knowledge of the local mechanical milieu within the bone. A comparison of these results with findings from actual *in vivo* loading data shows that overall changes in bone mass can be predicted very accurately without knowledge of the

underlying mechanics. Nevertheless, differences in local architecture can be noted between experiment and prediction, demonstrating the importance of incorporating local regulation of mechanical adaptation.

2.4.2 Biology

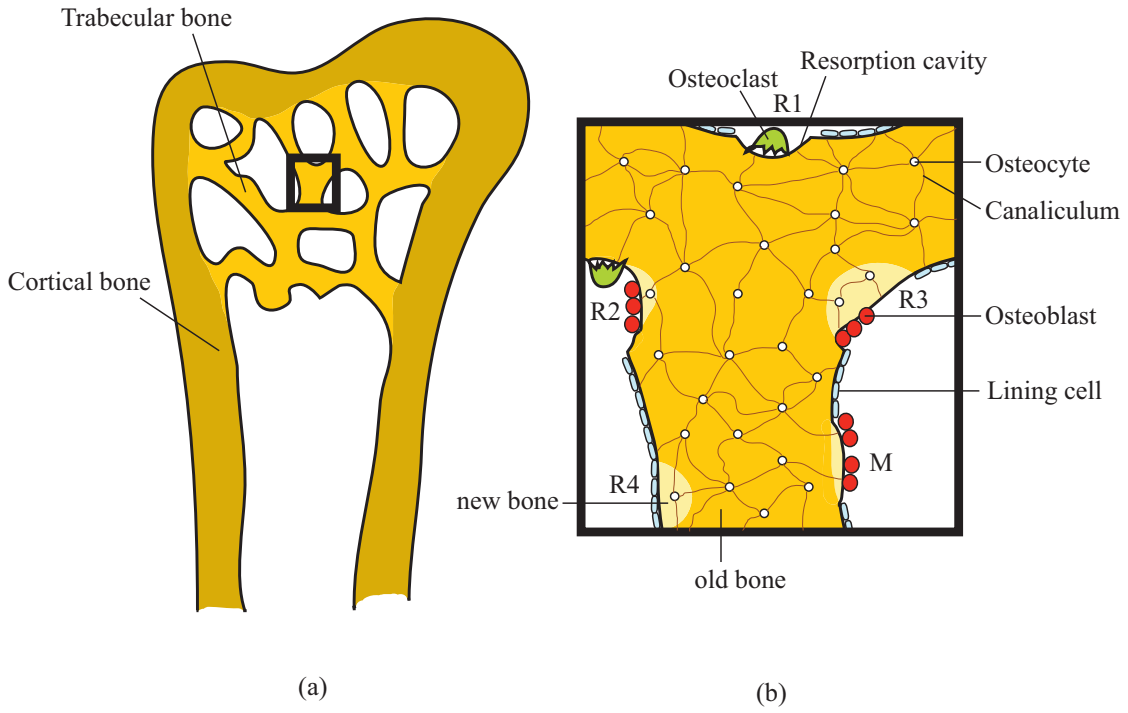

Figure 2.2: (a) Bone can be divided into cortical shell and trabecular compartment. Bone modelling and remodelling take place in both, but more in the trabecular compartment. Thus, (b) the cellular processes of modelling (M) and remodelling (R1−R4) are shown.

The actual change in the trabecular microstructure during mechanical adaptation is realized at the cellular level where the executive cells involved in the bone remodelling process are osteoblasts and osteoclasts (figure 2.2b). Osteoblasts are responsible for bone formation while osteoclasts resorb bone. The biochemical mechanisms triggering the activity and recruitment of these cell types, however, are still not identified [14]. Today, it is widely assumed that osteoblasts and osteoclasts are controlled by a sensing system of osteocytes [14–18]. Osteocytes are mechanosensitive cells [15]

lying within the so-called osteocyte lacunae deep within the mineralized matrix and are highly interconnected by cell processes, lying in small canaliculi (figure 2.2b). The canalicular network is extended throughout the whole bone matrix and thus possesses the characteristics to serve as a communication system [17]. For this reason, research has turned more and more towards the role of osteocytes and how they communicate with osteoblasts and osteoclasts to investigate processes related to mechanical bone adaptation [14, 19]. The transduction from an external mechanical force into a signal sensed by the osteocytes may take place by strain [20–22], micro-damage [23] or fluid flow [18, 24, 25]. For osteocytes to activate the executive cells, it is assumed that a cascade of biochemical processes incorporating an enzyme called nitric oxide synthase occurs [26–28].

The interactions between osteocytes, osteoblasts and osteoclasts are not known in detail. What is known is that during the bone remodelling process, osteoclasts first resorb a certain amount of bone and osteoblasts follow to refill the resulting resorption cavity (figure 2.2b). This unit of osteoclasts and osteoblasts is often referred to as the basic multicellular unit (BMU). It has been proposed that the activity of the BMU is governed by feedback from mechanical load transfer [21]. According to this theory, osteoblasts are recruited in response to an osteocytic signal associated with high strain energy density (SED) values, while osteoclasts are either recruited by a low SED signal (disuse) or they act in a spatially random fashion (in response to the random occurrence of microcracks resulting from daily loading; [29]). Other theories, however, assume high strains to produce microcracks and thus attract osteoclasts to remove the damaged bone [23, 30]. This controversy points to the fact that the actual cell activation mechanism has not yet been identified.

In the presence of post-menopausal osteoporosis, bone cells are impaired in their response to mechanical stimulation [31]. This in turn leads to bone loss and increased fracture risk. The pathological factors characterizing osteoporosis have been a topic of interest of many researchers to date, but are not the basis of this review.

2.4.3 *In silico* modelling

Organ-level approaches (continuum models)

To gain better insight into the physiological interplay between the mechanical environment and the biological response of bone at a macroscopic level, early theoretical models aimed to provide a more detailed mathematical description of the law es-

tablished by Wolff [1]. In these approaches, bone was considered as a continuum material and was described by its apparent density only. Cortical and trabecular components were accounted for by assigning two different ranges of apparent density [32], thus avoiding the need to describe their heterogeneous microstructures. Density-based simulations of trabecular bone adaptation have been addressed in many continuum approaches [20, 32–41] and have been reviewed before [42–44]. To name only some of the approaches, several groups [20, 32, 34, 45–48] proposed strain as the driving force for remodelling. A theoretical model using microdamage as a driving force was published by Prendergast & Taylor [23]. Thomsen et al. [49] focused on the simulation of osteoporotic bone loss on a continuum level by choosing a stochastic simulation approach.

The quantification of apparent bone density was without doubt a major advancement towards a better understanding of bone characteristics. However, with a greater understanding of the structural behaviour of bone, it became clear that the trabecular microstructure could not be ignored. With the arrival of new microstructural imaging techniques [50], new methods of investigation became accessible and made it possible to visualize the organization of the trabecular network. This enabled researchers to better investigate the effects of post-menopausal osteoporosis on the trabecular architecture or even the realignment of individual trabeculae as a consequence of changes in loading. These enhanced imaging capabilities also allowed new ways to validate existing theories, including tissue-level properties.

Tissue-level approaches

One of the first publications taking the intricate trabecular microstructure into account was published by Weinans et al. [47]. They presented a two-dimensional model based on finite-element (FE) analysis, which focused on the relationship between applied loads and the structural changes in single trabeculae. Trabeculae were modelled as a set of pixel elements and their morphological changes were simulated by removal or addition of the elements on the trabecular surface according to the local stresses and strains predicted by FE analysis. The theory behind the implemented algorithm was based on earlier work by Huiskes et al. [20]. However, the resulting two-dimensional artificial structures suffered from a so-called chessboard effect. This effect was expressed by pixel-sized holes within the two-dimensional representation of the bone structure. It was shown later that this behaviour was

an effect of the mathematical implementation, and a solution to this problem was presented by Mullender et al. [51], who allowed the number of osteocytes to be independent of the number of structural elements. Here, the authors assumed a certain sensing radius of the osteocytic signal, which was modelled as a decaying exponential function. From a biological point of view, this meant that several osteocytes could contribute to the stimulus an osteoblast receives. Evaluation of the model took place by visual inspection and comparison against the Weinans model.

Several studies based on the Mullender model followed [52, 53]. Mullender & Huiskes [17] demonstrated in a follow-up study that the mechanosensory system indeed is more likely to consist of osteocytes than of surface lining cells (figure 2.2b).

Adachi et al. [54] presented a competing two-dimensional FE model for trabecular surface remodelling, which assumed that an affinity for uniform stress conditions was the driving force behind bone remodelling. This algorithm was validated by applying it to a whole two-dimensional proximal femur using an artificially created trabecular microstructure.

Although these models appear to provide reasonable results when assessed qualitatively, one major limitation of all of the above models is that they lack quantitative validation using experimental datasets. A two-dimensional model validated against real experimental data was published for the first time by Tabor & Rokita [55]. They extended the stochastic continuum approach for osteoporosis that had been presented by Thomsen et al. [49] and modified the original algorithm, so that the state of bone was represented as the state of all pixels. Thus, it became possible to account for the structure of real trabeculae. Comparing the results of this approach with histomorphometric data resulted in a good agreement. A limitation of this model, however, was its two-dimensional design. Because trabecular bone is a three-dimensional structure, only three-dimensional simulation approaches are capable of predicting microstructural changes reliably. Thus, the evolution of microstructural approaches advanced more towards three-dimensional simulations. Two of the early three-dimensional approaches were presented by Tayyar et al. [56] and by Guo & Kim [57]. Both approaches focused on the simulation of bone loss over time by using artificial grids as input structures for successive bone removal. One of the first microstructural models using three-dimensional structures generated via micro-computed computer tomography (μCT) was presented by van der Linden et al. [58]. In this study, the authors investigated whether bone loss occurs

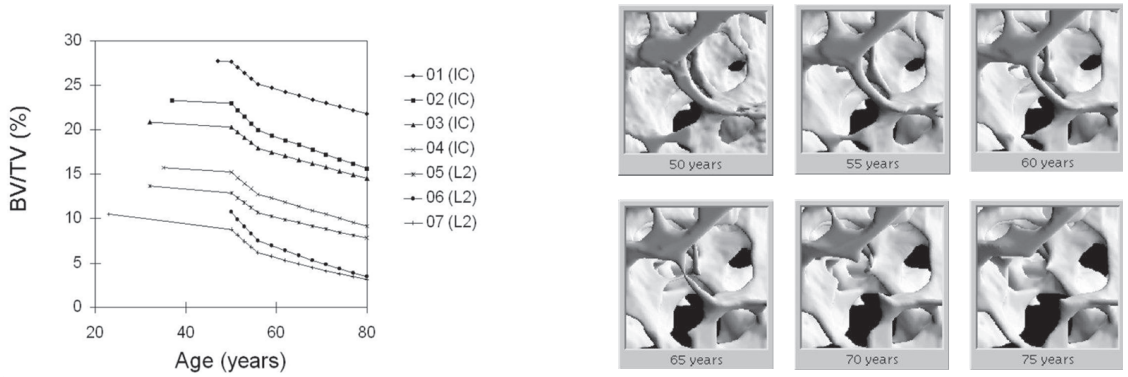

(a) (b)

Figure 2.3: (a) BV/TV in the course of age-related bone loss as determined by SIBA, starting at the individual ages of each of the seven donors. The onset of menopause was assumed to be at 50 years. (b) Series of simulated images of an iliac crest bone biopsy of a 47-year-old woman. The simulation illustrates the changes in bone architecture over time, where with increasing age the plate-like structure is partly resolved and the rods forming the network are more and more thinned until eventual perforation.

predominantly by a disconnection of trabeculae, by an accrual of loose fragments or by a formation deficit of osteoblasts. The simulated three-dimensional bone structures were applied to a quantitative bone morphometric analysis. The resulting bone morphometric parameters were then successfully compared with experimental results. From this study, the authors found that the osteoblastic formation deficit was responsible for the majority of total bone loss, while bone loss owing to a disconnection of trabeculae and loose fragments seemed to play a minor role. This result disagrees with a competing study [56] on artificial structures, indicating that bone loss occurs predominantly due to a perforation and subsequent removal of single trabeculae. In a further study, van der Linden et al. [59] used the developed model to predict the effects of an antiresorptive drug taken after menopause and found that late treatment can result in almost the same bone mass as early treatment after menopause; however, early treatment is shown to better conserve bone strength and stiffness.

Müller [60] focused on the same issue and introduced an algorithm for simulated bone atrophy (SIBA). In his model, bone loss was, for the first time, accounted for in a realistic time frame, spanning several decades of remodelling. The process of

osteoporotic bone loss was realized by means of a global iterative Gaussian filtration (osteoclastic resorption) and a subsequent thresholding procedure (osteoblastic refilling), employing several parameters to describe cellular activities in the different phases of hormonal development in women, i.e. pre-, peri- and post-menopausal phases. To validate this approach, the simulated structures were analysed and the resulting morphometric indices (bone volume density (BV/TV), specific bone surface (BS/BV), trabecular thickness (Tb.Th), trabecular spacing, trabecular number (Tb.N), degree of anisotropy and structure model index) from one simulated age group were compared with experimental results gained from the corresponding age group of seven human biopsies. Müller found no significant changes between the parameters from the simulation and experimental groups. Figure 2.3a shows the simulated course of BV/TV over time for seven individual specimens, resembling the actual course in ageing humans. Additionally, the simulated bone structures provided a realistic appearance (figure 2.3b). The conclusion of this study was that applying the thinning procedure without incorporation of strain knowledge may reflect a case where the osteocytes no longer sense strain- or flow-related impulses.

Most of the three-dimensional approaches simulating bone loss were developed to provide functionality in the case of post-menopausal osteoporosis or age-related changes; however, they do not simulate the remodelling process of healthy, normal bone in response to increased (or decreased) loading conditions. To simulate the behaviour of normal bone in the presence of changing loads, these approaches may be extended. There also exist approaches that were originally developed to simulate normal bone behaviour in response to external loads. In the following paragraphs, two of the most promising three-dimensional approaches for bone remodelling will be described along with an extension of the model presented by Müller [60].

Adachi et al. [61] published a three-dimensional microstructural extension of their two-dimensional model [54] for trabecular surface adaptation to new loading directions, which is based on the local uniform stress hypothesis. This considers the non-uniformity in the local stress distribution on the trabecular surfaces as the driving force of bone adaptation, directing structural changes towards a structure in which the stresses are distributed more homogeneously. In the first step, an FE analysis is performed in order to determine the local stress σ_c at any particular location x_c.

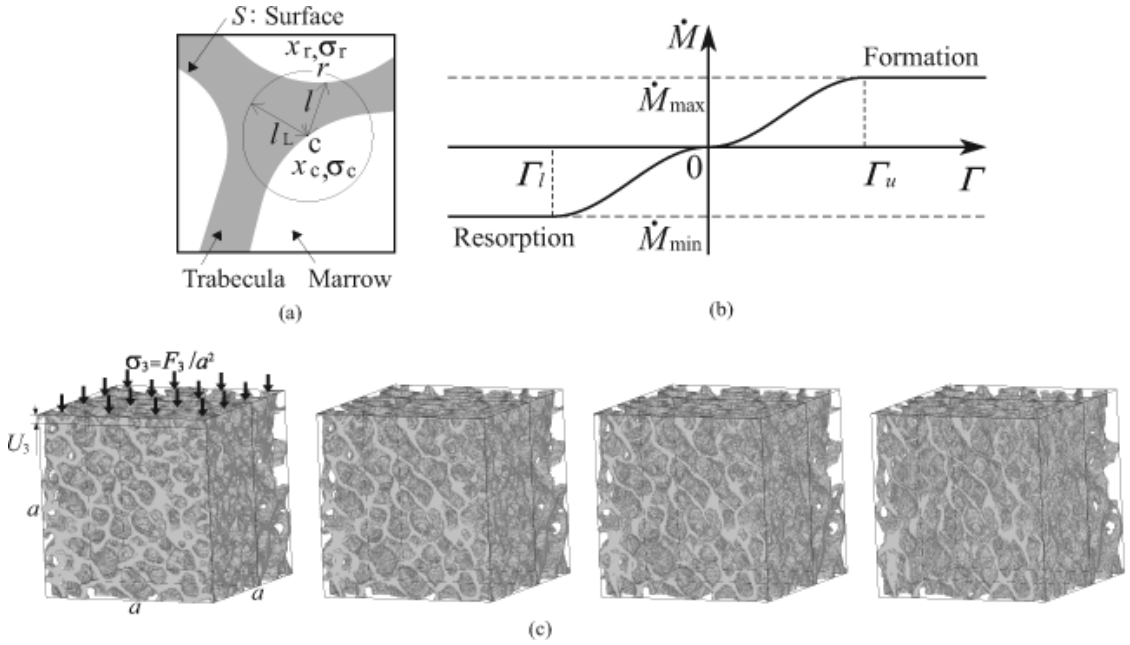

Figure 2.4: (a) The driving force of remodelling is defined as the relative difference between stress σ_c at the location x_c and σ_d determined by the weighted sum of the neighbouring stresses σ_r. (b) Remodelling rate equation M as a function of the driving force of remodelling Γ. (c) Changes in the three-dimensional architecture of a trabecular bone cube due to surface remodelling under compressive loading, starting from an initial voxel FE model based on a μCT digital image obtained from the canine distal femur. (Figure courtesy of Taiji Adachi.)

The non-uniformity of the stress distribution is then expressed by a function

$$\Gamma(x_c) = \ln(\frac{\sigma_c}{\sigma_d}), \tag{2.1}$$

where σ_d denotes the stress in the neighbourhood of σ_c and can be written as

$$\sigma_d = \frac{\int_S (w(l))\sigma_r dS}{\int_S (w(l))}, \tag{2.2}$$

where S is the trabecular surface and $w(l)$ is the weight function, considering the distance of a neighbouring point to the current one, e.g.

$$w(l) = 1 - \frac{l}{l_L} \tag{2.3}$$

as illustrated in figure 2.4a. The total amount of surface movement is determined by

substituting the value $\Gamma(x_c)$ into a function M as shown in figure 2.4b. The whole process is iterated until a remodelling equilibrium is attained. The authors validate their algorithm on cancellous bone (figure 2.4c) by comparing the morphometric indices of the artificially simulated structures with real *ex vivo* three-dimensional bone structures. This approach has not yet been used to investigate questions related to osteoporosis, although the potential might be there.

The second three-dimensional FE model for bone adaptation was proposed by Ruimerman et al. [62]. This model had been originally designed for growth and mechanical adaptation in trabecular bone. The authors follow the theory presented by Huiskes et al. [21]. According to this theory, osteoblasts form new bones relative to the mechanical signals they receive from osteocytes where the osteocytes emit signals according to the SED sensed in their environment. Osteoclasts are recruited by osteocyte apoptosis or micro-cracks, which occur in a spatially random manner. The coupling factor between osteoblast formation and osteoclast resorption is of a mechanical origin. Embedding these biological assumptions into mathematical equations is as follows. The total amount of bone formation at a particular location in the bone surface is given by

$$\frac{dm_{tot}(x,t)}{dt} = \frac{dm_{bl}(x,t)}{dt} - \frac{dm_{cl}(x,t)}{dt}, \tag{2.4}$$

where the amount of bone resorbed by osteoclasts is a function

$$\frac{dm_{cl}(x,t)}{dt} = -r_{cl}, \tag{2.5}$$

and the amount of bone formed by osteoblasts is

$$\frac{dm_{bl}(x,t)}{dt} = \tau(P(x,t) - k_{tr}), \tag{2.6}$$

where τ is the formation rate and k_{tr} is the formation threshold. The osteocyte stimulus function $P(x,t)$ is described by

$$P(x,t) = \sum_{i=1}^{N} f(x,x_i)\mu_i R(x_i,t), with f(x,x_i) = e^{-d(x,x_i)/D} \tag{2.7}$$

where $f(x,x_i)$ is the decay function representing the decrease in signal strength according to distance; μ is a mechanosensitivity factor; and $R(x_i,t)$ is the SED rate

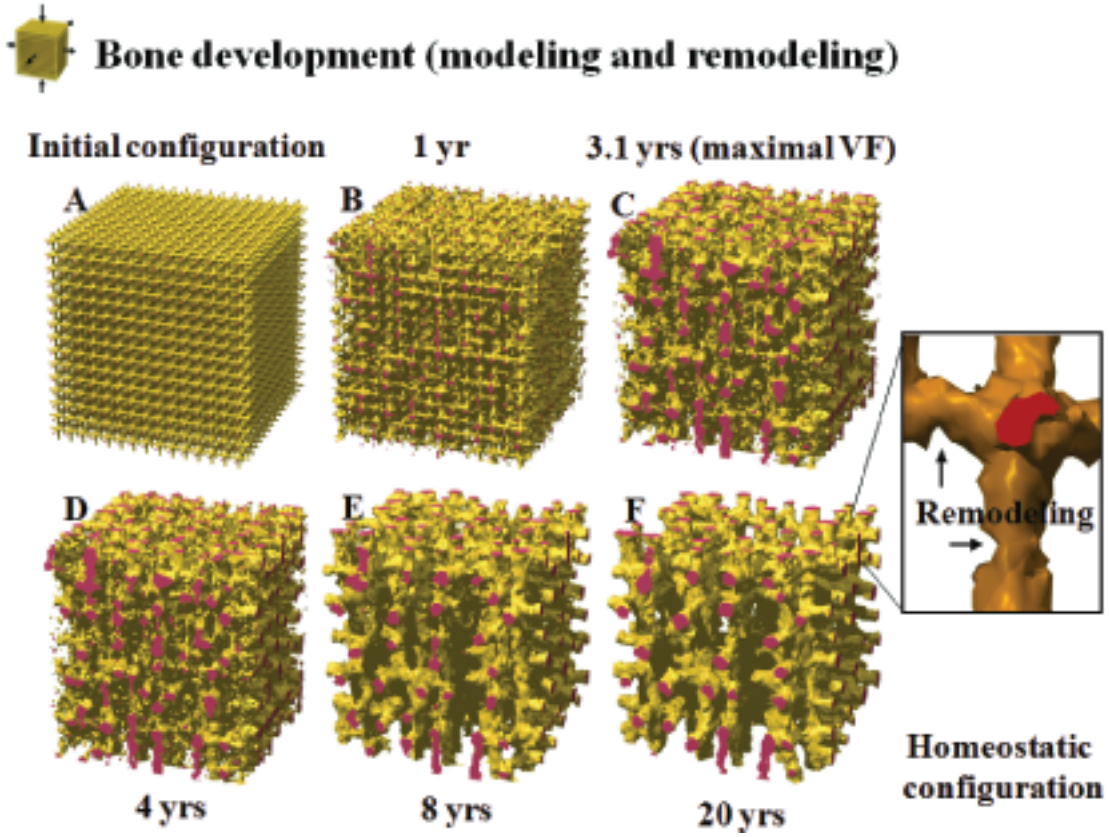

Figure 2.5: (A) Starting from a porous initial configuration representing bone in the post-mineralized foetal stage. During the simulation, (B−D) the structure developed in approximately 8 years into (E) a mature one. (F) From this point on the structure is maintained, while no more large architectural changes occur. Reprinted from Ruimerman et al. [62] with permission from Elsevier.

calculated by FE analysis.

Implementation of these equations resulted in a computer simulation model, which was validated using a $3 \times 3 \times 3$ mm^3 cube of artificially generated trabecular bone with respect to the following aspects. In a first study, Ruimerman et al. [62] successfully reproduced trabecular-like structures from a three-dimensional structured grid, which is illustrated in figure 2.5. Resulting morphometric indices resulted in reasonable dimensions; they also showed trabecular realignment after a change in the loading direction. In a second simulation series, alternative loading conditions were successfully applied to check whether the trabecular structure would adapt to a new equilibrium. Drastic reduction in loads resulted in disuse osteoporosis-like patterns with reduced bone mass and Tb.Th. In a third series, post-menopausal

osteoporosis was simulated by increasing the osteoclast activation frequency. This entailed an increase in the osteoclast resorption frequency due to the mathematical formulation of the theory, and an increase in osteoblast recruitment due to the underlying mechanics. Still, the simulation led to a new equilibrium with reduced Tb.Th and connectivity density and an increase in average SED. In a second study, Ruimerman et al. [63] compared alternatives with SED as the osteocytic stimulus, i.e. maximal principal strain and volumetric strain. The authors found by comparison with results from the literature that SED is the most likely signal sensed by osteocytes. Furthermore, they found that oestrogen deficiency after menopause can only be successfully simulated by assuming that oestrogen inhibits osteoclast but not both osteoclast and osteoblast activities under normal conditions. The novelty of this theory was that it explained the effects of mechanical forces on trabecular-bone growth, maintenance and adaptation by relating mechanical stimuli in the bone matrix to assumed expressions in the cells involved in bone metabolism [62]. The authors base their model on a number of assumptions that need still to be validated; however, the fact that they produce realistic results, speaks in favour of the model. One limitation might be that the volume of bone under investigation was relatively small, and thus it remains to be tested whether this model represents whole bone behaviour as well.

Extending and validating a model for bone adaptation

As *in silico* models provide an opportunity to test different hypotheses, this section gives an example of how simulations can be used to further our understanding of the biological behaviour of bone in the presence of external loading.

In silico approaches should, in general, be able to reflect as many physiological and pathological situations as possible. Here, SIBA as presented by Müller [60] was adapted in order to test the hypothesis that bone adaptation could be modelled by knowing the applied load only, without resolving the microstructural stresses and strains. This hypothesis was investigated by comparing the results of the simulation with real cross-sectional animal data gained from an experimental loading model, which was established to investigate the behaviour of bone in response to superphysiological loads. More details with respect to this model can be found elsewhere [64]. Briefly, the fifth caudal vertebrae (C5) of 4 groups of 10 C57BL/6 (B6), 12-week-old, female mice were loaded *in vivo* with amplitudes of 0 (control), 2, 4 and 8 N,

respectively, using a mechanical loading device (3000 cycles, 10 Hz, three times a week for four weeks). This treatment resulted in a substantial increase in BV/TV and other structural parameters for the different loading groups. The solid line in figure 2.6a illustrates the increase in BV/TV of the experiment.

With respect to the simulations, the Müller algorithm for bone loss [60] was used in such a way that binary input structures were blurred by applying the Gaussian filter and, in contrast to the original approach, a low subsequent threshold was chosen to simulate bone formation instead of bone loss. In order to account for direction-

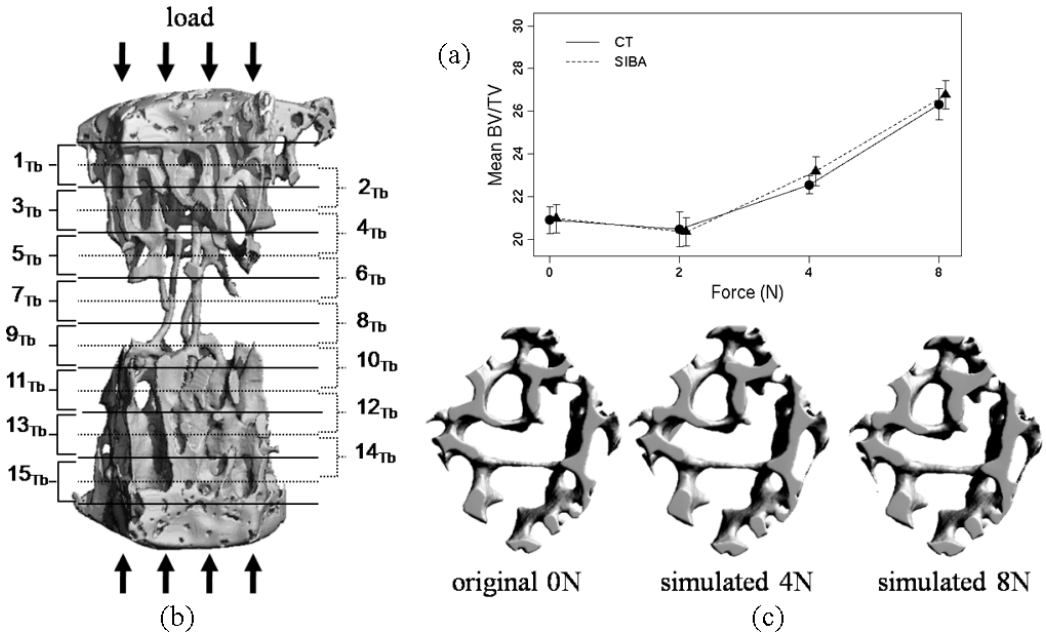

Figure 2.6: (a) Experimental (CT, solid line) and simulated (SIBA, dashed line) increase in BV/TV due to cyclic loading of murine trabecular C5 vertebrae for different loads applied and simulated, respectively. (b) Regional analysis by dividing the trabecular compartment into 15 overlapping subregions. (c) One subregion as computed from the simulations of mechanical loading with 4 N and 8 N loads. The original 0 N sample was used as the starting structure.

ality of the applied mechanical forces (in the axial direction of the vertebrae), the three-dimensional Gaussian filter kernel was compressed in the loading direction. The choice of the threshold and the size and extent of the Gaussian filter were obtained by optimally matching the simulated change in global mean BV/TV to the

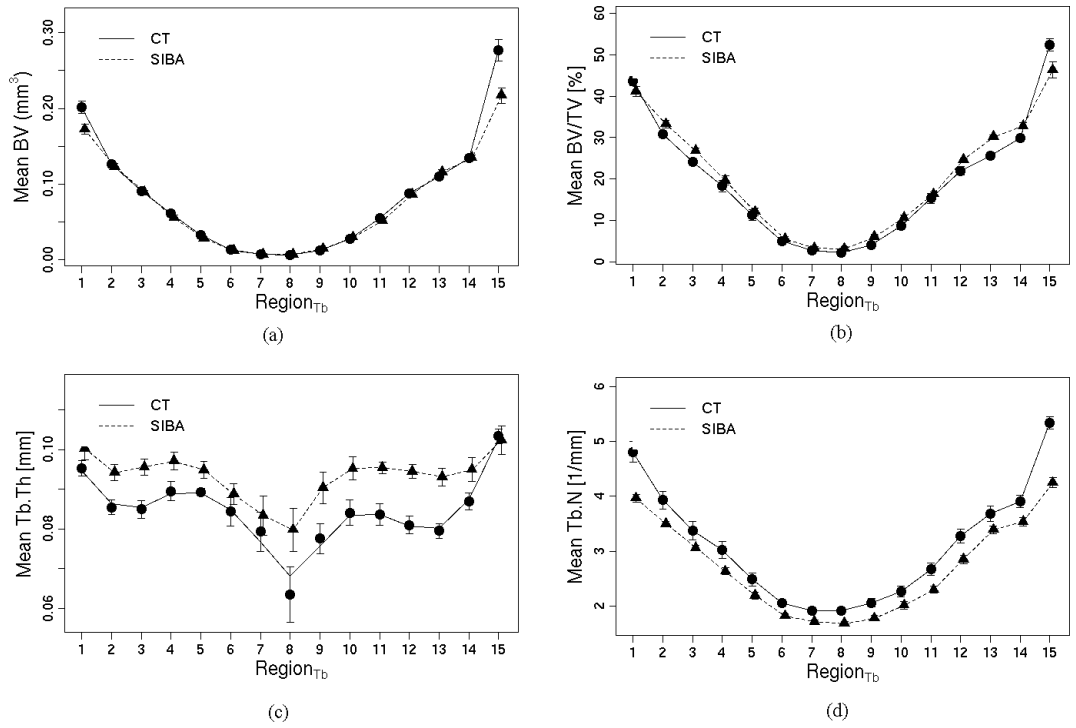

Figure 2.7: Regional analysis between experimental (CT, solid line) and simulated (SIBA, dashed line) structures of (a) BV, (b) BV/TV, (c) Tb.Th and (d) Tb.N.

experimental change in global mean BV/TV for all loading groups, as is illustrated in figure 2.6a. To compare the simulated datasets with *in vivo* loading datasets and to investigate how bone formation varied within the bone, the trabecular compartments of the caudal mouse vertebrae were divided into 15 subregions (figure 2.6b). Figure 2.6c shows simulated changes in the fifth subregion for loads of 4 and 8 N when using the 0 N group as input datasets. Quantitative results of the regional variations between the *in vivo* and the *in silico* datasets are presented in figure 2.7. As a first result, the experimental and simulated curves of BV (figure 2.7a) and BV/TV (figure 2.7b) through the regions seem to match very well. Thus, the agreement between the *in vivo* and *in silico* datasets strengthened the hypothesis that knowledge about the global applied load may be sufficient to simulate bone adaptation due to mechanical loading.

However, the simulated structures overestimated and underestimated Tb.Th (figure 2.7c) and Tb.N (figure 2.7d), respectively. An explanation of this second result may be given through the nature of the applied algorithm, which was designed for a uniform trabecular thickening and not for a structural reorganization including the

creation of new trabeculae. Thus, the experimental increase in bone mass coming from structural reorganization was simply compensated by an increase in Tb.Th.

The fact that differences in local architecture could be noted between experiment and prediction manifests a current limitation of the model and demonstrates the importance of incorporating local regulation mechanisms of mechanical bone adaptation. Nevertheless, the simulations revealed that bone adaptation in response to mechanical loading is more complicated than uniform trabecular thickening. Instead, structural reorganization including the formation of new trabeculae seems to take place. Little is known, however, about how new trabeculae are formed under physiological conditions. To tackle this question, it would be necessary to perform longitudinal studies where *in vivo* bone adaptation can be tracked in individual mice over time.

Multi-cell-level approaches

If we follow a hierarchical multi-scale approach, the next level of simulation would include cell-level and single-cell approaches. This section and the next section therefore give a short overview of current state of the art of *in silico* simulation models on cellular and single-cell levels.

At the tissue level, the localized activities of osteoclasts, osteoblasts and osteocytes are often implicitly merged to a scalar value, denoting bone formation or removal at a particular location. However, for a deeper understanding of how these cell types interact with each other to eventually renew or adapt the bone structure at the surface of a particular trabecula, it is important to depict these processes at a higher scale of resolution.

One of the first studies on a microscopic, but still multi-cellular, level was presented by Smit & Burger [65]. They built an FE model of a resorption cavity in a trabecula by means of a sphere residing in a simplified solid cylinder. Loading this FE model along the trabecular orientation resulted in elevated strain levels at the bottom of the resorption cavity. At the cavity border, however, low strains appeared in the direction of loading, while high strains occurred perpendicular to loading. From a biological point of view and under the assumption that osteoclasts remove bone at areas of low strain, this would mean that lateral osteoclastic excavation is inhibited, while remodelling in the longitudinal direction will proceed further. Although the authors assumed an idealized geometric structure and sim-

plified homogeneous material properties, these findings support the hypothesis that BMU coupling is regulated by strains.

McNamara et al. [30] extended this study by examining the strain distribution around a resorption lacuna by means of two-dimensional FE models of real μCT-scanned trabeculae. Their results supported the findings from Smit & Burger [65], and further disclosed that the magnitudes of the peak strains in trabeculae are sufficiently high to initiate micro-damage and propagate to structures local to the resorption site. In another study, McNamara & Prendergast [66] investigated whether an increased depth of resorption cavity, as occurs in osteoporosis, leads to a strain concentration capable of creating more micro-damage, such that osteoclasts 'chase' newly formed damage, leading to perforation. In this study, the mechanosensors are assumed to be the surface cells, i.e. osteoblasts and bone-lining cells. The results favour the concept of a critical cavity depth; larger cavities inevitably would lead to the loss of whole trabeculae. However, one limitation of this model might be that the sensing cells are located only on the trabecular surface and therefore will not be able to sense micro-damage occurring in areas deeply embedded in the bone matrix. In a subsequent study [67], it was hypothesized that bone remodelling may be regulated by signals due to both strain and microdamage. The authors concluded from their results that an algorithm of strain-adaptive remodelling below a critical damage threshold and damage-adaptive remodelling above the critical amount presents the best computational algorithm for simulation of bone remodelling and repair. With respect to the sensing cells, it was found that with osteocyte mechanosensation, damaged surface bone tissue was not completely removed nor was refilling of resorption cavities predicted. However, in a separate study that was mentioned in their paper, only the osteocyte sensor model, but not the bone lining cell model, was able to communicate a signal to the bone surface, which originated from damaged tissue residing in the core of trabeculae.

Mulvihill et al. [68] enhanced the above-proposed two-dimensional algorithms using a three-dimensional FE model of a cylindrical trabecular strut and found that, without restriction of osteoblast attachment at the resorption cavity, unusual bone formation behaviour was observed. At the border of the cavity, strain magnitudes were sufficient to form bone but not high enough to create micro-damage. These findings are in conflict with the suggestions made by Smit & Burger [65].

Another *in silico* approach investigating the remodelling process at a multicellular

level for both trabecular and cortical bone was presented by van Oers et al. [69]. They propose a unifying theory for osteonal and hemi-osteonal remodelling in a two-dimensional computer simulation model where osteoclasts are modelled explicitly using the Potts model for cell simulation [70]. Here, the authors follow the theory proposed by Huiskes et al. [21] and Ruimerman et al. [62] with enhanced attention to the osteoclast resorption function. It is postulated that osteoclast activity is inhibited by osteocytes instead of presuming random resorption along the bone surface. Osteoblasts only form bone at sites where the osteocyte signal exceeds a certain threshold for a particular period of time as occurring at the borders of a trabecular resorption cavity. In their study, it is found that stress concentrations around resorption cavities prevent osteoclasts from perforating trabeculae, and osteoblasts are recruited to refill resorption cavities.

Single-cell-level approaches

In an effort to gain a better understanding of how mechanoregulation in bone remodelling works, it could be of special interest to investigate more questions on the level of a single cell. In particular, osteocytes are widely assumed to play the role of mechanosensors in the bone matrix, based on the strain magnitude they perceive and thus they could play a pivotal role in bone adaptation. Since the shape of an osteocyte lacuna influences the mechanical strain perceived by the osteocyte, a study was performed by McCreadie et al. [71] to quantify the size and shape of osteocyte lacunae in trabecular bone near a typical fracture site. In their study, osteocytes are for the first time quantified in three dimensions, which was made possible by confocal microscopy images. In addition to the quantification of size and shape of the osteocytes, they proposed an ellipsoid as an appropriate geometric structure for an osteocyte lacuna. However, this study still neglected the interconnecting canaliculi. Bonivtch et al. [72] used the proposed geometric specification to perform a three-dimensional FE analysis on this structure, in order to investigate the microstructural response to the imposed macroscopic apparent strains. They developed a parametric model consisting of the osteocyte lacuna, a region of perilacunar tissue, canaliculi and the surrounding bone tissue. It was found that the maximum perilacunar tissue strain increased in a model without canaliculi by a factor of 1.5 and by a factor of 3.1 in a model incorporating the presence of canaliculi. The maximum strain always occurred at sites where the canaliculi entered the lacuna. Furthermore, it was found

that the predicted maximum perilacunar strain increased with a decrease in perilacunar tissue modulus and decreased with an increase in the tissue modulus, which entailed an increase in canalicular diameter. The authors concluded from this result that osteocytes may be able to change their local environment, i.e. the perilacunar tissue modulus. Whether the canalicular diameter indeed changes with an increase in tissue modulus remains to be verified experimentally.

A recent study [73] has examined quantitatively, based on earlier findings [74, 75], the effect of geometric and dimensional idealization on prediction of the mechanical signals imparted by fluid drag to cell surfaces. The study revealed that the physiologic geometry *per se* has a profound influence on the nano-scale flow regimes in bone, and that this influence imparts locally to cells through load-induced fluid flow.

McGarry & Prendergast [76] went one level further and tried to simulate an adherent general eukaryotic cell by an FE modelling approach. Applying forces in the pico-newton range to the model membrane nodes suggested a key role for the cytoskeleton in determining cellular stiffness. According to the authors, such a model could be useful when computing cellular structural behaviour in response to various *in vitro* mechanical stimuli, such as fluid flow or substrate strain to simulate mechanobiological processes. In any case, the simulation of mechanobiological and nanostructural coherences of cells and their properties, although not yet accounting for real bone adaptation but more focusing on micromechanics, has great potential to improve our understanding of the cellular interrelationships at a nanostructural level.

2.4.4 Conclusion and outlook

This paper gave an overview of current simulation models for macro-, meso- and nano-scales, and presented an extension of one of the existing simulation algorithms for trabecular bone remodelling. During the last few decades, more and more insights have been gained into the processes involved in bone adaptation, but also more and more questions have arisen regarding the underlying biochemical and mechanobiological pathways. With the availability of different imaging techniques to visualize and quantify different aspects of bone remodelling, we can create and validate simulation tools to reflect the behaviour of the human body at organ level, micro-level and single-cell level. The models presented here, which simulate the mechanical behaviour of bone at the organ level, represent bone by using its apparent

material properties and apparent mechanical strength. This plays a significant role in the understanding of the stability of our bones within the body. By neglecting the trabecular microstructure, however, these models can no longer be used when questions related to the microstructural arrangement of trabeculae arise. Knowledge and mathematical theories established at organ level were therefore developed to account for the trabecular microstructure.

A current limitation of the proposed microstructural models is that they are only validated qualitatively via visual inspection and quantitatively by comparing the simulation with cross-sectional experimental studies, due to a lack of *in vivo* imaging techniques. Furthermore, some of these approaches are based on artificially generated input structures, and thus it would need to be proven that the governing principles used in these artificial grids can be transferred to actual bone microarchitectures. The application of these models to real bone and their validation after several simulation steps is the next step towards a better understanding of the underlying biological processes involved in bone adaptation.

The extension of the bone loss simulating algorithm also includes bone adaptive mechanisms that incorporate actual bone architectures from *in vivo* loading studies, and shows that overall changes in bone mass can be predicted with knowledge of the applied load only. However, differences in local architecture could be noted between experiment and prediction, thereby demonstrating the importance of incorporating local regulation mechanisms of mechanical adaptation, i.e. the formation of new trabeculae. Some of the presented simulation approaches account implicitly for reorganization by the growth of new trabeculae, i.e. by tunnelling of an existing structure. It is, however, not clear whether new trabeculae really arise owing to tunnelling of existing structures or rather by bridging between existing trabeculae. The only way to check the exact mechanism is *in vivo* imaging of the bone microstructure. These imaging techniques are now available and allow tracking of microstructural changes over time. Thus, they would facilitate the vigorous validation and comparison of competing theories. In that sense, *in vivo* imaging provides new forms of evaluation, i.e. the validation of a model with respect to its ability to predict trabecular changes over time both spatially and temporally.

Nevertheless, caution must still be exercised when attempting to validate, particularly when such models use parameters to represent certain mechanisms at the nano-scale, which cannot be accurately quantified by experimental means. Further-

more, the issue of validation becomes more complicated in more complex models employing a large number of parameters: as the number of parameters increases so does the number of experiments required to verify the model's applicability to scientific questions.

Despite an inherent degree of uncertainty, the nano- to macro-scale models discussed here have great value from a speculative point of view, as during the development process, they have uncovered many biological questions and can thus guide research accordingly. Further research will then, in turn, provide invaluable feedback for the development of more sophisticated and more reliable hierarchical models, forming an iterative process that will progressively further our understanding of bone adaptation. This process could eventually lead to the development of novel strategies for the management of bone diseases such as osteoporosis.

Acknowledgement

The authors acknowledge funding from the Swiss National Science Foundation (PP 104317/1).

References

[1] J. Wolff. *Das Gesetz der Transformation der Knochen (The Law of Bone Remodelling)*. Springer-Verlag, Berlin, Germany, 1892.

[2] S. C. White, C. A. Berry, and R. R. Hessberg. Effects of weightlessness on astronauts–a summary. *Life Sci Space Res*, 10:47–55, 1972.

[3] G. D. Whedon, L. Lutwak, P. Rambaut, M. Whittle, C. Leach, J. Reid, and M. Smith. Mineral and nitrogen metabolic studies on skylab flights and comparison with effects of earth long-term recumbency. *Life Sci Space Res*, 14:119–27, 1976.

[4] G. D. Whedon, L. Lutwak, P. C. Rambaut, M. W. Whittle, J. Reid, M. C. Smith, C. Leach, C. R. Stadler, and D. D. Sanford. Mineral and nitrogen balance study observations: the second manned skylab mission. *Aviat Space Environ Med*, 47(4):391–6, 1976.

[5] P. C. Rambaut and R. S. Johnston. Prolonged weightlessness and calcium loss in man. *Acta Astronaut*, 6(9):1113–22, 1979.

[6] C. L. Donaldson, S. B. Hulley, J. M. Vogel, R. S. Hattner, J. H. Bayers, and D. E. McMillan. Effect of prolonged bed rest on bone mineral. *Metabolism*, 19(12):1071–84, 1970.

[7] V. Pavosky. Calcium metabolism during immobilization of the patient. *Zdrav Prac*, 27(4):suppl 15–21, 1977.

[8] G. P. Stupakov, A. I. Volozhin, and I. E. Didenko. Strength and mineral composition of human vertebrae during prolonged bed rest. *Biull Eksp Biol Med*, 91(5):544–6, 1981.

[9] B. L. Riggs and L. J. Melton 3rd. The worldwide problem of osteoporosis: insights afforded by epidemiology. *Bone*, 17(5 Suppl):505–511, 1995.

[10] J. A. Kanis and O. Johnell. Requirements for DXA for the management of osteoporosis in Europe. *Osteoporos Int*, 16(3):229–238, 2005.

[11] H. M. Frost. Skeletal structural adaptations to mechanical usage (satmu): 1. redefining wolff's law: the bone modeling problem. *Anat Rec*, 226(4):403–13, 1990.

[12] H. M. Frost. Skeletal structural adaptations to mechanical usage (satmu): 2. redefining wolff's law: the remodeling problem. *Anat Rec*, 226(4):414–22, 1990.

[13] L Geris, J. Vander Sloten, and H Van Oosterwyyck. In silico biology of bone modeling and remodeling - regeneration. *Philosophical Transactions of the Royal Society A*, 2009.

[14] S. C. Cowin. The significance of bone microstructure in mechanotransduction. *Journal of Biomechanics*, 40(Supplement 1):S105–S109, 2007.

[15] J. Klein-Nulend, A. van der Plas, C.M. Semeins, N.E. Ajubi, J.A. Frangos, P.J. Nijweide, and E.H. Burger. Sensitivity of osteocytes to biomechanical stress in vitro. *FASEB J*, 9(5):441–445, 1995.

[16] J. Klein-Nulend, R. G. Bacabac, and M. G. Mullender. Mechanobiology of bone tissue. *Pathol Biol (Paris)*, 53(10):576–80, 2005.

[17] M. G. Mullender and R. Huiskes. Osteocytes and bone lining cells: which are the best candidates for mechano-sensors in cancellous bone? *Bone*, 20(6):527–32, 1997.

[18] E. H. Burger and J. Klein-Nulend. Mechanotransduction in bone–role of the lacuno-canalicular network. *Faseb J*, 13 Suppl:S101–12, 1999.

[19] M. Mullender, A. J. El Haj, Y. Yang, M. A. van Duin, E. H. Burger, and J. Klein-Nulend. Mechanotransduction of bone cells in vitro: mechanobiology of bone tissue. *Med Biol Eng Comput*, 42(1):14–21, 2004.

[20] R. Huiskes, H. Weinans, H. J. Grootenboer, M. Dalstra, B. Fudala, and T. J. Slooff. Adaptive bone-remodeling theory applied to prosthetic-design analysis. *J Biomech*, 20(11-12):1135–50, 1987.

[21] R. Huiskes, R. Ruimerman, G. H. van Lenthe, and J. D. Janssen. Effects of mechanical forces on maintenance and adaptation of form in trabecular bone. *Nature*, 405(6787):704–706, 2000.

[22] Y. Han, S. C. Cowin, M. B. Schaffler, and S. Weinbaum. Mechanotransduction and strain amplification in osteocyte cell processes. *Proc Natl Acad Sci U S A*, 101(47):16689–94, 2004.

[23] P. J. Prendergast and D. Taylor. Prediction of bone adaptation using damage accumulation. *J Biomech*, 27(8):1067–76, 1994.

[24] M. L. Knothe Tate, U. Knothe, and P. Niederer. Experimental elucidation of mechanical load-induced fluid flow and its potential role in bone metabolism and functional adaptation. *Am J Med Sci*, 316(3):189–95, 1998.

[25] D. P. Nicolella, D. E. Moravits, A. M. Gale, L. F. Bonewald, and J. Lankford. Osteocyte lacunae tissue strain in cortical bone. *J Biomech*, 39(9):1735–43, 2006.

[26] C. H. Turner, Y. Takano, I. Owan, and G. A. Murrell. Nitric oxide inhibitor l-name suppresses mechanically induced bone formation in rats. *Am J Physiol*, 270(4 Pt 1):E634–9, 1996.

[27] K. E. Armour, K. J. Armour, M. E. Gallagher, A. Godecke, M. H. Helfrich, D. M. Reid, and S. H. Ralston. Defective bone formation and anabolic response to exogenous estrogen in mice with targeted disruption of endothelial nitric oxide synthase. *Endocrinology*, 142(2):760–6, 2001.

[28] A. Samuels, M. J. Perry, R. L. Gibson, S. Colley, and J. H. Tobias. Role of endothelial nitric oxide synthase in estrogen-induced osteogenesis. *Bone*, 29(1):24–9, 2001.

[29] D. Vashishth, J. Koontz, S. J. Qiu, D. Lundin-Cannon, Y. N. Yeni, M. B. Schaffler, and D. P. Fyhrie. In vivo diffuse damage in human vertebral trabecular bone. *Bone*, 26(2):147–52, 2000.

[30] L. M. McNamara, J. C. Van der Linden, H. Weinans, and P. J. Prendergast. Stress-concentrating effect of resorption lacunae in trabecular bone. *J Biomech*, 39(4):734–41, 2006.

[31] M. G. Mullender, S. D. Tan, L. Vico, C. Alexandre, and J. Klein-Nulend. Differences in osteocyte density and bone histomorphometry between men and women and between healthy and osteoporotic subjects. *Calcif Tissue Int*, 77(5):291–6, 2005.

[32] D. P. Fyhrie and D. R. Carter. A unifying principle relating stress to trabecular bone morphology. *J Orthop Res*, 4(3):304–17, 1986.

[33] H. M. Frost. *The Laws of Bone Structure*. Charles C. Thomas, Springfield, 1964.

[34] S. C. Cowin. Mechanical modeling of the stress adaptation process in bone. *Calcif Tissue Int*, 36 Suppl 1:S98–103, 1984.

[35] J. Reeve. A stochastic analysis of iliac trabecular bone dynamics. *Clin Orthop Relat Res*, 213:264–78, 1986.

[36] T.D. Brown, D.R. Pedersen, M.L. Gray, R.A. Brand, and C.T. Rubin. Toward an identification of mechanical parameters initiating periosteal remodeling: a combined experimental and analytic approach. *J Biomech*, 23(9):893–905, 1990.

[37] R. B. Martin. On the significance of remodeling space and activation rate changes in bone remodeling. *Bone*, 12(6):391–400, 1991.

[38] J. S. Thomsen, L. Mosekilde, and E. Mosekilde. Quantification of remodeling parameter sensitivity–assessed by a computer simulation model. *Bone*, 19(5):505–11, 1996.

[39] T. Adachi, Y. Tomita, and M. Tanaka. Computational simulation of deformation behavior of 2d-lattice continuum. *International Journal of Mechanical Sciences*, 40(9):857–866, 1998.

[40] C. M. Langton, T. J. Haire, P. S. Ganney, C. A. Dobson, and M. J. Fagan. Dynamic stochastic simulation of cancellous bone resorption. *Bone*, 22(4):375–80, 1998.

[41] C. J. Hernandez, G. S. Beaupre, and D. R. Carter. A model of mechanobiologic and metabolic influences on bone adaptation. *J Rehabil Res Dev*, 37(2):235–44, 2000.

[42] S. C. Cowin. Bone stress adaptation models. *J Biomech Eng*, 115(4B):528–33, 1993.

[43] C. R. Jacobs. The mechanobiology of cancellous bone structural adaptation. *J Rehabil Res Dev*, 37(2):209–16, 2000.

[44] RT Hart. Bone modeling and remodeling: theories and computation. *Bone Mechanics Handbook, 2nd edition,*, CRC Press, Boca Raton, Chapter 31:1–42, 2001.

[45] D. R. Carter and W. C. Hayes. Bone compressive strength: the influence of density and strain rate. *Science*, 194(4270):1174–6, 1976.

[46] G. S. Beaupre, T. E. Orr, and D. R. Carter. An approach for time-dependent bone modeling and remodeling–theoretical development. *J Orthop Res*, 8(5):651–61, 1990.

[47] H. Weinans, R. Huiskes, and H. J. Grootenboer. The behavior of adaptive bone-remodeling simulation models. *J Biomech*, 25(12):1425–41, 1992.

[48] B. Van Rietbergen, R. Huiskes, H. Weinans, D. R. Sumner, T. M. Turner, and J. O. Galante. ESB Research Award 1992. The mechanism of bone remodeling and resorption around press-fitted THA stems. *J Biomech*, 26(4-5):369–382, 1993.

[49] J. S. Thomsen, L. Mosekilde, R. W. Boyce, and E. Mosekilde. Stochastic simulation of vertebral trabecular bone remodeling. *Bone*, 15(6):655–66, 1994.

[50] L. A. Feldkamp, S. A. Goldstein, A. M. Parfitt, G. Jesion, and M. Kleerekoper. The direct examination of three-dimensional bone architecture in vitro by computed tomography. *J Bone Miner Res*, 4(1):3–11, 1989.

[51] M. G. Mullender, R. Huiskes, and H. Weinans. A physiological approach to the simulation of bone remodeling as a self-organizational control process. *J Biomech*, 27(11):1389–94, 1994.

[52] T. S. Smith, R. B. Martin, M. Hubbard, and B. K. Bay. Surface remodeling of trabecular bone using a tissue level model. *J Orthop Res*, 15(4):593–600, 1997.

[53] M. Zidi and S. Ramtani. Bone remodeling theory applied to the study of n unit-elements model. *J Biomech*, 32(7):743–7, 1999.

[54] T. Adachi, Y. Tomita, H. Sakaue, and M. Tanaka. Simulation of trabecular surface remodeling based on local stress nonuniformity. *The Japan Society of Mechanical Engineers*, 40(4):782–792, 1997.

[55] Z. Tabor and E. Rokita. Stochastic simulations of remodeling applied to a two-dimensional trabecular bone structure. *Bone*, 31(3):413–7, 2002.

[56] S. Tayyar, P. S. Weinhold, R. A. Butler, J. C. Woodard, L. D. Zardiackas, K. R. St John, J. M. Bledsoe, and J. A. Gilbert. Computer simulation of trabecular remodeling using a simplified structural model. *Bone*, 25(6):733–9, 1999.

[57] X. E. Guo, M. J. Eichler, E. Takai, and C. H. Kim. Quantification of a rat tail vertebra model for trabecular bone adaptation studies. *J Biomech*, 35(3):363–8, 2002.

[58] J. C. van der Linden, J. A. Verhaar, and H. Weinans. A three-dimensional simulation of age-related remodeling in trabecular bone. *J Bone Miner Res*, 16(4):688–96, 2001.

[59] J. C. van der Linden, J. A. Verhaar, H. A. Pols, and H. Weinans. A simulation model at trabecular level to predict effects of antiresorptive treatment after menopause. *Calcif Tissue Int*, 73(6):537–44, 2003.

[60] R. Müller. Long-term prediction of three-dimensional bone architecture in simulations of pre-, peri- and post-menopausal microstructural bone remodeling. *Osteoporos Int*, 16 Suppl 2:S25–35, 2005.

[61] T. Adachi, K. Tsubota, Y. Tomita, and S. J. Hollister. Trabecular surface remodeling simulation for cancellous bone using microstructural voxel finite element models. *J Biomech Eng*, 123(5):403–9, 2001.

[62] R. Ruimerman, P. Hilbers, B. van Rietbergen, and R. Huiskes. A theoretical framework for strain-related trabecular bone maintenance and adaptation. *J Biomech*, 38(4):931–41, 2005.

[63] R. Ruimerman, B. Van Rietbergen, P. Hilbers, and R. Huiskes. The effects of trabecular-bone loading variables on the surface signaling potential for bone remodeling and adaptation. *Ann Biomed Eng*, 33(1):71–8, 2005.

[64] D. J. Webster, P. L. Morley, G. H. van Lenthe, and R. Müller. A novel in vivo mouse model for mechanically stimulated bone adaptation - a combined experimental and computational validation study. *Comput Methods Biomech Biomed Engin*, 11(5):435–441, 2008.

[65] T. H. Smit and E. H. Burger. Is bmu-coupling a strain-regulated phenomenon? a finite element analysis. *J Bone Miner Res*, 15(2):301–7, 2000.

[66] L. M. McNamara and P. J. Prendergast. Perforation of cancellous bone trabeculae by damage-stimulated remodelling at resorption pits: a computational analysis. *Eur J Morphol*, 42(1-2):99–109, 2005.

[67] L. M. McNamara and P. J. Prendergast. Bone remodelling algorithms incorporating both strain and microdamage stimuli. *J Biomech*, 40(6):1381–91, 2007.

[68] B. M. Mulvihill, L. M. McNamara, and P. J. Prendergast. Should biological factors be considered when applying mechano-regulation algorithms to finite element models? *Proceedings of the 2007 Summer Workshop of the European Society of Biomechanics*, pages 114–115, 2007.

[69] R. F. van Oers, R. Ruimerman, E. Tanck, P. A. Hilbers, and R. Huiskes. A unified theory for osteonal and hemi-osteonal remodeling. *Bone*, 42(2), 2008.

[70] J. A. Glazier and F. Graner. Simulation of the differential adhesion driven rearrangement of biological cells. *Phys Rev E Stat Phys Plasmas Fluids Relat Interdiscip Topics*, 47(3):2128–2154, 1993.

[71] B. R. McCreadie, S. J. Hollister, M. B. Schaffler, and S. A. Goldstein. Osteocyte lacuna size and shape in women with and without osteoporotic fracture. *J Biomech*, 37(4):563–72, 2004.

[72] A. R. Bonivtch, L. F. Bonewald, and D. P. Nicolella. Tissue strain amplification at the osteocyte lacuna: a microstructural finite element analysis. *J Biomech*, 40(10):2199–206, 2007.

[73] E. J. Anderson and M. L. Knothe Tate. Idealization of pericellular fluid space geometry and dimension results in a profound underprediction of nano-microscale stresses imparted by fluid drag on osteocytes. *J Biomech*, 41(8):1736–46, 2008.

[74] A.E. Tami, P. Nasser, O. Verborgt, M.B. Schaffler, and M.L. Knothe Tate. The role of interstitial fluid flow in the remodeling response to fatigue loading. *J Bone Miner Res*, 17(11):2030–2037, 2002.

[75] R. Steck and M. L. Knothe Tate. In silico stochastic network models that emulate the molecular sieving characteristics of bone. *Ann Biomed Eng*, 33(1):87–94, 2005.

[76] J. G. McGarry and P. J. Prendergast. A three-dimensional finite element model of an adherent eukaryotic cell. *Eur Cell Mater*, 7:27–33; discussion 33–4, 2004.

Chapter 3

Dynamic bone morphometry from time-lapsed imaging

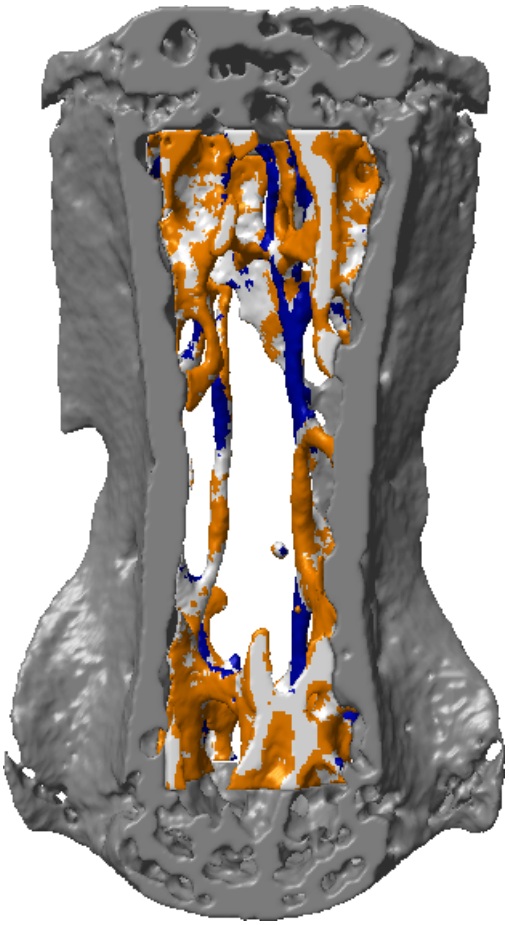

3.1 Quantitative outcomes after image registration of micro-computed tomography scans critically depend on interpolation technique

Friederike A. Schulte[1], Floor M. Lambers[1], Thomas L. Mueller[1], Martin Stauber[2] and Ralph Müller[1]

[1]Institute for Biomechanics, ETH Zurich, Zurich, Switzerland

Abstract:

Time-lapsed *in vivo* micro-computed tomography is a powerful tool to analyze longitudinal changes in the bone micro-architecture. Registration can overcome problems associated with spatial misalignment between scans; however, it requires image interpolation which might affect the outcome of a subsequent bone morphometric analysis. The impact of the interpolation error itself, though, has not been quantified to date. Therefore, the purpose of this study was to elaborate the effect of different interpolator schemes (nearest neighbor, tri-linear and B-spline) on bone morphometric indices. The lowest interpolation error was found using B-splines (1.4%), with no significant differences between reference values and values gained from interpolated images. Furthermore, the interpolation error was significantly higher when the registration was performed on binary instead of gray-scale images ($p<0.05$). These findings suggest that the evaluation of bone morphometry on interpolated images is accurate, at least when B-spline approximation is used for both the final transformation and during registration.

Keywords:

image registration; interpolation; post-processing; bone morphometry; *in vivo* micro-computed tomography

3.1.1 Introduction

Time-lapsed *in vivo* micro-computed tomography (micro-CT) is a powerful technique for monitoring longitudinal changes in the bone micro-architecture over time in single subjects. Its introduction for both human [1–3] and animal [4–6] research a few years ago has improved the understanding of bone modeling and remodeling in physiological and disease states considerably. With regard to the evaluation of *in vivo* data, it has been usual to apply the conventional morphometric measures developed for *in vitro* micro-CT data [7–11] in a first step. The advantage of longitudinal *in vivo* imaging is that it first minimizes the risk of inter-group changes being masked by intra-group variability. Second, it allows reduction of the number of subjects required per group.

It has been shown that the re-alignment of follow-up scans improves the reproducibility of bone morphometric indices in both animals [12] and humans [13]. This processing step ensures that the exact same region of interest can be evaluated in all images, although the time-lapsed scans may have been taken at slightly different positions and orientations. The mathematical tool required to re-align time-lapsed data sets is called rigid image registration. It searches iteratively for the best transformation matrix with which one image can be re-oriented so that it fits optimally onto another image. The registration procedure requires interpolation of the original voxel intensities to produce a new, re-oriented image. Common interpolation methods ranging from low to high computational complexity are nearest neighbor interpolation, tri-linear interpolation and B-spline approximation [14].

As the goal of the registration algorithm is to align the shape of the bone in a baseline and a follow-up scan, slight deviations in the texture information are not crucial for the alignment itself. However, if the re-aligned images are subsequently used for bone morphometric analysis, it is paramount to preserve as much as the original structural information in the image [15]. There is a possibility of applying the resulting transformation inversely onto the trabecular mask, using the original gray-scale images in order to avoid any interpolation effects on bone morphometric indices [12]. However, in some processing setups, the evaluation on re-aligned images may be considered advantageous. To date it is not clear if, and to what amount, interpolation affects the resulting bone morphometric indices. Furthermore, there are different possibilities for the point at which the required transformation can enter in the post-processing chain. This choice of entry might also influence the resulting

bone morphometric indices.

Thus, to investigate the registration error on bone morphometric indices, the aim of this study was to assess the effects of three different interpolators on micro-CT derived trabecular bone morphometric indices and to investigate at which stage in the post-processing order the transformation should be applied. To accomplish this aim, we used an animal model in which the 6^{th} caudal vertebra of C57BL/6 mice had been exposed to mechanical loading [16]. After completion of the experiment, the dissected vertebrae were scanned *ex vivo* in a repeated fashion. For the purpose of this study, it was hypothesized that different positionings or orientations, and their correction via image registration, would not show any effect on the outcome of a subsequent bone structural analysis.

3.1.2 Methods

Animals

The test data comprised 40 repeated micro-CT scans of the 6^{th} caudal vertebra of eight 19-week-old C57/B6 mice (RCC; Füllinsdorf, Switzerland), each scanned five times repetitively *ex vivo*. The entity of the samples was taken from a larger study in which mechanical loading of 0 N (control) or 8 N (loading) was applied *in vivo* to the 6^{th} caudal vertebra over a period of four weeks [16]. All *in vivo* animal procedures were approved by the local animal care and use committee (Kantonales Veterinäramt Zürich, Zürich, Switzerland). After completion of the *in vivo* experiment, the animals were sacrificed and the 6^{th} caudal vertebra was dissected. In the present study, three of the eight measured vertebrae belonged to the control group and five to the loading group.

Imaging

Each bone was scanned five times *in vitro* in an *in vivo* micro-CT scanner (vivaCT 40, Scanco Medical, Brüttisellen, Switzerland) with repositioning between the scans, with the same scanning protocol as the *in vivo* study (50 kVp, 200 ms integration time, no frame averaging). The nominal isotropic image resolution amounted to 10.5 μm. Image dimensions were $300 \times 300 \times 422$ voxels, i.e. $3.15 \times 3.15 \times 4.43$ mm^3.

Rigid image registration

During rigid image registration, one image is usually considered fixed and will here be called the reference image. The other image is considered moving and will here be referred to as the template image. In the present implementation, the transformation was defined by a rotation matrix, characterized by three Euler angles, and a translation vector composed of three translation values. The underlying fully-automated implementation was proposed by Thevenaz et al. [17]. In this approach, the search for the best set of transformation parameters was realized iteratively by a Levenberg-Marquardt gradient descent optimizer with optimization criterion being a least-squared-differences approach.

It is in the nature of the gradient-descent optimizer that it starts searching for a minimum in its vicinity. Thus there is the risk for the optimizer to get stuck in a local minimum instead of returning the global best fit. In order to minimize this risk, so-called pyramid approaches have been proposed [17–19], where the first match is returned on a coarse image resolution and refined by increasing the image size successively to its original resolution. In the current implementation, four of these pyramid levels were used. The interpolation technique during the optimization of the transformation matrix was B-splines [14,17].

In a first step, we validated the current registration implementation using an approach from the literature proposed by Boyd et al. [20]. This approach used fiducial markers as gold standard to calculate the target registration errors (TRE) on *in vivo* micro-CT data. It based on Mattes mutual information as optimization criterion in combination with tri-linear interpolation and was realized via the Insight Segmentation and Registration Toolkit (ITK). In our study, this solution was re-implemented and used as a reference technique to validate the current registration algorithm.

Specifically, we compared the amount of mismatching voxels which arise when the binarized and registered image is superimposed onto the binary reference image in both registration techniques. In a reproducibility study, this amount of mismatching voxels would ideally be zero. The amount and position of mismatching voxels is accountable for differences in bone morphometric indices. The quantity was given in percent as the amount of erroneous voxels per total bone volume (BV_e/TV). The underlying regression analysis between the two techniques was performed using the statistical software package R [21].

Interpolation

After registration, when the final transform is applied to the template image, interpolation is required because the new coordinate points may not coincide with the old coordinate points. In this case, a reasonable weighting of the neighboring intensity values is desired to define the intensity value at the new coordinate point.

The simplest interpolation function used in this study is called nearest neighbor interpolation (NNI). Strictly speaking, nearest neighbor is not an interpolation technique because it simply assigns the intensity of the nearest voxel in the transformed input image to the new coordinate point. Tri-linear interpolation (TRI) computes the output intensity value by weighting the eight neighboring intensity values by their distance to the new coordinate point. Furthermore, B-splines (BSP) can be used as an interpolation technique. B-splines use low-degree polynomials in each of the intervals and select the polynomial pieces so that they fit smoothly together. The B-spline function is an approximating function that passes near the points but not necessarily through them. Therefore, the data will also be modified if the image is resampled to the same grid [15]. B-splines can be implemented as third- or higher order polynomials. In this study, we used a third-order polynomial [17].

Data analysis

In a first setup, bone morphometric indices were calculated on the original image data using individual masks (ORG) as is common use in the field of *in vivo* micro-CT. To calculate bone morphometric indices, the 8×5 raw gray-scale volumes were filtered using a Gaussian-filter (sigma 1.2, support 1) to partially suppress noise. The filtered images were then segmented to separate bone from background using a fixed global threshold (22% of maximum grayscale value) and the trabecular compartment was separated from the cortical shell by a distance-transform-based algorithm [22]. Trabecular bone structure was analyzed by calculating bone volume fraction (BV/TV), bone volume (BV), specific bone surface (BS/BV), bone surface (BS), trabecular thickness (Tb.Th), trabecular separation (Tb.Sp) and trabecular number (Tb.N) [23].

All following setups required image interpolation. The experimental setups were defined as follows: The first scan of each series of five scans per animal was considered fixed. It differed from the following repeat scans in that it did not require interpolation. The remaining four scans were registered onto the first scan. In all

cases, the registration was performed on the raw unfiltered gray-scale images. After the registration, the transformed volumes were filtered and segmented and the bone morphometric indices were determined.

In particular, the second setup was based on the following motivation: To ensure the exact same trabecular region of analysis but avoid interpolation errors, some researchers proposed to determine the transformation matrix between two consecutive scans but then only transform the trabecular mask according to the achieved transformation matrix so that the bone morphometric indices can be calculated on the original images [12]. Therefore, we applied the resulting inverse transformation (INV; using NNI for binary images) onto the trabecular mask and evaluated the underlying bone structures in the original gray-scale images using this transformed mask.

In a third setup, the consecutive scans were registered and the images themselves were transformed via NNI, TRI or BSP. For bone morphometric analysis, always the same trabecular mask as in the fixed reference scan was used. Figure 3.1 shows a typical cut through a 6^{th} caudal vertebra. The dark gray area indicates the trabecular volume to be evaluated.

Reproducibility

In a first step, we investigated the effect of interpolation by making use of the reproducibility error of the underlying study. The reproducibility of a given measurement can best be described by its precision errors (PEs) [24]. For the seven morphometric indices, PEs were expressed both in absolute values (PE_{SD}) and as coefficients of variation ($\mathrm{PE}_{\%CV}$) of repeated measurements, as described in more detail elsewhere [25,26]. Furthermore, intra-class correlation coefficients (ICC) were calculated. ICC is defined as the intra-subject variance divided by the population variance, where a value of 0 denotes no reproducibility and a value of 1 perfect reproducibility. The ICC model, chosen for a reproducibility study with given repeated measurements, is the two-way mixed model. For all statistical analyses, the R software package was used [21]. All precision errors and ICCs were calculated for the original images with individual (ORG) and with inversely transformed masks (INV) as well as for the three different interpolators (NNI, TRI, BSP). Furthermore, a paired Student's t-test with Bonferroni-correction for multiple comparisons was performed between the repeated measurements. This test gives evidence if pooling

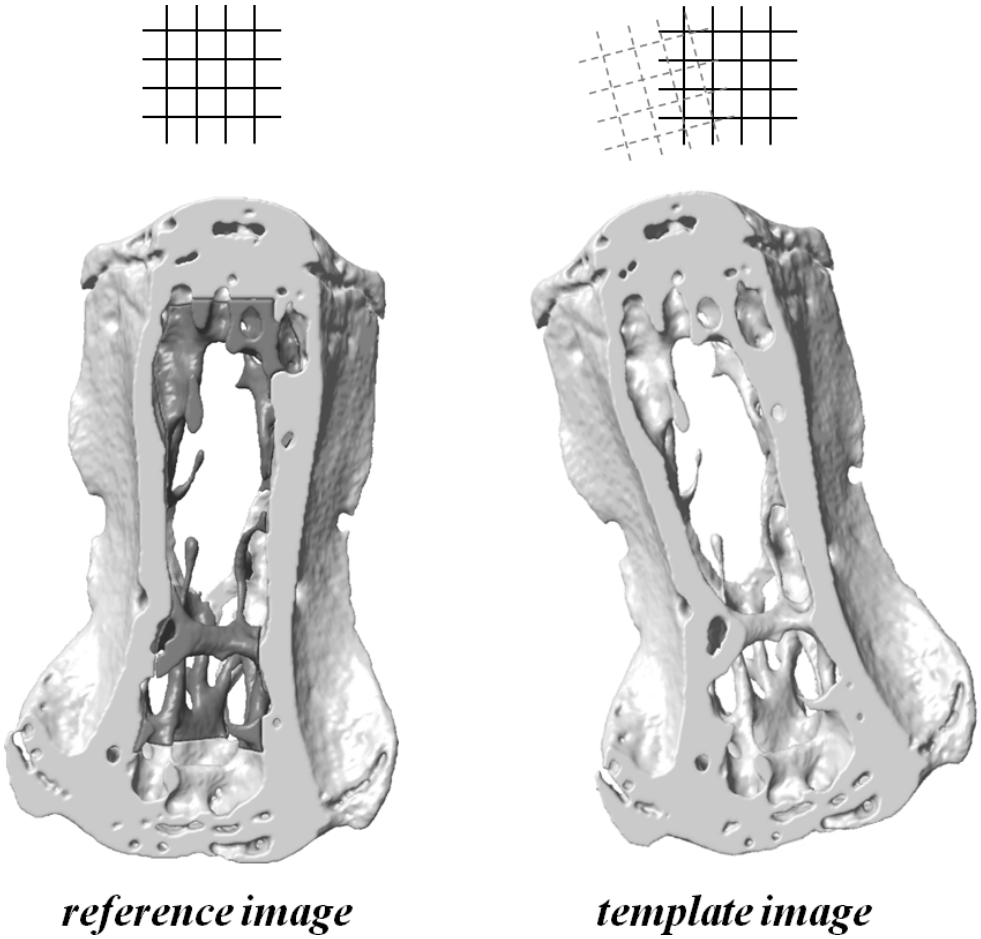

Figure 3.1: Representative image of the murine 6^{th} caudal vertebra (frontal view). The reference image shows the cortical shell and the trabecular compartment to be analyzed. The template image needs to be aligned to the reference image if the same trabecular mask should be used for evaluation. When transformed after registration, the coordinate system of the template image does not fit any more onto the reference coordinate system. To align the template coordinate system newly, interpolation is required.

of all repeated measurements is allowed. In the present case, this was of particular interest since in some setups the columns differed in that the first measurement did not require image interpolation while the other four measurements did.

Interpolation error

In a second step, we aimed at determining the actual amount of interpolation error. For this purpose, it seemed most appropriate to put the morphometric values

gained from the transformed images in relation to the values gained from the inverse transformation of the trabecular mask, where no interpolation is required on the measurement itself but the same volume of interest is evaluated. The interpolation error was then defined as the absolute percentage deviation from the "gold standard" technique (INV). Furthermore, a paired Student's t-test using Bonferroni-correction for multiple comparisons was used between interpolation errors gained from NNI, TRI and BSP. For this comparison, only the transformed images but not the first measurements were considered.

Post-processing order

The order in which a raw image is post-processed after image acquisition, is typically: gray-level filtration (e.g. Gaussian filtration; GAU) $\longrightarrow$ binarization (e.g. by using a fixed threshold; THR) $\longrightarrow$ morphometric measurements. Therefore, there are several possibilities where the registration (REG) can enter this processing chain; e.g. before the Gaussian-filter, after the Gaussian-filter, or after the threshold procedure. It is not clear to date whether and how this order affects the resulting bone morphometric indices.

To test the influence of the post-processing order, we prepared the four interpolated repeat scans (using B-splines) in the order REG-GAU-THR, GAU-REG-THR, and GAU-THR-REG. The transformation of the last series involved B-spline interpolation on binary images. In this case, the images were binary again after the registration. Trabecular bone morphometric indices were calculated as described earlier in all transformed images. For comparison of the different post-processing orders, the absolute difference from the gold standard in percent was determined for all repeat scans. A paired Student's t-test using Bonferroni-correction for multiple testing was calculated between the three groups (REG-GAU-THR, GAU-REG-THR, and GAU-THR-REG). P-values < 0.05 were considered significant.

3.1.3 Results

All registrations on the gray-scale images converged. Rotation angles ranged from -11.64° to 6.90° and translations ranged from -76.33 to 20.97 voxels which corresponds to a metric range from -486.5 μm to 72.5 μm. Figure 3.2 shows the results of the validation of the current registration algorithm comparing it to the reference algorithm from the literature [20]. The binary reference and repeat scans were su-

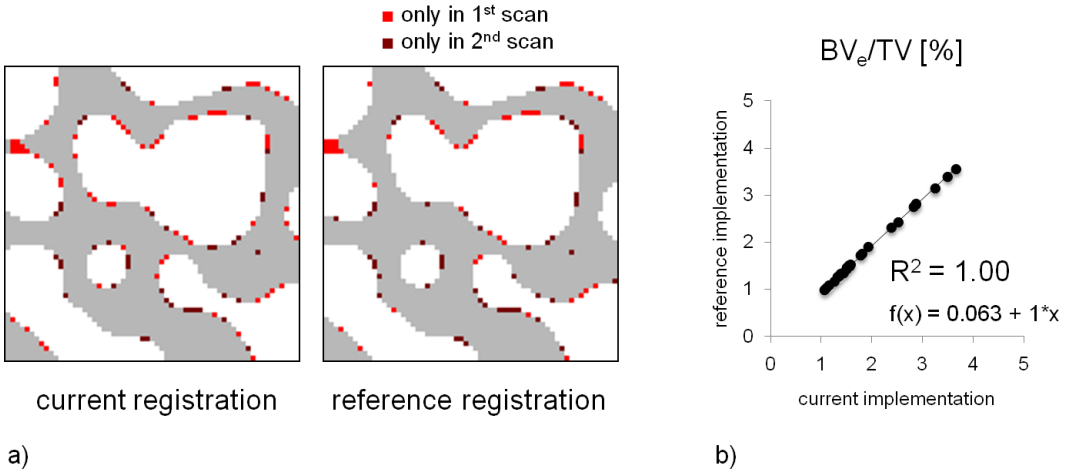

Figure 3.2: Validation of the proposed registration algorithm by means of a gold-standard reference from the literature [20]: a) Superimposition of two binary repeat scans resulting from (left) the current registration approach and (right) the reference registration algorithm. Dark red squares denote voxels only present in the second measurement while light red indicates voxels only present in the first measurement. Differences in the images result from differences in the two registration approaches (reference: Mattes mutual information optimization criterion and linear interpolation compared to the current least squared differences criterion and B-spline interpolation; 1 voxel = 10.5 μm). The percentage of erroneous voxels per TV is described as BV_e/TV. b) Linear regression analysis between BV_e/TV resulting from the current registration and the BV_e/TV resulting from the reference registration.

perimposed, indicating mismatching voxels that were either present in the first or the second scan, but not in both. Figure 3.2a (left) displays the reproducibility mismatch resulting from the current registration implementation and Figure 3.2a (right) shows the mismatch from the reference implementation. The percentage of erroneous voxels per trabecular bone volume (BV_e/TV) of both registration techniques correlated with $R^2 = 1.00$ with $f(x) = 1*x+0.063$ and amounted on average to 1.8% (Figure 3.2b).

Table 3.1 shows the results of the reproducibility examination of ORG and INV. In Table 3.2, the reproducibility of NNI, TRI and BSP is listed. For all different study setups (ORG, INV, NNI, TRI, BSP), the mean values, PE_{SD}, and $PE_{\%CV}$, and ICC are given. ORG showed $PE_{\%CV}$ ranging between 0.81% (Tb.Sp) and 3.93% (BV) while INV resulted in $PE_{\%CV}$ from 0.57% (Tb.Th) to 0.85% (Tb.N). The $PE_{\%CV}$

Table 3.1: Reproducibility of static bone morphometric indices via calculation on the original data using individual masks (ORG) and via inverse transformation of the masks only (INV). Reproducibility is expressed as precision error of the standard deviation (PE_{SD}), coefficient of variation ($PE_{\%CV}$) and intra-class correlations (ICC). The p-value denotes significant differences ($p<0.05$) between repeated scans, e.g. $p_{1,2}$ indicates significance between the first and the second measurement.

	Parameter	Mean	PE_{SD}	$PE_{\%CV}$ (%)	ICC	p-value
	BV/TV [%]	16.707	0.428	2.542	0.963	n.s.
	BV [mm^3]	0.327	0.013	3.926	0.925	n.s.
	BS/BV [mm^2/mm^3]	9.983	0.290	3.028	0.976	n.s.
ORG	BS [mm^2]	30.522	0.328	1.109	0.992	n.s.
	Tb.Th [mm]	0.084	0.001	1.185	0.986	n.s.
	Tb.Sp [mm]	0.371	0.003	0.807	0.994	n.s.
	Tb.N [1/mm]	2.463	0.026	1.056	0.988	n.s.
	BV/TV [%]	16.345	0.103	0.610	0.998	n.s.
	BV [mm^3]	0.316	0.002	0.808	0.998	n.s.
	BS/BV [mm^2/mm^3]	9.721	0.068	0.741	1.000	$p_{1,2}$-$p_{1,5}$
INV	BS [mm^2]	30.661	0.188	0.595	0.997	n.s.
	Tb.Th [mm]	0.084	0.000	0.569	0.997	n.s.
	Tb.Sp [mm]	0.372	0.003	0.776	0.995	n.s.
	Tb.N [1/mm]	2.451	0.022	0.850	0.992	n.s.

using nearest neighbor interpolation ranged from 0.41% (BS/BV) to 1.08% (Tb.N), using tri-linear interpolation from 0.41% (BS/BV) to 1.09% (Tb.N) and using B-spline interpolation from 0.21% (BS/BV) to 1.00% (Tb.N). ICC showed very high reproducibility with values between 0.925% and 0.994% for ORG, between 0.992% and 1.000% for INV, between 0.992 and 1.000 for NNI and TRI, and between 0.990 and 1.000 for BSP.

Pairwise Student's t-test with Bonferroni correction between the repeated measurements revealed that the scans could be pooled as expected when using original images with individual masks ($p>0.05$). The same applies for BSP interpolation where no significant differences were found in bone morphometric indices amongst the first untransformed and the following transformed images ($p>0.05$). TRI differed in BS/BV, BS, and Tb.Th ($p<0.05$) while NNI showed significant deviations in BS

Table 3.2: Reproducibility of static bone morphometric indices via nearest-neighbor (NNI), tri-linear (TRI), or B-spline (BSP) interpolation. Reproducibility is expressed as precision error of the standard deviation (PE_{SD}), coefficient of variation ($PE_{\%CV}$) and intra-class correlations (ICC). The p-value denotes significant differences ($p<0.05$) between repeated scans, e.g. $p_{1,2}$ indicates significance between the first and the second measurement.

	Parameter	Mean	PE_{SD}	$PE_{\%CV}$ (%)	ICC	p-value
	BV/TV [%]	16.453	0.101	0.567	0.998	n.s.
	BV [mm^3]	0.320	0.002	0.567	0.999	n.s.
	BS/BV [mm^2/mm^3]	9.864	0.042	0.412	1.000	n.s.
NNI	BS [mm^2]	30.788	0.195	0.614	0.997	$p_{1,2}$,$p_{1,3}$,$p_{1,5}$
	Tb.Th [mm]	0.084	0.000	0.602	0.996	n.s.
	Tb.Sp [mm]	0.371	0.003	0.701	0.997	n.s.
	Tb.N [1/mm]	2.470	0.027	1.077	0.992	$p_{1,4}$
	BV/TV [%]	16.461	0.103	0.583	0.998	n.s.
	BV [mm^3]	0.320	0.002	0.583	0.998	n.s.
	BS/BV [mm^2/mm^3]	9.754	0.040	0.408	1.000	$p_{1,3}$
TRI	BS [mm^2]	30.431	0.244	0.790	0.997	$p_{1,2}$-$p_{1,5}$
	Tb.Th [mm]	0.085	0.001	0.845	0.996	$p_{1,2}$-$p_{1,4}$
	Tb.Sp [mm]	0.374	0.003	0.891	0.996	n.s.
	Tb.N [1/mm]	2.427	0.027	1.088	0.992	n.s.
	BV/TV [%]	16.453	0.100	0.564	0.998	n.s.
	BV [mm^3]	0.320	0.002	0.564	0.999	n.s.
	BS/BV [mm^2/mm^3]	9.809	0.020	0.205	1.000	n.s.
BSP	BS [mm^2]	30.615	0.188	0.595	0.997	n.s.
	Tb.Th [mm]	0.084	0.000	0.571	0.997	n.s.
	Tb.Sp [mm]	0.372	0.004	0.901	0.993	n.s.
	Tb.N [1/mm]	2.451	0.026	0.996	0.990	n.s.

and Tb.N ($p<0.05$). Although being proposed as the gold standard for bone morphometric analysis on transformed images, INV differed significantly in BS between the first and all following transformed measurements ($p<0.05$). Further investigation of this discrepancy discovered that the inverse transformation of the trabecular mask resulted in a significantly lower tissue volume (0.52%) than the mask used in the first repeat scan ($p<0.05$) as determined by a paired Student's t-test. In general, the fact that, if significant differences occurred, they occurred between the first and any of the transformed scans but not amongst the transformed scans themselves, suggests that the transformation is responsible for these discrepancies.

Figure 3.3 gives a visual impression of the changes in gray-scale scans between

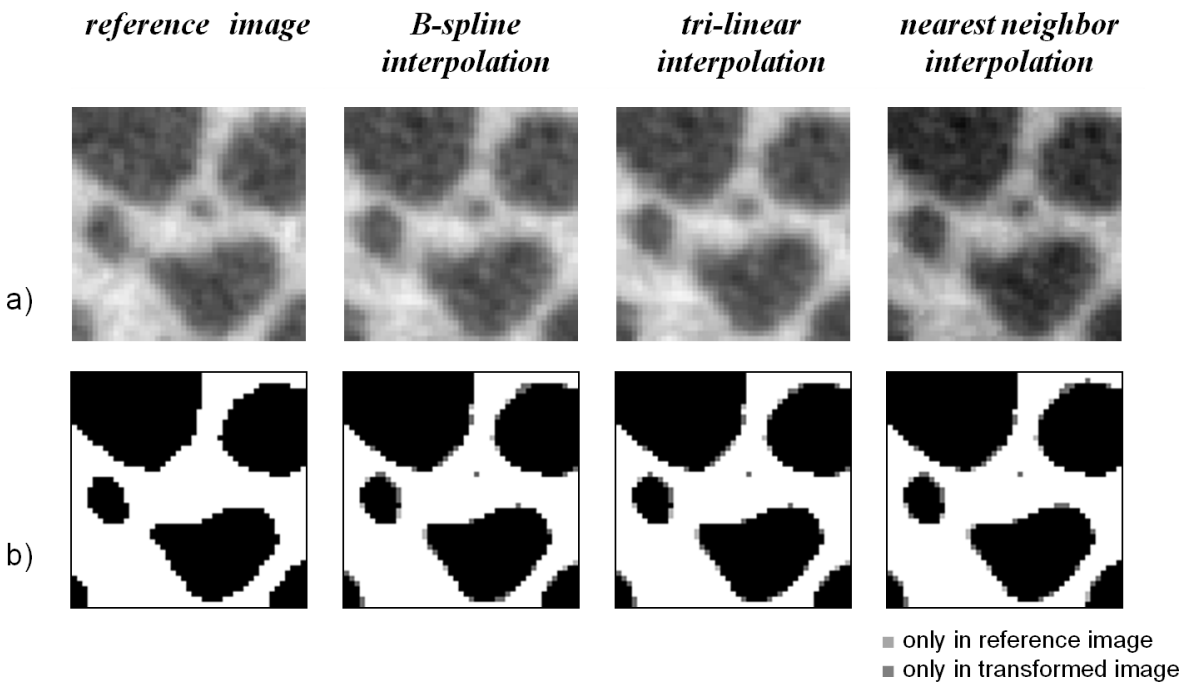

Figure 3.3: a) Gray-scale and b) corresponding binary trabecular image detail of the first repeat scan not requiring image interpolation, the same detail acquired via nearest neighbor interpolation, via tri-linear interpolation and via B-spline approximation. Visually it is hard to distinguish the three interpolation techniques. Tri-linearly interpolated images appear slightly smoother while nearest neighbor interpolated images seem a bit more jagged than the original gray-scale image. Superimposition of binary scans highlights small changes in the bone structure resulting from image interpolation. (1 voxel = 10.5 μm)

interpolators and the corresponding differences in binary images. Superimposition of the first untransformed and the transformed binary images highlighted the critical voxels responsible for possible changes in bone morphometric indices.

Although INV showed differences in BS, it was still taken as reference technique to determine the actual amount of interpolation error for all other indices, disregarding BS. Figure 3.4a shows the absolute interpolation errors for the three interpolation techniques. BSP returned the lowest interpolation error for BS/BV, Tb.Th, Tb.Sp and Tb.N ($p<0.05$), ranging from 0.2% to 1.4%. TRI ranged between 0.5% and 1.4% and NNI between 0.4% and 1.9%. Furthermore, the interpolation error of BS/BV and Tb.Th in each animal is plotted in Figure 3.4b and c. In both images, B-spline interpolated values can be found close to the zero baselines. TRI slightly underestimates BS/BV and overestimates Tb.Th while NNI performs the other way round.

In Figure 3.5, the effects of the post-processing order including a registration step are displayed. In this step, the 32 template values were calculated for the three processing orders (REG-GAU-THR, GAU-REG-THR and GAU-THR-REG). The absolute interpolation errors are plotted for each processing order, ranging from 0.2% to 1.4% for REG-GAU-THR and GAU-REG-THR, and from 0.7% to 7.9% for GAU-THR-REG. One image pair in GAU-THR-REG only converged after a manual change in the initial guess for the transformation matrix. In general, GAU-THR-REG was significantly different from the other two processing orders in BS/BV, Tb.Th and Tb.N ($p<0.05$), but no significant differences could be found between REG-GAU-THR and GAU-REG-THR.

3.1.4 Discussion

The study of longitudinal changes due to disease, pharmaceutical or physiological intervention requires accurate analysis of the bone structure. Rigid image registration enables follow-up measurements to be aligned and thus to analyze an identical trabecular region at multiple time points. However, interpolation might affect the resulting bone morphometric indices in a registered and thus transformed image. This study focused on the effects of different interpolators on the trabecular morphometric indices. Furthermore, the influence of the post-processing order including the transformation step was investigated.

Any kind of post-processing of micro-CT scans might influence the bone morpho-

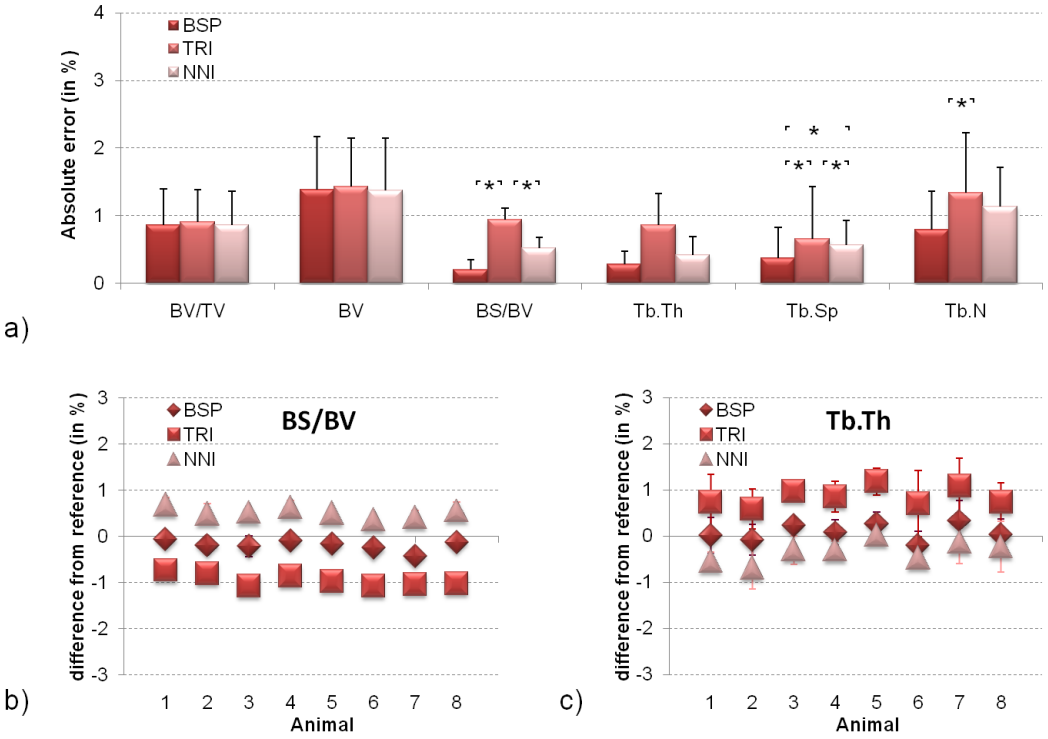

Figure 3.4: a) Absolute percentage errors in relation to INV in bone morphometric indices (* $p<0.05$). b), c) Assessment of different interpolators on BS and Tb.Th analyzed for the eight animals of the study.

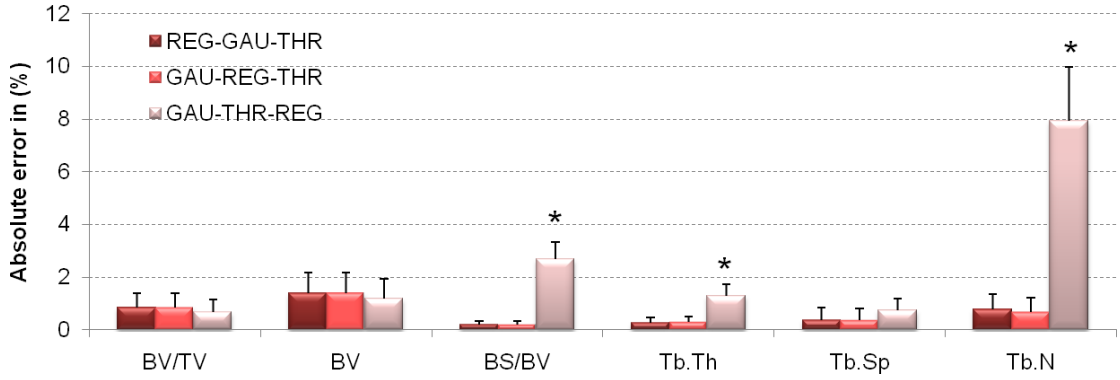

Figure 3.5: Post-processing B-spline interpolation errors expressed as absolute percent difference from the gold standard reference values for the static bone morphometric indices. The abbreviations denote the post-processing order: REG = registration, GAU = Gaussian filter, THR = thresholding. GAU-THR-REG differed significantly from the other two arrangements in BS/BV, BS, Tb.Th and Tb.N (* $p<0.05$).

metric indices. Nevertheless, with the introduction of a new imaging technology for longitudinal scans, the incorporation of a registration step seemed reasonable since it offers more advanced evaluation of longitudinal data [12, 27, 28]. So far, it has been proposed to handle the arising interpolation error by avoiding the evaluation on registered images and to apply the inverse transformation on the trabecular mask but not on the image itself [12]. Here, we determined the amount of interpolation error in order to investigate whether the evaluation of bone morphometric indices on a transformed image is still justifiable.

The results of this study showed that the precision errors coming from the inverse transformation of the mask and from three different interpolator schemes were almost identical (Table 3.1 and 3.2). Registration improved the reproducibility error as was already pointed out by other studies [12, 15]. Furthermore, we showed that B-spline approximation was the only technique besides the setup with original masks which did not result in significant deviations between the untransformed and the follow-up transformed repeat measurements in the underlying reproducibility setup. The deviation from the gold standard technique (INV) was lower for BSP than for TRI and NNI in most bone morphometric indices (maximum 1.4%). Nevertheless, it is important to note that BSP was also used for the optimization of the registration procedure. Therefore, we cannot rule out the possibility that the choice of optimization also influenced image interpolation and subsequent morphometric analysis. Therefore a combination of TRI optimization and TRI interpolation might fare equally well in the quantitative analysis. What we can say though is that BSP optimization and interpolation work together very well and therefore it is suggested that these results justify the use of BSP interpolation for subsequent bone morphometric analysis on with B-Spline interpolation registered images.

Boyd et al. [20] proposed to perform a registration procedure on gray-scale instead of binary images. This suggestion seems reasonable as gray-scale images provide a lot more intensity information for finding the best match between any two images. Our results support this proposal. Furthermore, we give values on the effect of the post-processing order. For the evaluation of bone morphometric indices, it does not matter if a raw gray-scale image is first registered or first Gaussian filtered. However, a transformation should not be performed on segmented images if possible since registration of segmented data may result in errors of up to 7.9% (Tb.N) as compared to the non-interpolated reference value.

This study has several limitations. First, the design of the underlying study is an *ex vivo* setup. Nevertheless, here, the aim was to investigate the interpolation effect on bone structural indices, not to elaborate on the reproducibility of *in vivo* imaging. In this study, the reproducibility of bone structural indices had to be shown to verify if the first untransformed scan and the follow-up transformed measurements could be pooled and therefore be considered equal. Several studies exist showing the reproducibility of longitudinal measurements *in vivo* (0.47% - 3.92%) [12,13] and *ex vivo* (0.17% - 3.54%) [13,25] for the herein investigated bone morphometric indices.

A second limitation of the current study is that it was performed on high-resolution animal data (10.5 μm) where one trabecula typically had a thickness of 8 voxels. Compared to lower image resolutions as typically encountered in clinically used human high-resolution peripheral quantitative computed tomography (HR-pQCT) scans, the impact of the bone surface was reduced which is the obvious contact point of interpolation effects. The influences of the interpolation technique are thus expected to be less pronounced than might be the case in HR-pQCT data at an approximately 10 times lower spatial image resolution. Nevertheless, a study with a similar aim performed on magnetic resonance imaging (MRI) scans of human proximal femurs with $234 \times 234 \times 1000$ μm^3 image resolution came to almost the same conclusions. BSP and NNI were not significantly different from the reference bone morphometric index while TRI was not recommended [15].

In conclusion, we assessed the effect of three different interpolators on the subsequent bone morphometric analysis and investigated at which stage in the post-processing order interpolation should occur. We found that B-spline approximation - in contrast to nearest neighbor or tri-linear interpolation - did not alter the trabecular bone morphometric indices calculated from transformed *in vivo* micro-CT scans, at least provided that B-spline approximation was also used for the registration. With an error of less than 1.4%, a post-processing step including the registration of time-lapsed gray-scale images via B-spline interpolation is considered justifiable for the subsequent calculation of trabecular bone morphometric indices. Quantification of the interpolation error is required to establish the adequacy of image registration techniques including subsequent quantitative evaluation of micro-CT images. With adequate validation techniques, image registration has the potential to become a fundamental technique in experimental and clinical imaging studies for the investigation of bone diseases and related interventions.

Acknowledgements

The authors would like to acknowledge David Christen for the support with the Insight Segmentation and Registration Toolkit (ITK) which was needed to implement the reference registration algorithm [20]. ITK is an open source software package available at www.itk.org. Furthermore, funding from the European Union for the osteoporotic virtual physiological human project (VPHOP FP7-ICT2008-223865) is gratefully acknowledged.

References

[1] R. Müller, T. Hildebrand, H. J. Häuselmann, and P. Rüegsegger. In vivo reproducibility of three-dimensional structural properties of noninvasive bone biopsies using 3D-pQCT. *J Bone Miner Res*, 11(11):1745–1750, 1996.

[2] P. Augat, C. L. Gordon, T. F. Lang, H. Iida, and H. K. Genant. Accuracy of cortical and trabecular bone measurements with peripheral quantitative computed tomography (pqct). *Phys Med Biol*, 43(10):2873–83, 1998.

[3] X. Banse, J. P. Devogelaer, and M. Grynpas. Patient-specific microarchitecture of vertebral cancellous bone: a peripheral quantitative computed tomographic and histological study. *Bone*, 30(6):829–35, 2002.

[4] J. E. M. Brouwers, B. van Rietbergen, R. Huiskes, and K. Ito. Effects of pth treatment on tibial bone of ovariectomized rats assessed by in vivo micro-ct. *Osteoporos Int*, 20(11):1823–35, 2009.

[5] J.A. Gasser and J. Yam. In vivo non-invasive monitoring of changes in structural cancellous bone parameters with a novel prototype microct in rats. *J Bone Miner Res*, 17(Suppl. 2), 2002.

[6] S. K. Boyd, P. Davison, R. Müller, and J. A. Gasser. Monitoring individual morphological changes over time in ovariectomized rats by in vivo micro-computed tomography. *Bone*, 39(4):854–62, 2006.

[7] T. Hildebrand and P Rüegsegger. A new method for the model-independent assessment of thickness in three-dimensional images. *J Microsc*, 185:67–75, 1997.

[8] T. Hildebrand, A. Laib, R. Müller, J. Dequeker, and P. Rüegsegger. Direct three-dimensional morphometric analysis of human cancellous bone: microstructural data from spine, femur, iliac crest, and calcaneus. *J Bone Miner Res*, 14(7):1167–1174, 1999.

[9] T. Hildebrand and P. Rüegsegger. Quantification of bone microarchitecture with the structure model index. *Comput Methods Biomech Biomed Engin*, 1(1):15–23, 1997.

[10] A. Odgaard, E.B. Jensen, and H.J. Gundersen. Estimation of structural anisotropy based on volume orientation. a new concept. *J Microsc*, 157(Pt 2):149–162, 1990.

[11] A. Odgaard. Three-dimensional methods for quantification of cancellous bone architecture. *Bone*, 20(4):315–328, 1997.

[12] K. K. Nishiyama, G. M. Campbell, R. J. Klinck, and S. K. Boyd. Reproducibility of bone micro-architecture measurements in rodents by in vivo micro-computed tomography is maximized with three-dimensional image registration. *Bone*, 46(1):155–61, 2010.

[13] J. A. MacNeil and S. K. Boyd. Bone strength at the distal radius can be estimated from high-resolution peripheral quantitative computed tomography and the finite element method. *Bone*, 42(6):1203–1213, 2008.

[14] P. Thevenaz, T. Blu, and M. Unser. Interpolation revisited. *IEEE Trans Med Imaging*, 19(7):739–58, 2000.

[15] J. Blumenfeld, C. Studholme, J. Carballido-Gamio, D. Carpenter, T. M. Link, and S. Majumdar. Three-dimensional image registration of mr proximal femur images for the analysis of trabecular bone parameters. *Med Phys*, 35(10):4630–9, 2008.

[16] F. M. Lambers, G. Kuhn, F. A. Gerhard, and R. Müller. In vivo micro computed tomography allows monitoring of load induced microstructural bone adaptation. *Bone*, 44(S2):300, 2009.

[17] P. Thevenaz, U. E. Ruttimann, and M. Unser. A pyramid approach to subpixel registration based on intensity. *IEEE Trans Image Process*, 7(1):27–41, 1998.

[18] F. Maes, D. Vandermeulen, and P. Suetens. Comparative evaluation of multiresolution optimization strategies for multimodality image registration by maximization of mutual information. *Medical Image Analysis*, 3(4):373–386, 1999.

[19] C. Studholme, D. L. Hill, and D. J. Hawkes. Automated three-dimensional registration of magnetic resonance and positron emission tomography brain images by multiresolution optimization of voxel similarity measures. *Med Phys*, 24(1):25–35, 1997.

[20] S. K. Boyd, S. Moser, M. Kuhn, R. J. Klinck, P. L. Krauze, R. Müller, and J. A. Gasser. Evaluation of three-dimensional image registration methodologies for in vivo micro-computed tomography. *Ann Biomed Eng*, 34(10):1587–99, 2006.

[21] R Development Core Team. *R: A language and environment for statistical computing*. R Foundation for Statistical Computing, Vienna, Austria, 2007.

[22] T. Kohler, M. Stauber, L. R. Donahue, and R. Müller. Automated compartmental analysis for high-throughput skeletal phenotyping in femora of genetic mouse models. *Bone*, 41(4):659–667, 2007.

[23] M. L. Bouxsein, S. K. Boyd, B. A. Christiansen, R. E. Guldberg, K. J. Jepsen, and R. Müller. Guidelines for assessment of bone microstructure in rodents using micro-computed tomography. *J Bone Miner Res*, 25(7):1468–86, 2010.

[24] C. C. Glüer, G. Blake, Y. Lu, B. A. Blunt, M. Jergas, and H. K. Genant. Accurate assessment of precision errors: how to measure the reproducibility of bone densitometry techniques. *Osteoporos Int*, 5:262–270, 1995.

[25] T. L. Mueller, M. Stauber, T. Kohler, F. Eckstein, R. Müller, and G. H. van Lenthe. Non-invasive bone competence analysis by high-resolution pQCT: an in vitro reproducibility study on structural and mechanical properties at the human radius. *Bone*, 44(2):364–371, 2009.

[26] T. Kohler, M. Beyeler, D. Webster, and R. Müller. Compartmental bone morphometry in the mouse femur: reproducibility and resolution dependence of microtomographic measurements. *Calcif Tissue Int*, 77(5):281–290, 2005.

[27] J. H. Waarsing, J. S. Day, J. C. van der Linden, A. G. Ederveen, C. Spanjers, N. De Clerck, A. Sasov, J. A. N. Verhaar, and H. Weinans. Detecting and

tracking local changes in the tibiae of individual rats: a novel method to analyse longitudinal in vivo micro-ct data. *Bone*, 34(1):163–169, 2004.

[28] F. A. Schulte, F. M. Lambers, G. Kuhn, and R. Müller. In vivo micro-computed tomography allows direct three-dimensional quantification of both bone formation and bone resorption parameters using time-lapsed imaging. *Bone*, 48(3):433–442, 2011.

3.2 *In vivo* micro-computed tomography allows direct three-dimensional quantification of both bone formation and bone resorption parameters using time-lapsed imaging

Friederike A. Schulte[1], Floor M. Lambers[1], Gisela Kuhn[1], and Ralph Müller[1]

[1]Institute for Biomechanics, ETH Zurich, Zurich, Switzerland

published in:
Bone
48:433-442, 2011

Abstract:
Bone is a living tissue able to adapt its structure to external influences such as altered mechanical loading. This adaptation process is governed by two distinct cell types: bone-forming cells called osteoblasts and bone-resorbing cells called osteoclasts. It is therefore of particular interest to have quantitative access to the outcomes of bone formation and resorption separately. This article presents a non-invasive three-dimensional technique to directly extract bone formation and resorption parameters from time-lapsed *in vivo* micro-computed tomography scans. This includes parameters such as Mineralizing Surface (MS), Mineral Apposition Rate (MAR), and Bone Formation Rate (BFR), which were defined in accordance to the current nomenclature of dynamic histomorphometry. Due to the time-lapsed and non-destructive nature of *in vivo* micro-computed tomography, not only formation but also resorption can now be assessed quantitatively and time-dependent parameters Eroded Surface (ES) as well as newly defined indices Mineral Resorption Rate (MRR) and Bone Resorption Rate (BRR) are introduced. For validation purposes, dynamic formation parameters were compared to the traditional quantitative measures of dynamic histomorphometry, where MAR correlated with R=0.68 and MS with R=0.78 ($p<0.05$). Reproducibility was

assessed in 8 samples that were scanned 5 times and errors ranged from 0.9% (MRR) to 6.6% (BRR). Furthermore, the new parameters were applied to a murine *in vivo* loading model. A comparison of directly extracted parameters between formation and resorption within each animal revealed that in the control group, i.e., during normal remodeling, MAR was significantly lower than MRR ($p<0.01$), whereas MS compared to ES was significantly higher ($p<0.0001$). This implies that normal remodeling seems to take place by many small formation packets and few but large resorption volumes. After 4 weeks of mechanical loading, newly extracted trabecular BFR and MS were significantly higher ($p<0.01$) in the loading compared to the control group. At the same time, ES was significantly decreased ($p<0.01$). This indicates that modeling induced by mechanical loading takes place primarily by increased area, not width of formation packets. With these results, we conclude that the noninvasive direct technique is well suited to extract dynamic bone morphometry parameters and eventually gain more insight into the processes of bone adaptation not only for formation but also resorption.

Keywords:
bone formation; bone resorption; dynamic morphometry; mechanical loading; *in vivo* micro-computed tomography

3.2.1 Introduction

Bone is able to change its microstructure by mechanisms called modeling and remodeling. Modeling is needed to adapt the micro-architecture to external influences such as changes in mechanical loading [1]. Remodeling keeps the structure capable of coping with daily physical requirements [2]. This adaptation process is governed by bone-forming cells called osteoblasts and bone-resorbing cells called osteoclasts. As a result, formation and resorption are two separate processes whose coordinated execution eventually results in a global net gain or loss of bone tissue. In order to investigate this cellular interplay on an experimental basis, it is of particular interest to have quantitative access to the outcomes of bone formation and bone resorption separately.

Traditionally, the outcomes of dynamic bone cell activity are measured by two-dimensional (2D) histomorphometry. In order to quantify rates of bone formation,

the bone is stained *in vivo* with a substance able to incorporate into actively mineralizing osteoid, e.g., calcein or tetracyclin. A short time period between a first and a second labeling injection allows a time-dependent assessment of the mineralization fronts, visible as epifluorescent lines. From these lines, a number of bone formation parameters including Bone Formation Rate (BFR), Mineral Apposition Rate (MAR), and Mineralizing Surface (MS) are determined [3].

Conversely, histomorphometric assessment of bone resorption suffers from the lack of an equivalent dynamic marker [4]. Alternatively, people study resorption cavities in terms of their relative and absolute extent [4]. Eroded Surface (ES) is measured as the percentage of crenated surfaces per total surface; furthermore, markers exist that are able to visualize the osteoclast number and activity (Oc.N) [5]. Nevertheless, these bone resorption parameters are, in contrast to the available bone formation parameters, only snapshots of a single moment and do not allow an assessment of temporal rates of bone resorption. Besides the difficulty in assessing rates of bone resorption, quantitative histomorphometry suffers from its destructive, laborious, and operator-dependent nature [6, 7].

Thus, there is a need for an alternative assessment of bone formation and bone resorption rates. This should be non-destructive and allow time-lapsed *in vivo* measurements of these rates. Waarsing et al. [8] proposed a three-dimensional (3D) method to analyze *in vivo* scans from a non-invasive micro-computed tomography (micro-CT) system. This technique was based on image registration of two subsequent scans of the same animal, where voxels only present in the earlier measurement were considered resorbed bone volumes and voxels only present in the latter measurement were considered formed bone. Qualitative comparison of endosteal formation areas indicated by *in vivo* micro-CT and calcein labeling resulted in very good agreement. Here, we go one step further and show that it is not only possible to detect and track local changes but also to quantify the formation and resorption rates.

The following three steps are necessary to propose a new technique for the calculation of established parameters. First, the results from the new technique need to be compared to the results from the established method. Second, the reproducibility of the new technique needs to be shown. Third, the new method has to be applied to experimental data in order to verify its sensitivity. For this reason, we validated the new 3D technique against traditional quantitative histomorphometry, investigated

its reproducibility, and applied it to an experimental *in vivo* animal loading model. The focus of this article was on the validation of the new algorithm. Nevertheless, the evaluation of the *in vivo* model also provided new insights into trabecular bone formation and resorption during normal remodeling and during mechanical loading.

3.2.2 Materials and Methods

Materials

All experimental data used in this study were taken from an animal *in vivo* loading model following the approach of Webster et al. [9]. Briefly, *in vivo* bone adaptation was induced in 15-week-old female C57BL/6 mice (RCC, Füllinsdorf, Switzerland) by subjecting their sixth caudal vertebra to mechanical loading at 0 or 8 N for 3000 cycles at 10 Hz, 3 times per week for 4 weeks. Loading was applied through pins inserted in the adjacent vertebrae with a previously developed device [10]. Contrary to the original cross-sectional experiment [9, 10], the loaded vertebra was scanned weekly with *in vivo* micro-CT (vivaCT 40, Scanco Medical, Brüttisellen, Switzerland) at an isotropic voxel resolution of 10.5 μm. In order to prevent motion artifacts, the tails were tightly clamped. Previous radiation control studies showed that no radiation effects could be observed in mice scanned 5 times as compared to animals where no *in vivo* imaging was performed (data not shown). During all treatments, the animals underwent isoflurane anesthesia. All animal procedures were approved by the local animal care and use committee (Kantonales Veterinäramt Zürich, Zürich, Switzerland).

For comparison between micro-CT and histomorphometry, data from an experiment with 6 loaded and 6 control mice were used. For quantitative comparison, data from a larger experiment with 9 loaded and 8 control mice were taken. In this experiment, *in vivo* loading resulted in a 22% net gain of trabecular bone volume fraction (BV/TV) and a 13% increase in trabecular thickness (Tb.Th) for the loaded group, and a 7% net gain of trabecular BV/TV for the control group. These results confirmed adequate trabecular bone remodeling and were thus considered appropriate for this article.

For histomorphometry, calcein (Sigma-Aldrich, Buchs, Switzerland) was injected on the days of the 4^{th} and the 5^{th} micro-CT measurement (21 and 28 days after start of loading). Mice were sacrificed 24 h after the second injection. The dissected vertebrae were fixed in phosphate-buffered formaldehyde and then sub-

mitted to a dehydration process in an ascending series of ethanol solutions (70%, 80%, 90%, 96%, 100%), before degreasing in xylene. Samples were infiltrated for 7 days at 4 °C in MMA (methyl methacrylate) solution. This solution consisted of methacrylic acidmethylester (Fluka, Basel, Switzerland), dibuthylphthalate (Merck, Darmstadt, Germany), and perkadox 16 (Dr. Grogg Chemie AG, Stettlen-Deisswil, Switzerland) in a proportion 89.5:10:0.5. Thereafter, the samples polymerized at room temperature. Sagittal sections of 6-μm thickness were prepared using a microtome (Leica SP1400, Wetzlar, Germany). Afterwards, fluorescent images were taken from these sections using a fluorescence microscope (Zeiss, Aalen, Germany) and stitched together with Photoshop CS3 (Adobe, San Jose, USA). Histomorphometric analysis was executed using Image Pro Analyzer 6.3 (Media Cybernetics, Silver Spring, USA). For statistical analysis, the software package R (R, Auckland, New Zealand) was used.

Image processing

In order to assess bone formation and resorption sites separately, we followed the approach of Waarsing et al. [8], where a latter measurement of an *in vivo* measured animal was superimposed onto an earlier measurement of the same animal. Bone areas only present in the earlier measurement were considered resorbed bone areas, while areas only present in the latter measurement corresponded to formed bone areas [8, 11, 12].

Superimposing measurements taken from one animal at different points in time requires a procedure called image registration because the mouse tail cannot be fixed twice in the exact same position. Therefore, data sets of different measurements have to be matched by rotating and translating one record with respect to the other. Several registration algorithms have been proposed in the field of micro-computed tomography [8, 11, 13]. The approach applied here consists of an intensity-based least-squares algorithm proposed by Thevenaz et al. [14]. B-splines were chosen as the interpolation method [15].

In the image processing chain, the unfiltered initial grayscale scan (week 0) was aligned according to its principal axis, and the unfiltered second grayscale scan (week 4) was registered to it. Both transformed measurements were Gaussian filtered (support 1, sigma 1.2) and thresholded at a global level (threshold 220). Afterwards, the binary registered data set of week 4 was added onto the binary data set of week

0. This procedure resulted in a three-colored image containing voxels present in both volumes, voxels only present in the former volume, and voxels only present in the latter volume (see Fig. 3.6a). These three-colored data sets served as input for the direct extraction of dynamic bone formation and bone resorption rates.

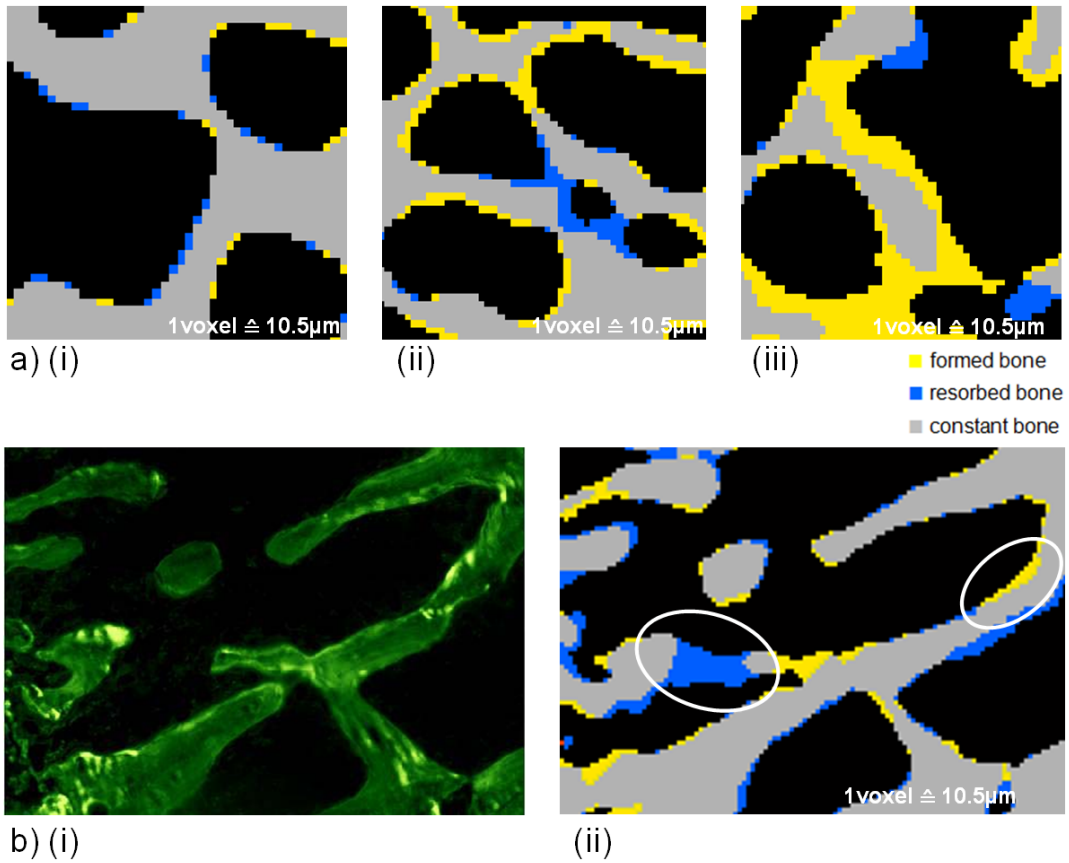

Figure 3.6: (a) Color-coded 2D images of a registered repeat scan at the same point in time (i), after 4 weeks of normal remodeling (ii) and after 4 weeks of mechanical loading (iii). Yellow denotes formed bone areas; blue, resorbed bone areas. Constant areas are colored in gray. (b) Detail of trabecular bone indicating bone formation sites, either by histological calcein staining (i) or by means of micro-CT (ii). Yellow areas on the right correspond to calcein-labeled sites, whereas blue areas denote bone resorption that cannot be visualized in histology.

Dynamic bone morphometry

Histomorphometry defines the Mineral Apposition Rate (MAR) as the distance between the midpoints or the corresponding edges of two consecutive labels, divided by the time between the label injections, given in micrometer per day (μm/d) [3]. In histomorphometry, there is no corresponding parameter such as Mineral Resorption Rate (MRR), given in μm/d. Mineralizing Surface (MS) is defined by the total extent of labeled surface, usually normalized by total bone surface (BS) and given in percentage. The extent of labeled surface can be specified as the mean between separately measured first and second label length, the second label length alone, or the total label length, where the specification and validation of the chosen method are, according to Parfitt et al. [3], the responsibility of the investigator. Eroded Surface (ES) is usually determined by the length of crenated surfaces per total bone surface, also given in percentage. From these directly measured parameters, Bone Formation Rate (BFR) can be derived as the product of MAR and MS. Normalization can take place by a number of referents, e.g., by bone volume (BV) or by bone surface (BS) [3]. Corresponding units are %/d or $\mu m^3/\mu m^2/d$. Bone Resorption Rate (BRR), in %/d or in $\mu m^3/\mu m^2/d$, cannot be measured directly but can be estimated indirectly as the Bone Formation Rate increased or decreased by an assumed or measured rate of change of bone volume [3].

Rigid registration of time-lapsed *in vivo* micro-CT images allows simultaneous assessment of bone formation and resorption sites by quantification of the triangulated formed and resorbed bone volumes. This information can then be used to directly extract MAR, MS, and BFR. At the same time, parameters of bone resorption such as MRR, ES, and BRR can be determined. To avoid confusion between histomorphometric and micro-CT-derived parameters, we will label the 3D micro-CT parameters with an asterisk (*).

MAR* can be calculated by isolating the volumes of formed bone from the three-colored image and applying a distance transformation algorithm to them. For this purpose, we used the algorithm that was originally written by Hildebrand et al. [16] to calculate trabecular thickness. MAR* is then defined as the mean thickness of the formed bone volume divided by the number of days between the measurements and is given in μm/d. Resorbed bone volume can be isolated in the same way, and the newly defined parameter Mineral Resorption Rate (MRR*, in μm/d) can be calculated.

MS* is defined as the percentage of formed bone surface per total bone surface in percentage. In micro-CT, the amount of formed bone surface can be extracted again from the three-colored image by separation of the contact areas between formed and constant bone voxels. Total bone surface (BS) is defined as the amount of bone surface available in the data set of week 0. ES*, given in percentage, is extracted analogously by dividing the amount of resorbed bone surface by total bone surface.

In histomorphometry, BFR is typically either defined as the formed bone volume per bone volume or surface per day. Therefore, we also distinguish between these two referents and define BFR^*_{BV} (BFR^*_{BS}) as the amount of formed bone volume per original bone volume (bone surface) per day. The corresponding units are %/d and $\mu\mathrm{m}^3/\mu\mathrm{m}^2/\mathrm{d}$, respectively. The amount of formed bone volume is directly determined with the new 3D technique by the volume of formed areas. Total BV (BS) is calculated by the volume (surface) of the measurement in week 0. Bone Resorption Rate BRR^*_{BV} is defined analogously as the amount of resorbed bone volume per total volume, with corresponding unit %/d. BRR^*_{BS} describes the amount of resorbed bone volume per total bone surface, given in $\mu\mathrm{m}^3/\mu\mathrm{m}^2/\mathrm{d}$. If not otherwise specified, we will, in the following, refer to BFR* as BFR^*_{BV} and to BRR* as BRR^*_{BV}.

2D comparison of micro-CT and histomorphometry bone formation parameters

For comparison between bone formation rates gained by micro-CT and histomorphometry, respectively, a group of 12 mice (6 control, 6 loading) was used as explained in the Materials section. Independent parameters MAR and MS were determined by analyzing the trabecular regions of histological slices (1 slice per sample) using a semiautomatic analysis software. MS was defined as the sum of the length of double label plus the length of single label along the entire trabecular bone surface divided by total bone surface. Single-labeled areas in histology indicate that remodeling has ended before the time of second label injection or has only started after the time of first label injection. The micro-CT images, however, contain strictly spoken only double-labeled areas showing all bone changes within the defined time interval. For this reason, it seemed the fairest comparison between histomorphometry and micro-CT morphometry to take all labeled areas equally into account. Subsequently, the corresponding micro-CT-slices were extracted from the 3D volumes by registration of a micro-CT scan of the remaining parts of the cut vertebrae. The cut

area then corresponded to the adjacent histological slice (Fig. 3.6b). This procedure allowed direct 2D comparison of the information available in the histological and the micro-CT slices, respectively.

Comparison of 2D and 3D micro-CT bone formation parameters

The extraction of 3D rates from 2D information entails several potential error sources. This concerns the indirect derivation of BFR as the product of MAR and MS, the constraint to a small region of analysis (1 slice), and most probably an overestimation of MAR due to the oblique presentation of single trabeculae in 2D cut planes, where histomorphometry proposes a correction factor of 1/1.2 [17].

In order to assess the limitations of 2D analysis, we compared 2D and 3D measures of bone formation, both assessed from the time-lapsed micro-CT images. Direct bone formation parameters were extracted using 17 samples (8 control, 9 loading) and calculated over a period of 4 weeks. The volume of consideration was constrained to the trabecular compartment, which was defined using an automatic distance-based segmentation algorithm [18].

First, 3D BFR*, being calculated as the mean product of 3D MAR* and 3D MS*, was compared to directly calculated 3D BFR*. Second, in order to simulate the 2D situation for MAR*, the calculation of MAR* was constrained to circles instead of spheres along the sagittal cut plane. Third, the effect of constraining the measurement to one slice was determined. This was done by automatically calculating MAR* for each sagittal slice separately. To exclude regions of low trabecular bone, only the inner 50% of the sagittal slices, perpendicular to the long axis of the bone, were taken into account. The fluctuation throughout the slices was expressed by the coefficient of variation (%CV).

Reproducibility

Reproducibility was assessed in the *in vivo* model over a period of 4 weeks. For ethical reasons, the repeated measurements were taken after sacrifice at the end of the experiment. This was considered justifiable since Nishiyama et al. had shown earlier that *in vivo* micro-CT is as reproducible as *ex vivo* micro-CT [19]. Eight mouse vertebrae (3 control, 5 loading) were chosen at random and measured 5 times each in the *in vivo* micro-CT scanner with repeated repositioning between the scans. The repeated scans thus corresponded to the last *in vivo* measurements

after 4 weeks and were registered to their respective initial scan. With this setup, parameters BFR^*_{BV}, BFR^*_{BS}, BRR^*_{BV}, BRR^*_{BS}, MAR*, MRR*, ES*, and MS* were calculated.

Precision errors (PEs) have been defined to best characterize the reproducibility of a given bone measurement technique [20]. Therefore, the new dynamic bone parameters were expressed both in absolute values and as coefficients of variation (%CV) of repeated measurements. As another measure of reproducibility, we calculated intraclass correlation coefficients (ICC). ICCs are quantitative measurements of how strongly units in the same group resemble each other. Values can lie between 0 and 1, where 1 denotes perfect reproducibility. The underlying ICC model was a two-way model that assumes randomly selected subjects and a fixed number of measurements, where the measurements are the only ones of interest. Furthermore, the confidence intervals (CIs) of PEs and ICCs were calculated using a Chi-squared distribution. A more detailed description about the definition of precision errors, intraclass correlation coefficients, and confidence intervals, as calculated in this study, can be found in Kohler et al. [21] or Mueller et al. [22].

Dynamic 3D morphometry in an *in vivo* animal model of bone adaptation

In a last step, the newly defined parameters were assessed for an *in vivo* loading model. For a direct comparison between loading and control treatment, a total of 17 mice (8 control, 9 loading) was used as described earlier. Trabecular bone formation and resorption rates were calculated as a mean over the whole duration of the experiment, i.e., a period of 4 weeks. Differences in dynamic parameters between loading and control treatment were assessed by an unpaired Student's t-test. Furthermore, differences between formation and resorption rates within one animal were calculated using pairwise Student's t-test and presented separately for control and loading animals. Differences in variances were calculated using an f-test. Furthermore, linear regression analysis correlating the newly defined parameters with changes after 4 weeks in standard structural indices such as bone volume density (BV/TV), bone volume (BV), specific bone surface (BS/BV), bone surface (BS), trabecular thickness (Tb.Th), trabecular spacing (Tb.Sp), and trabecular number (Tb.N) was performed. This step was necessary to verify the independency of the newly defined dynamic bone morphometry parameters.

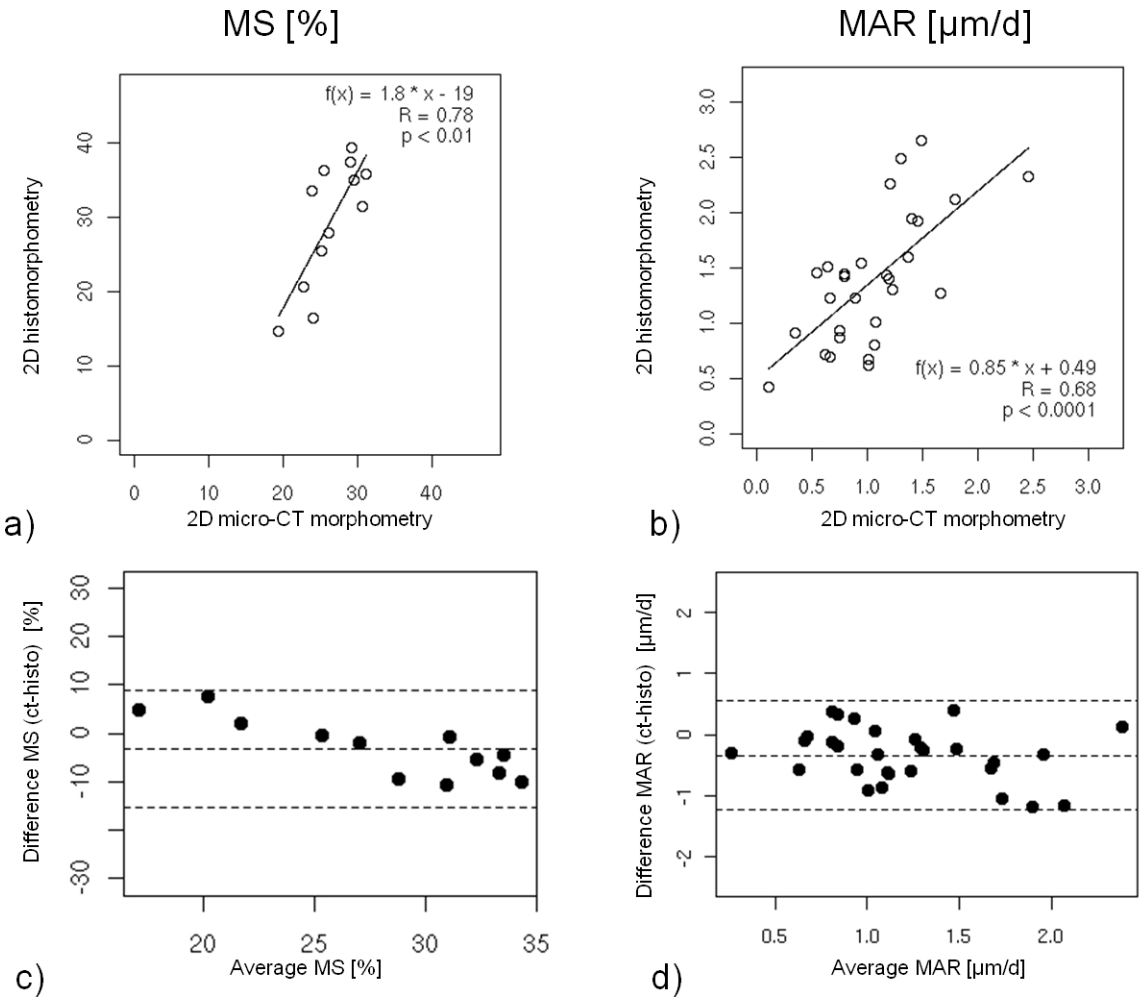

Figure 3.7: Linear regression curves of MS (a) and MAR (b) as calculated from 2D histomorphometry and corresponding micro-CT slices. MS was correlated between corresponding slices, whereas MAR was correlated for paired double labels. Panels c and d represent the actual data graphically in a Bland-Altman plot. The three lines denote the mean of the difference ± 1.96 times the standard deviation.

3.2.3 Results

2D comparison of micro-CT and histomorphometry bone formation parameters

The new visualization technique via micro-CT images allows the simultaneous illustration of formation and resorption sites. Fig. 3.6a (i) shows the 'error' between two reproducibility scans, whereas Fig. 3.6a (ii) and (iii) denote the changes in a control and a loaded animal after 4 weeks. For comparison, Fig. 3.6b presents a trabecular region labeled with calcein staining (i) and labeled with the newly developed micro-CT technique (ii) after 7 days. Yellow regions in the micro-CT image correspond to calcein-labeled regions in the histological slice. Blue regions in the micro-CT image denote resorbed bone areas, which cannot be directly visualized by means of histology. Quantitative correlation of MS and MAR, as calculated semi-automatically from histological slices and the corresponding micro-CT slices, is presented in Fig. 3.7. The 12 correlation points in Fig. 3.7a correspond to the 12 samples in the animal study ($R=0.78$, $p<0.01$). MAR was assessed per double label visible in both representations (29 data points) and correlated with $R=0.68$ ($p<0.0001$) as illustrated graphically in Fig. 3.7b. While it is commonly accepted to access the validity of a new technique by comparison against some type of gold standard, in this case, the gold standard might not really be valid in that there is appreciable scatter with standard histology. For this reason, the actual data are additionally shown in a Bland-Altman diagram in Fig. 3.7c and d (MS and MAR) where the difference between both techniques is plotted on the y-axis and the actual values, on the x-axis. As can be seen, the histomorphometric values are systematically higher than micro-CT-derived values. Furthermore, the Bland-Altman plots show that the degree of fluctuation is smaller for MS than for MAR. Nevertheless, a significant correlation exists in the Bland-Altman plot comparing histomorphometric and micro-CT derived MS ($R=0.84$). This can probably be best explained by the difference in image resolution between the two techniques.

Comparison of 2D and 3D micro-CT bone formation parameters

The correlation between directly and indirectly (=MAR*MS) calculated 3D BFR* is presented in Fig. 3.8a ($R=0.98$; $p<0.0001$). Indirectly calculated BFR* is systematically higher than directly assessed BFR* and can be described by the function

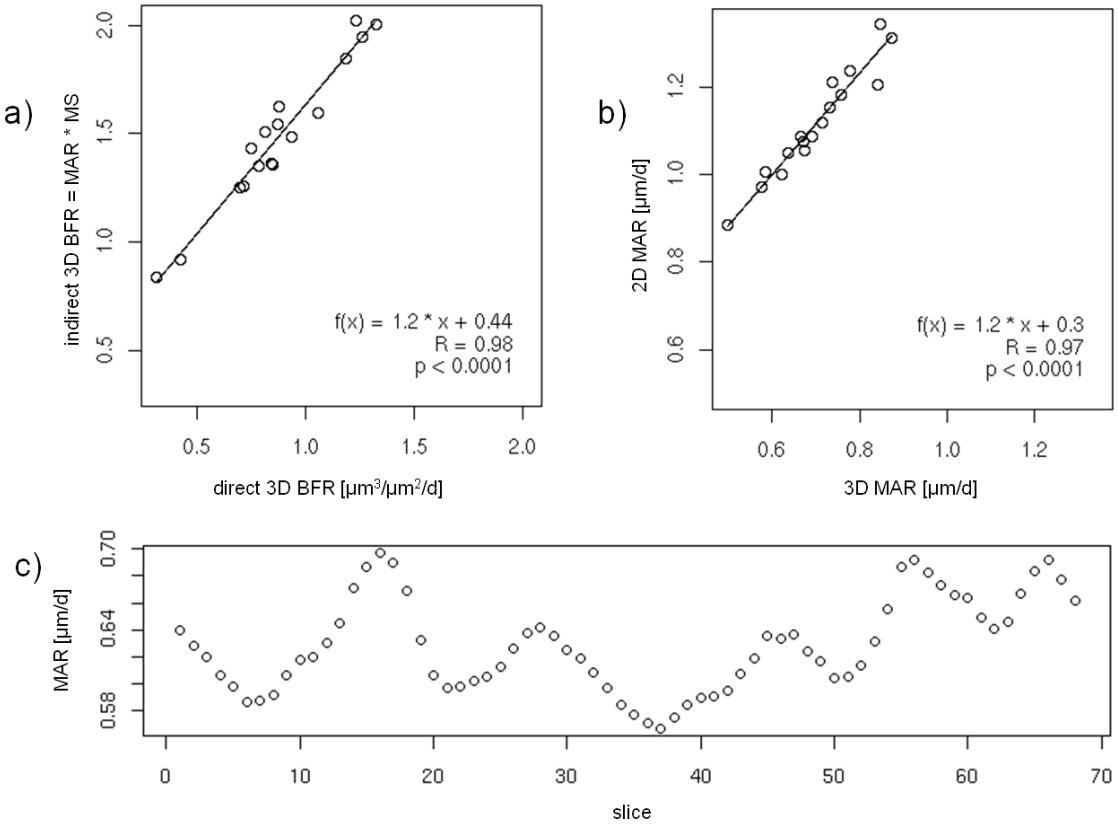

Figure 3.8: (a) Correlation curve of direct 3D BFR^*_{BV} and indirect 3D BFR^*_{BV} calculated from 3D MAR* and 3D MS*. (b) Correlation curve of 2D MAR* calculated as the mean of 2D MAR* in each sample compared to directly calculated 3D MAR*. (c) Variation of MAR* in one animal through the inner 50% of trabecular sagittal slices.

$f(x) = 1.2 * x + 0.4$. 2D and 3D MAR* correlate with R=0.97 (p<0.0001), where 3D MAR* can be derived from 2D MAR* as a function $f(x) = 1.2 * x + 0.3$ (see Fig. 3.8b). This is in accordance with the scaling factor of 1.2 proposed by Birkenhager-Frenkel et al. [17]. 2D MAR* was calculated in each animal by taking the mean of 2D MAR* over all slices. While the analysis in histology is usually constrained to one or a few slices per sample, the 3D analysis with micro-CT allows the determination of the coefficient of variation (%CV) through consecutive slices. As an example, the variation in MAR* was calculated and visualized in a single sample (Fig. 3.8c). In this sample, %CV amounted to 7.9%.

Table 3.3: Reproducibility of 3D dynamic morphometry.

Parameter	Mean	PE_{SD}	$PE_{\%CV}$ (%)	$CI_{95\%}PE_{\%CV}$	ICC	$CI_{95\%}ICC$
MAR* [μm/d]	0.82	0.012	1.75	1.40-2.31	0.991	0.976-0.998
MRR* [μm/d]	0.98	0.008	0.92	0.74-1.21	0.999	0.998-1.000
MS* [%]	61.34	0.742	1.17	0.94-1.54	0.989	0.970-0.998
ES* [%]	19.21	0.810	5.04	4.05-6.67	0.965	0.908-0.992
BFR^*_{BV} [%/d]	1.23	0.022	2.40	1.93-3.17	0.995	0.985-0.999
BRR^*_{BV} [%/d]	0.41	0.011	6.58	5.29-8.70	0.998	0.996-1.000
BFR^*_{BS} [$\mu m^3/\mu m^2$/d]	0.33	0.006	2.40	1.93-3.17	0.996	0.989-0.999
BRR^*_{BS} [$\mu m^3/\mu m^2$/d]	0.11	0.003	6.58	5.29-8.70	0.999	0.996-1.000

Reproducibility

The precision errors $PE_{\%CV}$ of the newly defined formation and resorption parameters ranged from 0.92% (MRR*) to 6.58% (BRR*). ICCs were lying in a range of 0.965 (ES*) and 0.999 (MRR*, BRR^*_{BS}). A full overview of mean values, PE_{SD}, $PE_{\%CV}$, ICCs, as well as the 95% CIs for $PE_{\%CV}$ and ICC is given in Table 3.3. $PE_{\%CV}$ for formation parameters had values from 1.17% (MS*) to 2.40% (BFR*), which was lower than $PE_{\%CV}$ for resorption parameters ranging from 0.92% (MRR*) to 6.58% (BRR*). Fig. 3.9a displays the regression analysis for BV/TV and ES* as calculated from each of the 40 reproducibility scans. Each cluster belongs to one of the eight animals and consists of 5 repeated measurement points. Despite the good correlation, the clusters are still well distinguishable. Given the fact that variation between animals and between groups was an order of magnitude larger than the precision errors, the newly introduced parameters can be considered highly reproducible.

Dynamic 3D morphometry in an *in vivo* animal model of bone adaptation

In a last step, the newly defined 3D formation and resorption parameters were applied to an experimental animal model. Furthermore, to see which indices might have the potential for giving new information beyond structural indices, we performed linear regressions with the %changes in BV/TV, BV, BS/BV, BS, Tb.Th, Tb.N, and Tb.Sp from week 0 to week 4 as independent variables. The full results are presented in Table 3.4. The highest correlation values between dynamic indices

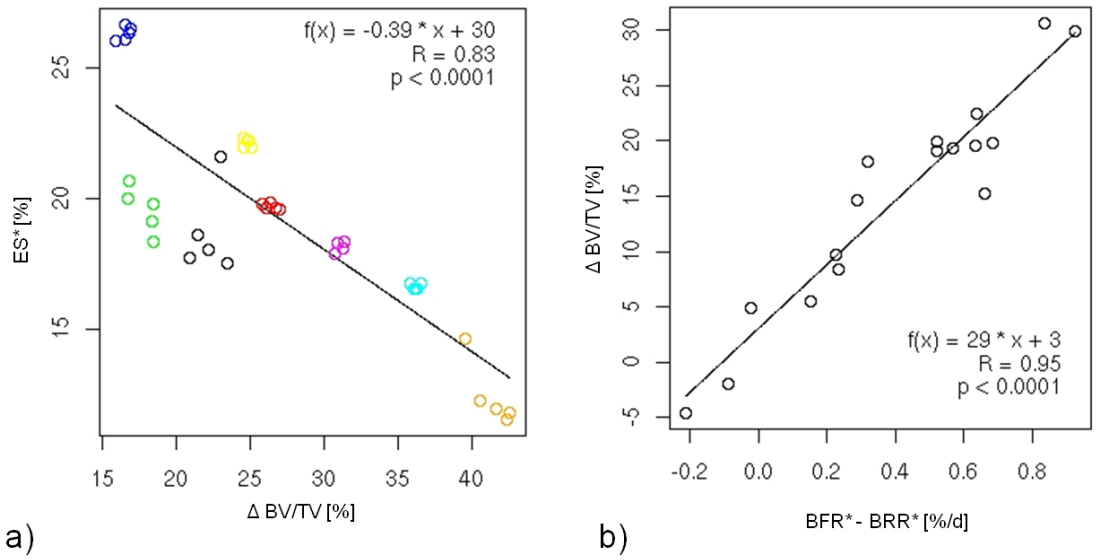

Figure 3.9: (a) Significant correlation between ΔBV/TV [%] and ES* [%] with underlying data being the total of 40 reproducibility scans. Despite a good correlation, the 8 clusters belonging to the 8 measured animals are still well distinguishable and the 5 repeat measurements per animal lie close together. (b) Significant correlation between BFR*-BRR* [%/d] and ΔBV/TV [%]. This correlation is higher than any single new parameter correlated with changes in the established morphometric indices.

and changes in static morphometric indices were found for MS* and BFR* (up to R=0.88), and the lowest correlation values, for MRR* and BRR* (up to R=0.62). This step was necessary to show if the dynamic indices contain unique information and cannot be substituted by changes in static morphometric indices. In comparison to correlations of the individual new parameters, the regression line of %change in BFR* minus BRR* and ΔBV/TV was also plotted and correlated with R=0.95 (see Fig. 3.9b). As can be noted, BFR* minus BRR* is constantly lower than ΔBV/TV (Fig. 3.9b and Table 3.4). The volumes of formed and resorbed bone are by definition enclosed by the lowest possible triangulated surface. With this definition, it was ensured that the volumes being considered formed or resorbed bone volumes were under no circumstances overestimated.

Table 3.4: Correlation coefficients R between dynamic morphometry and changes in static structural indices calculated between week 0 and week 4.

Parameter	ΔBV/TV	ΔBV	ΔBS/BV	ΔBS	ΔTb.Th	ΔTb.N	ΔTb.Sp
MAR*	n.s.	n.s.	0.57^a	n.s.	0.68^a	n.s.	n.s.
MRR*	n.s.	n.s.	n.s.	n.s.	n.s.	n.s.	n.s.
MS*	0.87^a	0.80^a	0.84^a	n.s.	0.81^a	n.s.	n.s.
ES*	0.85^a	0.73^a	0.78^a	n.s.	0.68^a	n.s.	n.s.
BFR^*_{BV}	0.70^a	0.64^a	0.82^a	n.s.	0.88^a	n.s.	n.s.
BRR^*_{BV}	0.51^a	n.s.	n.s.	n.s.	n.s.	0.49^a	0.51^a

$^a p < 0.05$

Qualitative differences between a loaded and a control mouse are illustrated in Fig. 3.10. This figure shows the 3D extent of formation sites (in yellow) and resorption sites (in blue) in the trabecular compartment after 4 weeks. The loaded vertebra shows more formation sites than the control one, but resorption is still ongoing despite the mechanical loading regime. Quantitative differences are shown in Table 3.5 and Figs. 3.11 and 3.12. Table 3.5 contains the mean and standard deviation of the static and dynamic morphometric indices after 4 weeks of control or loading treatment. As can be seen in Fig. 3.11, BFR* and MS* were significantly

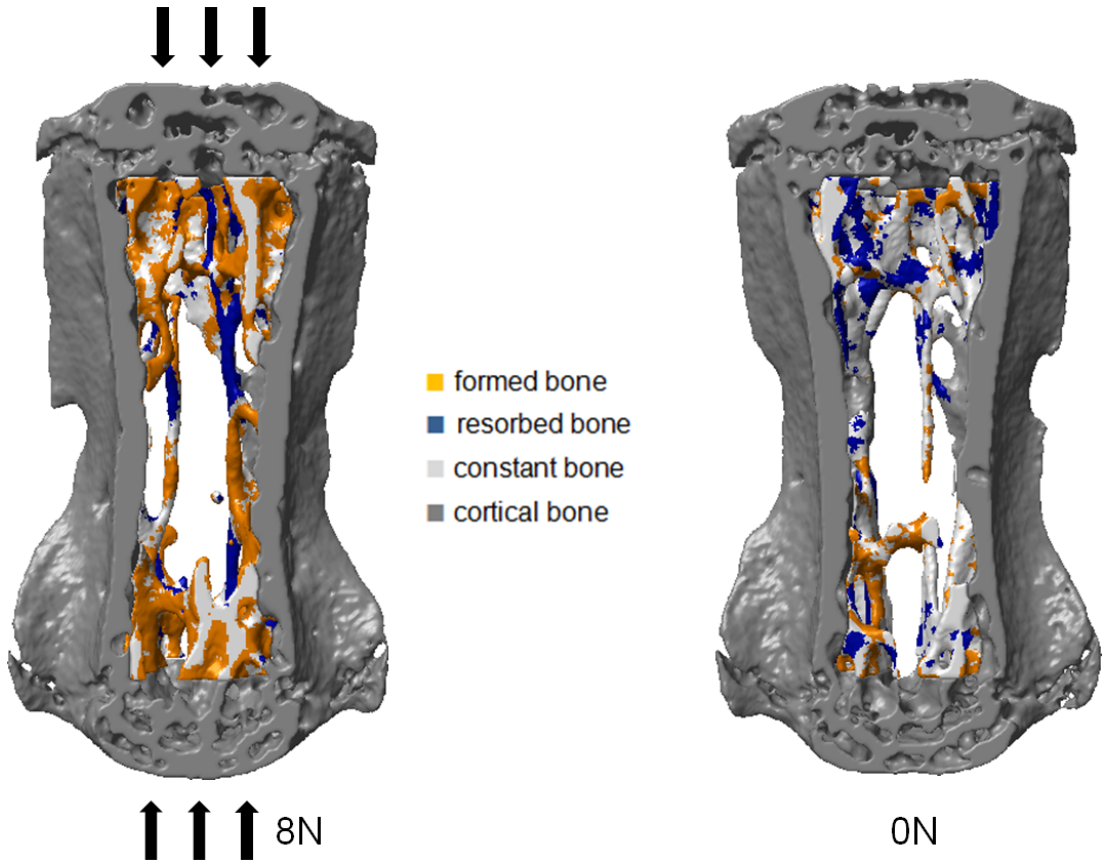

Figure 3.10: Three-dimensional visualization of formation and resorption sites in the trabecular compartment of a loaded (left) and a control (right) animal after 4 weeks. Yellow areas denote formation, and blue areas, resorption. The loaded vertebra shows more formation sites than the control one, but resorption is still ongoing despite the mechanical loading regime.

higher in the loading group than in the control group ($p<0.01$) after 4 weeks. At the same time, ES* was significantly decreased ($p<0.01$). In general, it was found that the bone resorption parameters showed less variation in the loading group than in the control group, where standard deviations for BFR*, ES*, and MS* were significantly lower after 4 weeks of loading compared to the control group (Table 3.5). This implies that mechanical loading is characterized primarily by an increase in formation sites, but not in the thickness of formed bone areas. At the same time, more control is exerted in the resorption cycles, indicated by the significantly decreased variances in bone resorption rates (Table 3.5).

Second, the average differences between formation and resorption parameters within each individual animal were compared (Fig. 3.12). While BFR* and BRR* were not significantly different in the control group, BFR* was significantly higher than BRR* in the loaded group ($p<0.0001$). MAR* was significantly lower than MRR* in both the control group ($p<0.01$) and the loading group ($p<0.0001$). In contrast, MS* was significantly higher than ES* in both the control group and the loading group ($p<0.0001$). These results imply that already during normal remodeling, formation takes place by many thin layers of formed bone packets, while resorption is characterized by few but deep resorption sites.

3.2.4 Discussion

In the present study, we introduced a non-destructive 3D technique to extract bone formation parameters (BFR, MS, and MAR) from time-lapsed *in vivo* micro-CT images. Furthermore, a direct assessment of time-dependent bone resorption parameters (BRR, ES, and MRR) was presented for the first time.

As with every new technique that is introduced to calculate previously well-defined and validated parameters, it needs to be shown that the new technique yields very similar results to the established method. Furthermore, its reproducibility and sensitivity need to be investigated. We therefore performed linear regressions for established bone formation parameters such as MAR and MS, which resulted in a good agreement between histology and micro-CT ($R=0.68$ and 0.78). The coefficients of correlation were comparable to values found in the literature comparing traditional static bone morphometric indices such as BV/TV, Tb.Th, Tb.N, etc. ranging from $R=0.60$ to 0.98 [23–26]. Reproducibility errors $PE_{\%CV}$ lie in the same range as $PE_{\%CV}$ that were reported for established bone morphometric parameters (0.94% -

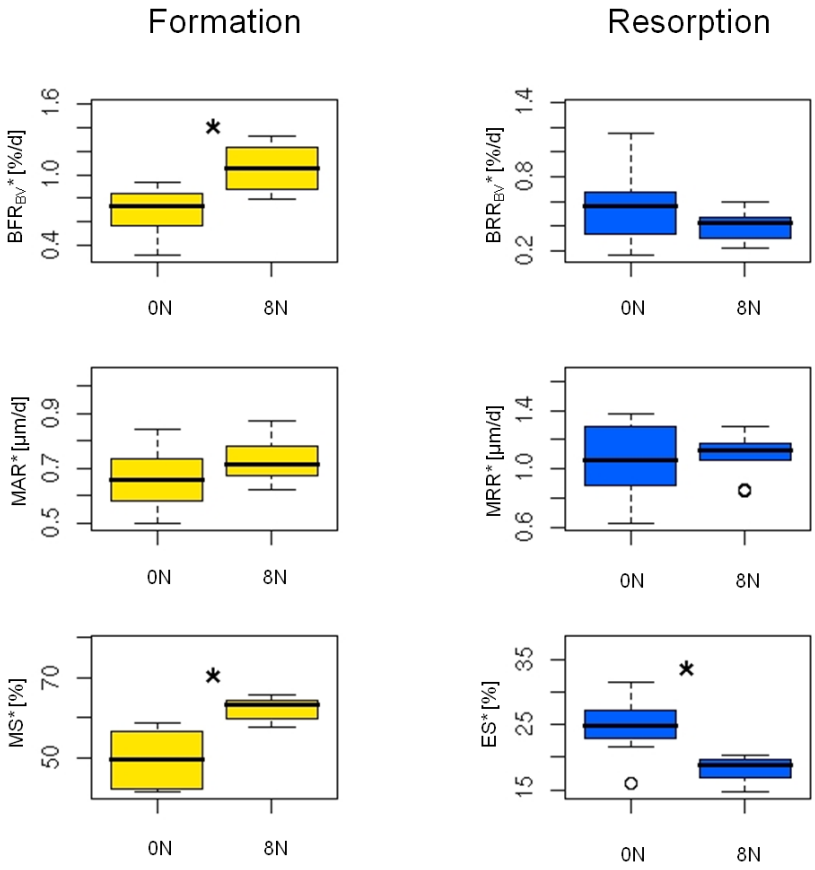

Figure 3.11: Boxplots showing the differences between (a) loading (8 N) and control (0 N) group. The bottom and top of the box represent the 25^{th} and 75^{th} percentile with the median (band near the middle of the box). The extremes of the whiskers extend to 1.5 times the interquartile range of the data. Any data not included between the whiskers are plotted as an outlier with a small circle in the boxplot (*p<0.01; **p<0.001; ***p<0.0001).

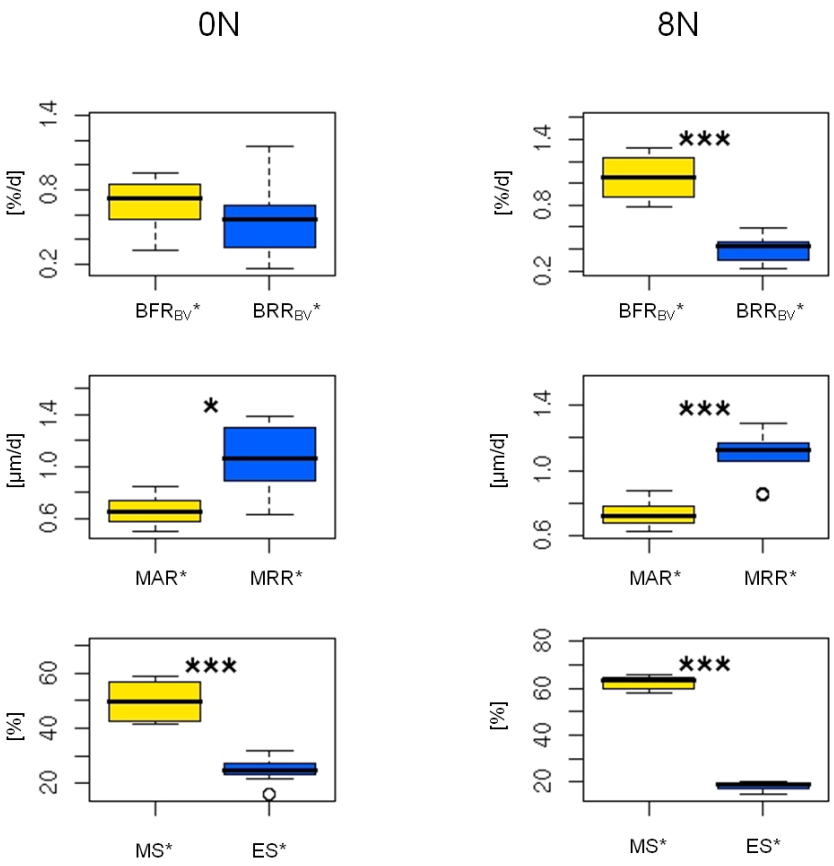

Figure 3.12: Boxplots showing the differences between formation and resorption parameters as calculated for each animal separately. The bottom and top of the box represent the 25^{th} and 75^{th} percentile with the median (band near the middle of the box). The extremes of the whiskers extend to 1.5 times the interquartile range of the data. Any data not included between the whiskers are plotted as an outlier with a small circle in the boxplot (*p<0.01; **p<0.001; ***p<0.0001).

Table 3.5: Mean values of control and loading mice calculated by means of *in vivo* micro-computed tomography.

Parameter	Mean, 0N	Mean, 8N	SD, 0N	SD, 8N
ΔBV/TV [%]	7.08	21.58^a	8.08	5.26
ΔTb.Th [%]	5.40	13.43^a	4.49	3.60
ΔTb.N [%]	-0.70	0.74	3.06	4.94
MAR* [μm/d]	0.66	0.74	0.11	0.08
MRR* [μm/d]	1.06	1.09	0.27	0.16
MS* [%]	49.76	62.55^a	7.79	2.87^a
ES* [%]	24.72	18.14^a	4.63	1.86^a
BFR^*_{BV} [%/d]	0.69	1.05^a	0.22	0.21
BRR^*_{BV} [%/d]	0.55	0.40	0.31	0.12^a
BFR^*_{BS} [$\mu m^3/\mu m^2$/d]	0.18	0.28^a	0.06	0.05
BRR^*_{BS} [$\mu m^3/\mu m^2$/d]	0.15	0.11	0.08	0.03^a

$^a p < 0.05$

8.40%) [19] and are far lower than the reproducibility errors reported in histomorphometry (8.5% (MAR) - 40% (ES)), mostly related to inter-observer variations [6]. When comparing the ranges of MAR*, BFR*, MS*, and ES* to the ranges reported in literature, a good agreement was found. In general, there are values reported from 0.40 to 2.13 μm/d for MAR, 0.04 to 0.75 $\mu m^3/\mu m^2$/d for BFR_{BS}, 11.11 to 54.90% for MS, and 8.10 to 32.00% for ES at various trabecular sites in C57BL/6 control mice [9, 27–32]. By comparison, our results for the control group yielded values of 0.66 μm/d for MAR*, 0.18 $\mu m^3/\mu m^2$/d for BFR^*_{BS}, 49.8% for MS*, and 24.7% for ES* (see Table 3.5).

Compared to histomorphometry, the direct parameters are extracted non-invasively. This also allows longer periods of investigation in contrast to histology, where label resorption usually restricts the applied time interval. Dynamic bone morphometry can be applied to longitudinal studies, which aim at comparing the temporal changes in dynamic parameters, e.g., before and after treatment, whereas with histology, animals would have to be sacrificed at multiple points in time. Our method reduces the number of animals required in an experiment. The new parameters include 3D information of the whole compartment, instead of only one

or a few random 2D slices. Furthermore, the fully automatic character of the new technique does not only save manpower but also alleviates the inter-observer and intra-observer errors, which are considered problematic in histomorphometry [33].

However, the most important advantage of the new quantification method may be the direct assessment of time-dependent bone resorption rates. The quantification of bone resorption rates opens new ways of measuring changes between treatment groups in a quantitative manner. This will be advantageous especially in the study of diseases such as osteoporosis and its treatment.

Although resorption parameter ES already exists in histology, it was refrained from a direct comparison. ES in histology can be seen as a snapshot measuring the momentary activity of osteoclasts. The high resolution of histological slices allows identification of single resorption cavities. However, there is no predefined temporal starting point in histology such as calcein labels for formation indices. On the other hand, ES* calculated from micro-CT images is defined as the direct counterpart to Mineralizing Surface and returns the net resorption over a certain time period. Therefore, a direct comparison would result in comparing two different quantities and did not seem appropriate.

A general limitation of the presented method is the current image resolution of *in vivo* scanners. In histomorphometry, short time periods can be addressed giving insight into the activity of particular bone cells; this is not possible with the micro-CT technique. Here, the minimum time interval is dependent on the voxel size of the imaging system. As an example, if MAR is expected to be around 1 μm per day with current image resolution at 10.5 μm, a considered period of 7 days will actually yield formation values below image resolution. For the underlying mechanical loading data, the authors found a time interval of 7 days to be sufficient for a voxel size of 10.5 μm. This was verified by the good correlation between histomorphometry and micro-CT morphometry. Nevertheless, it is very likely that a higher image resolution would lead to even higher reproducibility and thus even better reliability of the new 3D technique. For this reason, it would not be necessary but advantageous in terms of reliability for the present time interval to go smaller on voxel size. However, no *in vivo* scanner with higher voxel size is on the market today.

Bland-Altman plots (Fig. 3.7c and d) demonstrated that micro-CT derived values are systematically lower than the values from histology. These differences can

probably be best explained by the difference in image resolution between micro-CT and histology. On the other side, histology only captures double labels if bone has grown over the full period of 7 days, while the micro-CT technique also displays areas where bone has grown within for example 5 days, but the value for MAR is still divided by the full period of 7 days and thus underestimated. Bone tissue that has only grown for 1 day is not represented in the micro-CT representation, leading to a systematic underestimation of MS. The significant correlation of the Bland-Altman plot of MS (Fig. 3.8c) demonstrates the resolution dependency. Very low values of MS* are underestimated and higher values overestimated with respect to histomorphometric results for MS. These resolution-dependent problems could be circumvented by a larger period of investigation.

For this reason, the micro-CT technique is better suited as a long-term technique, while histomorphometry remains the method of choice for investigation of short time periods and the activity of particular individual bone cells (e.g., osteoblast and osteoclast number, osteoid surfaces and thickness, etc). In consequence to the above-mentioned limitations, the micro-CT technique quantifies the outcome of formation and resorption as an average over a certain period of time and thus returns the mean of total formation and resorption activity but not the behavior of particular bone cells.

In conclusion, we present a non-invasive, direct, 3D, fully automated quantification procedure for dynamic bone morphometry by means of time-lapsed *in vivo* micro-computed tomographic images. This technique facilitates the access to dynamic bone changes during *in vivo* experiments and allows, for the first time, new insight into time-dependent bone resorption rates. Using this technique, we showed that mechanical loading leads to an increase in bone formation rates mainly caused by increased sites of bone formation, not the width of formed bone areas. At the same time, mechanical loading results in a more controlled process of bone resorption cycles. With these results, we conclude that non-invasive extraction of dynamic bone morphometry has great potential in improving our understanding of the interplay between the different cell types involved during the modeling and remodeling of bone.

Acknowledgements

The authors would like to thank Dr. Brigitte von Rechenberg from the Musculoskeletal Research Unit of Vetsuisse Faculty, University of Zurich, Zurich, Switzerland, for the generous offer to use their histology laboratory equipment, and Sabina Wunderlin for cutting the histological samples. Furthermore, the authors thank Dr. Itai Bab for helpful discussions with regard to the transfer from histomorphometric to micro-CT parameters, as well as Drs. Heike Hall, Duncan Webster, and Elad Wasserman for practical advice and for the introduction to the microscope and quantitative histomorphometric analysis. Funding from the European Union for the osteoporotic virtual physiological human project (VPHOP FP7-ICT2008-223865) is gratefully acknowledged.

References

[1] H. M. Frost. Skeletal structural adaptations to mechanical usage (satmu): 1. redefining wolff's law: the bone modeling problem. *Anat Rec*, 226(4):403–13, 1990.

[2] H. M. Frost. Skeletal structural adaptations to mechanical usage (satmu): 2. redefining wolff's law: the remodeling problem. *Anat Rec*, 226(4):414–22, 1990.

[3] A. M. Parfitt. Trabecular bone architecture in the pathogenesis and prevention of fracture. *Am J Med*, 82(1B):68–72, 1987.

[4] J. P. Roux, M. E. Arlot, E. Gineyts, P. J. Meunier, and P. D. Delmas. Automatic-interactive measurement of resorption cavities in transiliac bone biopsies and correlation with deoxypyridinoline. *Bone*, 17(2):153–6, 1995.

[5] C. Minkin. Bone acid phosphatase: tartrate-resistant acid phosphatase as a marker of osteoclast function. *Calcif Tissue Int*, 34(3):285–90, 1982.

[6] J. E. Compston, S. Vedi, and A. J. Stellon. Inter-observer and intra-observer variation in bone histomorphometry. *Calcif Tissue Int*, 38(2):67–70, 1986.

[7] C. D. Wright, S. Vedi, N. J. Garrahan, M. Stanton, S. W. Duffy, and J. E. Compston. Combined inter-observer and inter-method variation in bone histomorphometry. *Bone*, 13(3):205–8, 1992.

[8] J. H. Waarsing, J. S. Day, J. C. van der Linden, A. G. Ederveen, C. Spanjers, N. De Clerck, A. Sasov, J. A. N. Verhaar, and H. Weinans. Detecting and tracking local changes in the tibiae of individual rats: a novel method to analyse longitudinal in vivo micro-ct data. *Bone*, 34(1):163–169, 2004.

[9] D. Webster, E. Wasserman, M. Ehrbar, F. Weber, I. Bab, and R. Müller. Mechanical loading of mouse caudal vertebrae increases trabecular and cortical bone mass-dependence on dose and genotype. *Biomech Model Mechanobiol*, 9(6):737–47, 2010.

[10] D. J. Webster, P. L. Morley, G. H. van Lenthe, and R. Müller. A novel in vivo mouse model for mechanically stimulated bone adaptation - a combined experimental and computational validation study. *Comput Methods Biomech Biomed Engin*, 11(5):435–441, 2008.

[11] K. A. Powell, L. Latson, M. O. Ibiwoye, A. Wolfman, M. D. Grabiner, M. Zborowski, Y. Sakai, and R. J. Midura. In vivo longitudinal assessment of bone resorption in a fibular osteotomy model using micro-computed tomography. *Iowa Orthop J*, 25:123–8, 2005.

[12] J. E. M. Brouwers, B. van Rietbergen, R. Huiskes, and K. Ito. Effects of pth treatment on tibial bone of ovariectomized rats assessed by in vivo micro-ct. *Osteoporos Int*, 20(11):1823–35, 2009.

[13] S. K. Boyd, S. Moser, M. Kuhn, R. J. Klinck, P. L. Krauze, R. Müller, and J. A. Gasser. Evaluation of three-dimensional image registration methodologies for in vivo micro-computed tomography. *Ann Biomed Eng*, 34(10):1587–99, 2006.

[14] P. Thevenaz, U. E. Ruttimann, and M. Unser. A pyramid approach to subpixel registration based on intensity. *IEEE Trans Image Process*, 7(1):27–41, 1998.

[15] P. Thevenaz, T. Blu, and M. Unser. Interpolation revisited. *IEEE Trans Med Imaging*, 19(7):739–58, 2000.

[16] T. Hildebrand, A. Laib, R. Müller, J. Dequeker, and P. Rüegsegger. Direct three-dimensional morphometric analysis of human cancellous bone: microstructural data from spine, femur, iliac crest, and calcaneus. *J Bone Miner Res*, 14(7):1167–1174, 1999.

[17] D. H. Birkenhager-Frenkel and J. C. Birkenhager. Bone appositional rate and percentage of doubly and singly labeled surfaces: comparison of data from 5 and 20 microns sections. *Bone*, 8(1):7–12, 1987.

[18] T. Kohler, M. Stauber, L. R. Donahue, and R. Müller. Automated compartmental analysis for high-throughput skeletal phenotyping in femora of genetic mouse models. *Bone*, 41(4):659–667, 2007.

[19] K. K. Nishiyama, G. M. Campbell, R. J. Klinck, and S. K. Boyd. Reproducibility of bone micro-architecture measurements in rodents by in vivo microcomputed tomography is maximized with three-dimensional image registration. *Bone*, 46(1):155–61, 2010.

[20] C. C. Glüer, G. Blake, Y. Lu, B. A. Blunt, M. Jergas, and H. K. Genant. Accurate assessment of precision errors: how to measure the reproducibility of bone densitometry techniques. *Osteoporos Int*, 5:262–270, 1995.

[21] T. Kohler, M. Beyeler, D. Webster, and R. Müller. Compartmental bone morphometry in the mouse femur: reproducibility and resolution dependence of microtomographic measurements. *Calcif Tissue Int*, 77(5):281–290, 2005.

[22] T. L. Mueller, M. Stauber, T. Kohler, F. Eckstein, R. Müller, and G. H. van Lenthe. Non-invasive bone competence analysis by high-resolution pQCT: an in vitro reproducibility study on structural and mechanical properties at the human radius. *Bone*, 44(2):364–371, 2009.

[23] T. Uchiyama, T. Tanizawa, H. Muramatsu, N. Endo, H.E. Takahashi, and T. Hara. A morphometric comparison of trabecular structure of human ilium between microcomputed tomography and conventional histomorphometry. *Calcif Tissue Int*, 61(6):493–498, 1997.

[24] R. Müller, S. C. Gerber, and W. C. Hayes. Micro-compression: a novel technique for the nondestructive assessment of local bone failure. *Technol Health Care*, 6(5-6):433–444, 1998.

[25] I Tamminen, A Aula, H Isaksson, J S Jurvelin, and H Kröger. Metabolic status of human trabecular bone affects reproducibility and agreement of microct and histomorphometry. *36th European Symposium on Calcified Tissues, Vienna, Austria*, 44(2):P334, 2009.

[26] V. David, N. Laroche, B. Boudignon, M. H. Lafage-Proust, C. Alexandre, P. Ruegsegger, and L. Vico. Noninvasive in vivo monitoring of bone architecture alterations in hindlimb-unloaded female rats using novel three-dimensional microcomputed tomography. *J Bone Miner Res*, 18(9):1622–31, 2003.

[27] H. Zhou, A. Iida-Klein, S. S. Lu, M. Ducayen-Knowles, L. R. Levine, D. W. Dempster, and R. Lindsay. Anabolic action of parathyroid hormone on cortical and cancellous bone differs between axial and appendicular skeletal sites in mice. *Bone*, 32(5):513–20, 2003.

[28] M. H. Sheng, D. J. Baylink, W. G. Beamer, L. R. Donahue, K. H. Lau, and J. E. Wergedal. Regulation of bone volume is different in the metaphyses of the femur and vertebra of c3h/hej and c57bl/6j mice. *Bone*, 30(3):486–91, 2002.

[29] J. C. Fritton, E. R. Myers, T. M. Wright, and M. C. van der Meulen. Bone mass is preserved and cancellous architecture altered due to cyclic loading of the mouse tibia after orchidectomy. *J Bone Miner Res*, 23(5):663–71, 2008.

[30] L. Machado do Reis, C. B. Kessler, D. J. Adams, J. Lorenzo, V. Jorgetti, and A. M. Delany. Accentuated osteoclastic response to parathyroid hormone undermines bone mass acquisition in osteonectin-null mice. *Bone*, 43(2):264–73, 2008.

[31] S. Itoh, F. Yoshitake, H. Narita, K. Ishihara, and S. Ebisu. Gab2 plays distinct roles in bone homeostasis at different time points. *J Bone Miner Metab*, 25(2):81–5, 2007.

[32] A. Iida-Klein, S. S. Lu, F. Cosman, R. Lindsay, and D. W. Dempster. Effects of cyclic vs. daily treatment with human parathyroid hormone (1-34) on murine bone structure and cellular activity. *Bone*, 40(2):391–8, 2007.

[33] E. Bonucci, P. Ballanti, C. Della Rocca, S. Milani, V. Lo Cascio, and B. Imbimbo. Technical variability of bone histomorphometric measurements. *Bone Miner*, 11(2):177–86, 1990.

Chapter 4

Local trigger for mechanotransduction

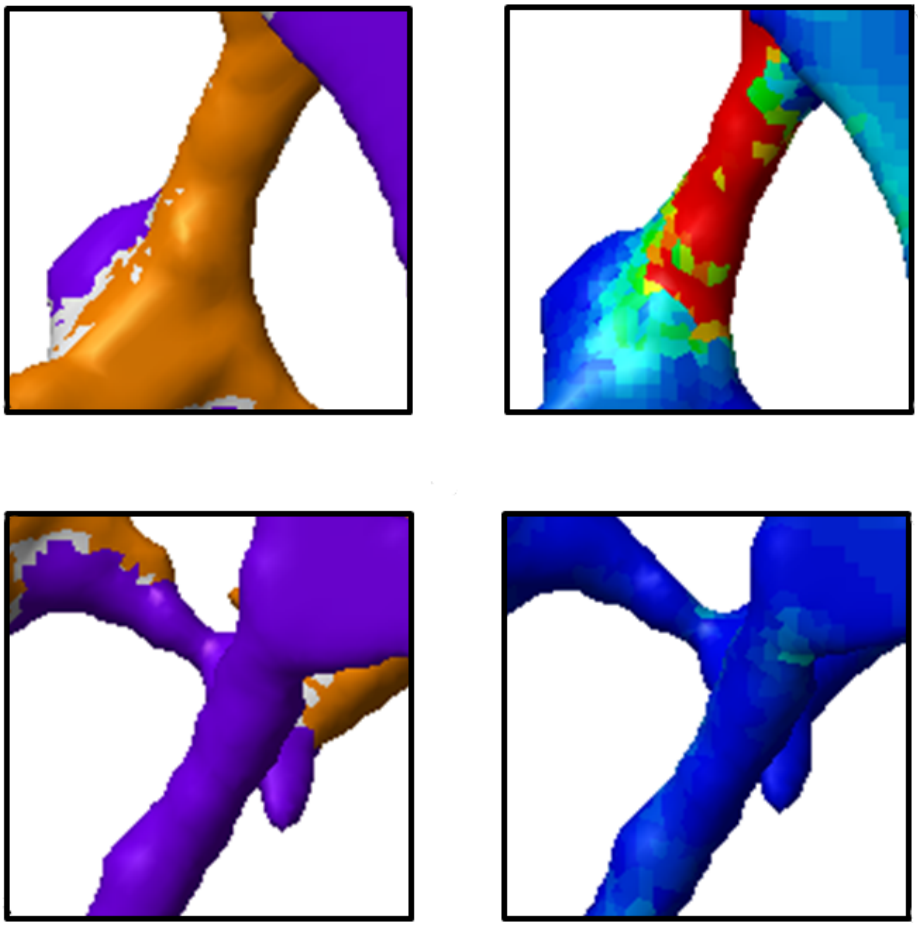

Local mechanical environment regulates osteoblast and osteoclast activity

Friederike A. Schulte[1], Davide Ruffoni[1], Floor M. Lambers[1], Gisela Kuhn[1], David Christen[1], Duncan J. Webster[1] and Ralph Müller[1]

[1]Institute for Biomechanics, ETH Zurich, Zurich, Switzerland

Abstract:

During life bone has the ability to adapt to changes in the loading environment [1,2] and to preserve its mechanical integrity [3,4]. Such remarkable features are based on a continuous remodeling process taking place at the cellular level by bone resorbing osteoclasts and bone forming osteoblasts [5]. It is well accepted that, at a global level, bone adaptation is mechanically controlled, as suggested by *in vivo* [6, 7] and *in vitro* [8, 9] studies. However, a quantitative proof of the link between local mechanical forces in the bone tissue and cell action is still missing. Here, we characterize the interplay between bone formation/resorption and mechanical stimuli in healthy and diseased states. Our approach combines three-dimensional *in vivo* micro-computed tomography measurements of bone formation and resorption in the caudal vertebrae of mice in response to defined mechanical loads [10, 11] and ovariectomy, with *in silico* evaluations of the corresponding local mechanical environments. Significant differences in strain energy density (SED) are found at sites of bone formation, quiescence and resorption, for both the healthy and estrogen deficiency state ($p<0.05$). By connecting the surface SED with the probabilities of subsequent formation/resorption events, we obtain for the first time an

experimentally derived quantitative biological formulation of the mechanical control of bone remodeling. Furthermore, our results show that the functioning of the mechanosensory system is transiently altered by estrogen removal. Most important, the measured pattern of formation, quiescence and resorption probabilities as a function of SED contradicts the common idea of a region at the cellular level (the so-called lazy zone [12, 13]) where the effects of bone formation and resorption are balanced. We believe that the new insight concerning the local regulatory mechanism will enhance our ability to understand the effects of physical activity, diseases, aging and pharmaceutical treatment on bone adaptation and maintenance.

Introduction

Shape, structure and material properties of most biological tissues often emerge in response to external environmental stimuli [14]. In living bone, the predominant physical stimulus which regulates bone mass, shape and internal micro-architecture, is most probably mechanical loading [2]. The ideas of functional adaptation and mechanical control of bone mass and architecture were introduced more than a century ago by Roux [15] and Wolff [16]. Based on those concepts, Frost [17, 18] proposed the so-called mechanostat theory, which states that bone keeps strain-levels within a given range by means of a mechanical feedback loop. This classical view suggests that tissue strains are constantly monitored and that bone formation occurs when strains are larger than a certain set point, while bone resorption only takes place when strains fall below another, lower set point. In between, there is a lazy zone where no net remodeling takes place. It has been proposed that various medications and hormonal changes may influence the values of these set points [19].

Although the mechanostat concept suitably explains both homeostasis and changes in bone mass at the organ-level [18], it presents a deterministic view where adaptation occurs in a completely predictable fashion. At the local cellular level, osteoblasts and osteoclasts are not only regulated by local mechanical forces but also by hormones and biological factors, which act independently of load. Other researchers [1, 15, 20] therefore proposed that bone adaptation is more realistically represented as a stochastic process where bone formation and resorption are described as probabilistic functions of mechanical stimuli. To capture this, phenomenological-

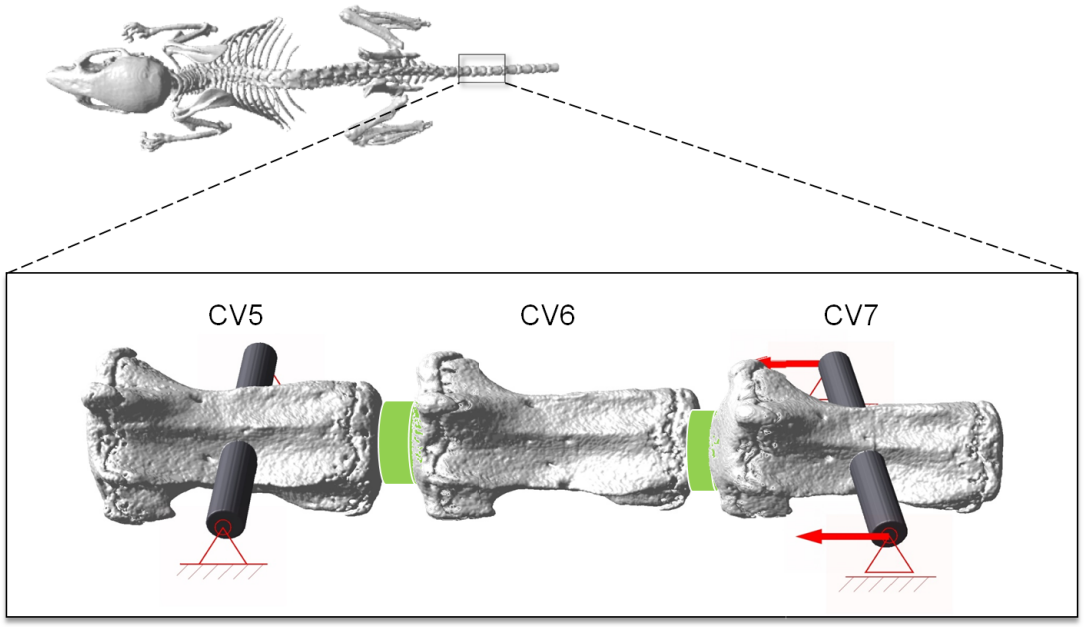

Figure 4.1: Experimental setup. The 6^{th} caudal vertebra (CV6) is cyclically loaded by a force of 8 N. Controlled application of the force is given through the pins inserted in the adjacent vertebrae (CV5 fixed, CV7 displaced).

based remodeling rules have been established.

Whilst the numerical implementations of the proposed theoretical frameworks have captured certain aspects of bone adaptation observed experimentally [1, 21–23], a realistic description of the mechanosensory system in term of remodeling rules based on experimental data is still missing.

Furthermore, it is not clear if and to which extent the mechanical control of bone remodeling at the tissue level changes in response to physical activity, bone diseases or after pharmaceutical treatments. With this study we first aimed to prove the existence of a control mechanism of bone formation and resorption at the local cellular level. Secondly, we investigated how the mechanism changes in a model of bone disease. Finally, we formulated a realistic description of local biological rules of bone remodeling.

Recently we have established a mouse model which permits the study of bone remodeling *in vivo* (Figure 4.1). Using this model we have shown trabecular bone in the 6^{th} caudal vertebra (CV6) to be responsive to mechanical loading in healthy C57BL/6 (B6) mice [7, 10]. Furthermore, in performing ovariectomy on B6 mice, we have also successfully replicated the bone deterioration seen in post-menopausal

osteoporosis [24]. In the work presented here, using time-lapsed *in vivo* micro-CT images, we correlate sites of local bone formation, resorption and quiescence with micro-finite element models of loaded and ovariectomized caudal vertebrae to characterize the relationship between cellular activity and the local mechanical environment for healthy and diseased states.

Materials and Methods

Animal procedures: Animals were purchased from RCC (Füllinsdorf, Switzerland). All experiments were carried out with the approval from the local animal care and use committee (Kantonales Veterinäramt Zürich, Zürich, Switzerland).

Mechanical loading: In vivo bone adaptation was induced in 15-week-old, female C57BL/6 mice by subjecting the sixth caudal vertebra (CV6) to mechanical loading at 8 N (loading; n=9) or 0 N (control; n=8) through pins inserted in the adjacent vertebrae 3 times per week for 4 weeks according to an established loading protocol [11]. The CV6 was scanned weekly with *in vivo* micro-CT (vivaCT 40, Scanco Medical, Brüttisellen, Switzerland) at an isotropic voxel resolution of 10.5 μm.

Ovariectomy: 15-week old C57BL/6 mice were ovariectomized (OVX, n=9) or sham operated (SHM, n=7). *In vivo* micro-CT scans of the sixth caudal vertebra were performed on the day of operation and consecutively every two weeks over a twelve-week period.

Finite element analysis: Three-dimensional micro-FE models were generated by directly converting all voxels of the micro-CT image to 8 node hexahedral elements, with each model consisting of approximately 1.8 million elements. A Young's modulus of 14.8 GPa, and a poisson's ratio of 0.3 were assigned [11]. Compressive static loads (8 N for loading, 0.1 N for control, OVX and SHM animals) were applied to the CV6 through simplified intervertebral disks. The models were solved with ParFE [25] (http://parfe.sourceforge.net) running at the Swiss National Supercomputing Centre (CSCS, Manno, Switzerland).

Statistics: Results are presented with mean ± standard error. Box plots include data from the 25^{th} to 75^{th} percentile. For all statistical analyses a two-tailed paired (within animal) or unpaired (between groups) Student's t-test with Bonferroni-correction was performed after testing for equal variance of sample by Kolmogorov-Smirnof test. Over time, two-tailed repeated measures ANOVA with Bonferroni-

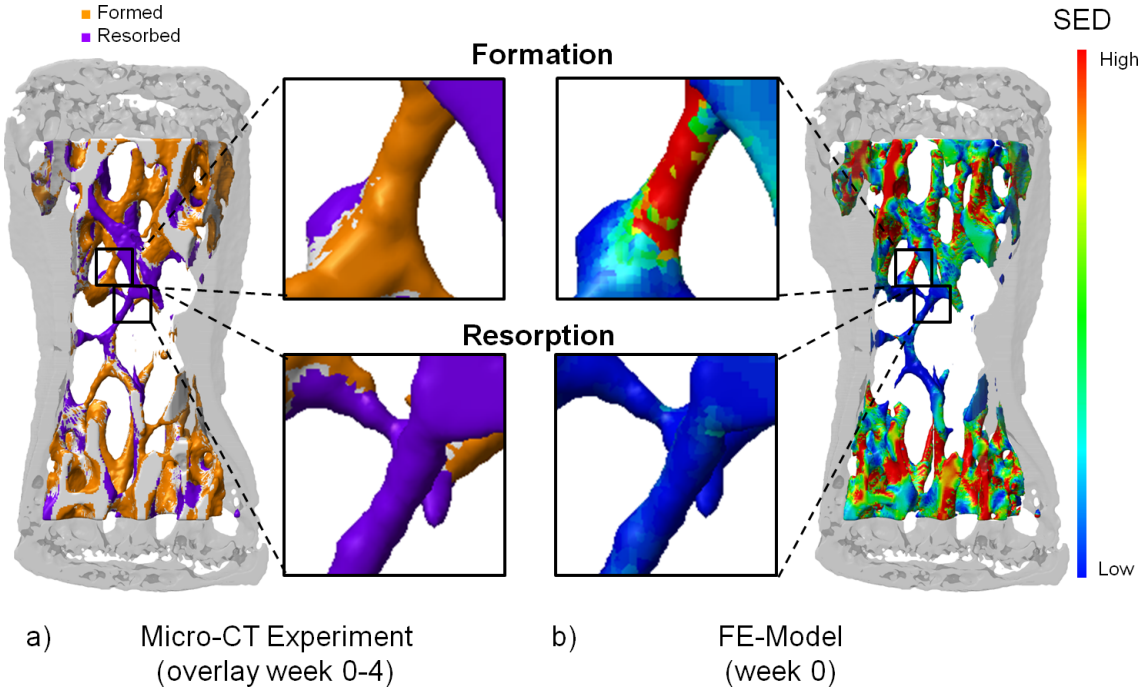

Figure 4.2: Comparison of local bone formation and resorption sites and mechanical stimulus. (a) Three-dimensional trabecular bone formation and resorption sites measured over 4 weeks, including a magnified view of formation and resorption sites for individual trabeculae. (b) Corresponding strain energy density (SED) prevailing at the time of basal scan. The same details as in (a) are enlarged, showing the corresponding SED-conditions. High strains (red) correspond to formation (yellow), while low strains (blue) are found at similar locations as bone resorption (purple).

correction for multiple comparisons was used. Statistics was calculated with the software package R [26]. $p < 0.05$ was considered significant.

Results

Bone formation and resorption sites were identified from superimposition of binary *in vivo* micro-CT scans of the same vertebra taken at different time points during each experiment (Figure 4.2a). The local mechanical environment, characterized by the SED was derived from micro-finite element (micro-FE) simulations of the baseline vertebra subjected to the experimental loading conditions (Figure 4.2b). To quantify the relationship between the local SED and cellular activity, each voxel on the bone surface was classified into either being formed (F), constant (C) or

resorbed (R). The mean value of the SED in each of these three groups was calculated from the baseline scan of each mouse. Initial, visual comparisons of local bone formation and resorption sites and the corresponding SED values suggested that high mechanical stimuli coincided with bone formation and low mechanical stimuli with bone resorption, respectively (Figure 4.2). Mechanical loading of CV6 led to a significant increase in the trabecular bone volume fraction (BV/TV) after four weeks of experiment compared to the control group (19.5%, n=17, repeated measures ANOVA, $p<0.0001$, Figure 4.3a, b). Comparison between remodeling sites and mechanical environment took place on a weekly format. Mean SED at formation sites was 13.7±4.5% higher than mean SED at constant sites ($p<0.0001$) and, at the same time, mean SED at resorption sites was 22.8±3.4% lower than mean SED at constant sites (Student's t-test with Bonferroni-correction; $p<0.0001$; Figure 4.3c) with respect to the first week of experiment. The same mechanobiological analysis performed over the following week-intervals, i.e. from week 1 to 2, 2 to 3 and 3 to 4, led to a similar result (both $p<0.0001$, repeated measures ANOVA with Bonferroni-correction). The same pattern was observed in the animals of the control group (n=8), assuming a much lower load due to everyday activity: mean SED at locations of bone formation was 13.9±7.6% higher and mean SED at resorption sites was 16.4±6.1% lower in comparison to mean SED at constant surfaces (repeated measures ANOVA with Bonferroni-correction; $p<0.0001$ and $p<0.05$, Figure 4.3d). Furthermore, no significant differences between loaded and control group were found in the percentage differences of SED from constant level at formation/resorption locations (repeated measures ANOVA, both $p>0.05$). These findings indicate that both osteoblastic and osteoclastic activities are controlled by local mechanical stimuli and the same mechanism which allows bone to adapt to changes in the loading environment seems to control also bone remodeling in daily loading.

Next, we investigated to which extent pathological variations in the hormonal levels interfere with the local regulatory mechanism of bone remodeling. After performing ovariectomy (OVX), a significant loss of BV/TV was measured due to estrogen deficiency in the CV6 compared to the SHM group (31.7%; n=16; repeated measures ANOVA; $p<0.0001$; Figure 4.3e, f). In this experiment the remodeling sites were quantified within 2-week-intervals and the same low load as in the control animals was assumed to calculate SED values. By comparing mean SED with remodeling locations, evidence of local mechanical regulation was found also in the diseased state.

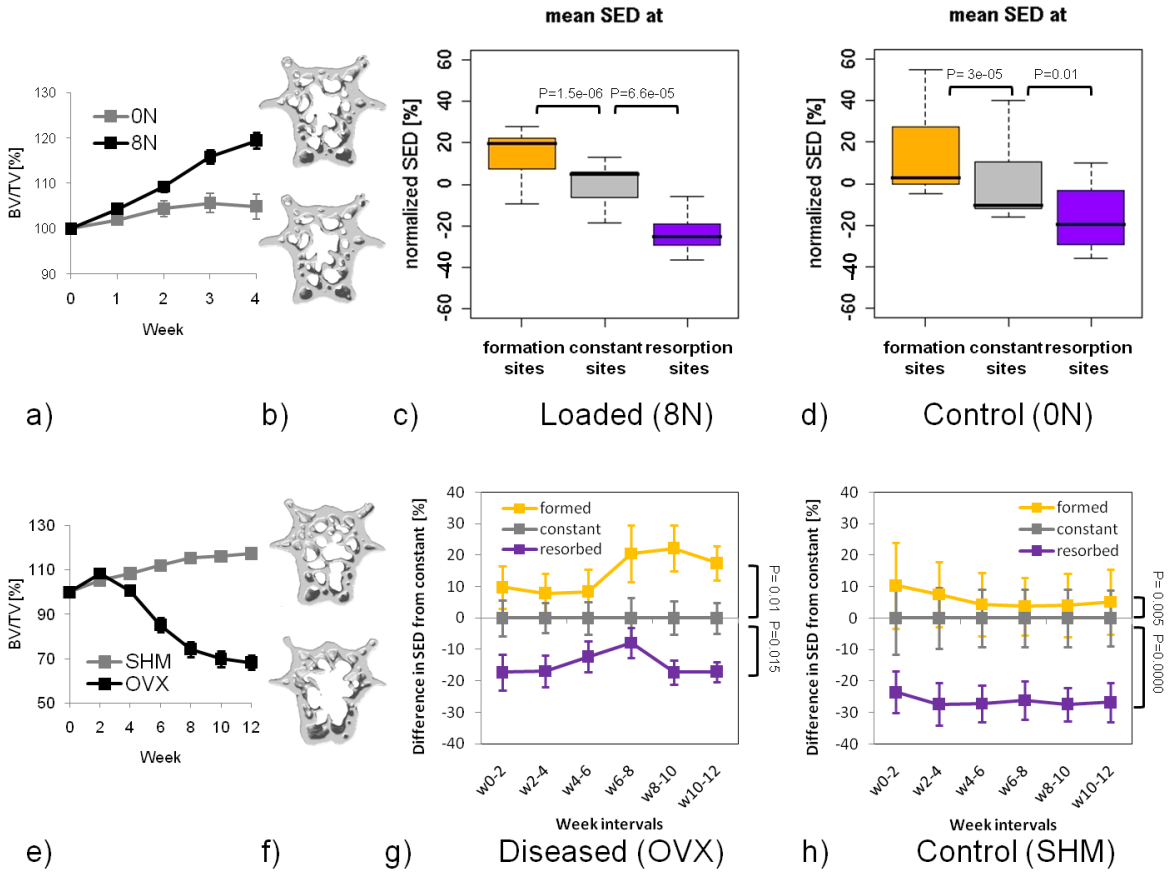

Figure 4.3: Structural details of *in vivo* experiment as well as increased and decreased mean SED preceding bone formation and resorption. (a) Increase in trabecular bone volume fraction (BV/TV) after mechanical loading at 8 N (loading) and constant BV/TV in 0 N group (control). (b) Sagittal section through the diaphyseal CV6 at the basal scan and after 4 weeks of mechanical loading. (c) Comparison between mean SED in formation, constant and resorption sites from week 0 to week 1 in the loaded animals. All values are normalized to the mean value of the constant group to highlight percentage differences from normal levels. (d) Same comparison from week 0 to 1 in the control animals (e) Decrease in BV/TV over 12 weeks following ovariectomy (OVX) and slight increase in BV/TV after SHAM-operation (SHM). (f) Sagittal section through CV6 at 0 and 12 weeks after ovariectomy. (g) Comparison between mean SED at formation, constant and resorption sites over all time intervals after ovariectomy. All values are given in percentage values and are normalized to the mean value of the constant group at the zero baseline. (h) Same comparison in SHM group of ovariectomy experiment over all time intervals.

In fact, mean SED values in regions of bone formation (resorption) were significantly above (below) values at constant bone surfaces over all time intervals (both $p<0.05$, repeated measures ANOVA with Bonferroni-correction, Figure 4.3g). The same behavior characterized the sham operated group (SHM; repeated measures ANOVA with Bonferroni-correction; $p<0.01$, $p<0.001$, Figure 4.3h). However, extent of percentage increase of SED was significantly higher and percentage reduction significantly smaller in OVX compared to SHM animals (repeated measures ANOVA with Bonferroni-correction; $p<0.01$). Taken together, our findings indicate the existence of a local mechanical regulation mechanism which is still active in the case of hormonal perturbations. In order to formulate a quantitative description of the mechano-regulatory system, the relation between mechanical stimuli and remodeling events was further explored. Considering the stochastic aspects which are present in bone remodeling [23,27] and also the unknowns related to loading conditions and metabolic processes [27,28], we adopted a probabilistic viewpoint [20,23]. The total probabilities of bone formation P_f and resorption P_r at the different time intervals were computed by dividing the number of formed and resorbed voxels calculated between two consecutive measurements by the total amount of voxels on the initial trabecular surface. Mechanical loading led to an increase in bone mass by increasing P_f and decreasing P_r compared to the control group (repeated measures ANOVA; $p<0.001$, Figure 4.4a), indicating a larger part of surface was occupied by formation sites. An opposite effect was observed following OVX: initially, P_r increased and P_f decreased, at later points, P_f approached the value of the SHM group (repeated measures ANOVA with Bonferroni-correction; both $p<0.001$, see Figure 4.4b). Local remodeling rules for the behavior of osteoblasts and osteoclasts as a function of the mechanical environment were obtained by analyzing the frequency distributions of SED at sites of formation, quiescence and resorption for specific time intervals. E.g. in the interval from week 0 to 1, for every SED value (bin width 0.05), the local probabilities of bone formation p_f, quiescence p_c, and resorption p_r were computed by counting the relative number of voxels being added, constant and removed from the bone surface between two consecutive measurements. First, to rule out the influence of differences in formed and resorbed bone volumes (e.g. as a result of loading or OVX, see Figure 4.4a and b), the frequency distributions were normalized to unit area. Next, in order to allow comparison of individual animals and treatments, SED was normalized by the corresponding maximum SED value observed in each animal.

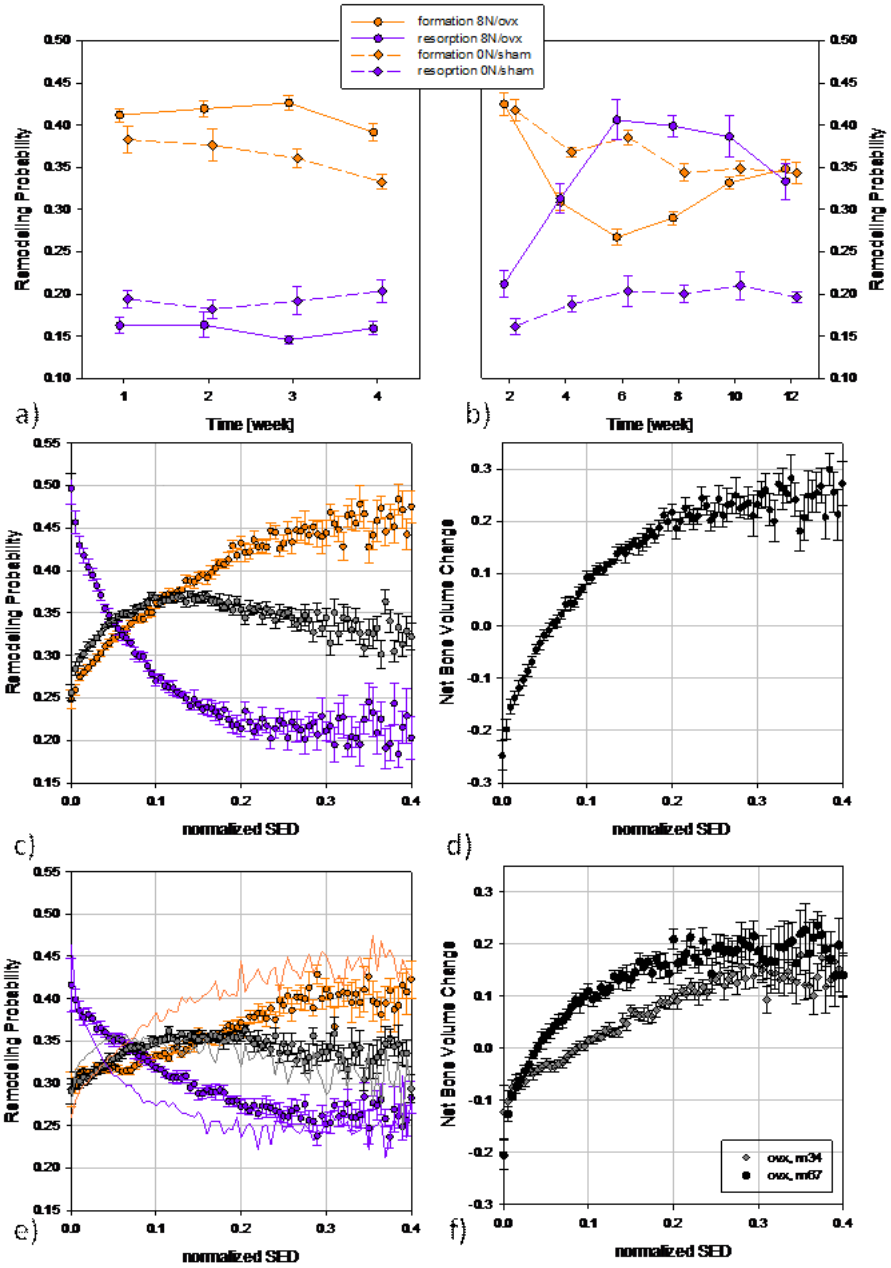

Figure 4.4: Remodeling probability curves. (a) Time evolution of the probabilities of surface remodeling (P_f, P_r) for loading and control group. The fact that P_f was always higher than P_r also in the control group reflects a constant bone growth. (b). Time evolution of the probabilities of surface remodeling (P_f, P_r) for OVX and SHM group. The typical bone loss observed in the OVX animals can be explained by P_r being higher than P_f. (c) Remodeling rule connecting the local probabilities of bone formation, quiescence and resorption with the mechanical stimulus for the loaded animals. (d) Net bone volume change of loading group between week 0 and 1. (e) Remodeling rules following OVX in two different time intervals (dots, week 4-6; lines, week 10-12). (f) Net bone volume change of OVX group in time intervals week 4-6 and week 10-12. Y-axes in (c)-(f) are truncated at 40% of maximum value due to small count number at higher SED values.

Figure 4.4c shows the remodeling probabilities as a function of SED obtained by averaging the individual remodeling rules of the loaded animals over the first week interval. At low SED it is more likely for bone to be resorbed, whereas in regions of high SED, probability of bone formation is greater. The same behavior (within one standard deviation range, data not shown) was obtained over the remaining time intervals as well as for the control group. p_f and p_r could be fitted by exponential functions:

$$p_f(SED) = \alpha_f + \beta_f * [1 - exp^{(-\gamma_f * SED)}] \tag{4.1}$$

with α_f=0.257, β_f=0.237, γ_f=5.762), R=0.995.

$$p_r(SED) = \alpha_r + \beta_r * exp^{(-\gamma_r * SED)} \tag{4.2}$$

with α_r=0.207, β_r=0.268, γ_r=13.908), R=0.995.

The net remodeling change in relation to SED was derived by summation of the formation and resorption probabilities at every SED value (Fig. 4.4d). The remodeling curves in the estrogen depleted animals had a similar behavior compared to the healthy scenario confirming the presence of local mechanical regulation; however, some differences were evident (Fig. 4.4e). Considering the time interval of highest bone loss (week 6-8, Figure 4.3e) the range of SED where $p_r > p_f$ was almost 1.5 times larger for OVX than for the loading group (Figure 4.4e). Additionally, in this period, a reduced mechanical sensitivity may be assumed since both p_r and p_f varied within a range which was about 50% smaller for OVX compared to the loading group. At later stages (week 10-12) the healthy behavior was partly recovered (Figure 4.4e) but still the functional parameters describing the remodeling rules were significantly different from the healthy conditions (Student‘s t-test with Bonferroni-correction; $p<0.05$). The partial recovery is also reflected in the curves of net remodeling change after ovariectomy in the two different time intervals (Figure 4.4f).

In both healthy and diseased states, bone resorption and formation occurred with a certain probability different from zero over the full range of mechanical stimuli present at the bone surface. In addition, in our remodeling rules there was not a defined region where the two probabilities were equal, i.e. where the effects of bone formation and resorption cancel out resulting in zero net changes in bone mass.

Furthermore, the maximum probability for constant bone (37%) never reached the maximum probabilities of formation or resorption (50%). This contrasts the common understanding of bone remodeling being at the local level controlled by two set-points which would divide the full range of stimuli into a "lazy zone" and two intervals of action. Instead, the processes of resorption, quiescence and formation measured by experiment have a more stochastic appearance and with this, display smoother transitions between the remodeling processes.

Conclusion

In conclusion, we showed that both osteoblastic and osteoclastic activity is subjected to a local mechano-regulatory mechanism which is maintained even after estrogen depletion. Furthermore, we have unraveled the nature of such regulation by calculating phenomenological remodeling rules from *in vivo* measurements of bone remodeling and adaptation. It is hoped that such kind of experimental *in vivo* analysis will eventually lead to a better understanding of mechanobiology and with this, a better understanding of the biological mechanisms which regulate the processes in the skeletal system.

Acknowledgements

The authors would like to thank Andreas J. Wirth for his introduction and support in micro-finite element analysis calculations using ParFE and Kathleen Koch for her assistance with the animal experiments. Furthermore, the authors acknowledge Richard Weinkamer for discussions with respect to local strain control. Computational time was granted by the Swiss National Supercomputing Centre (CSCS, Manno, Switzerland) and funding from the European Union for the osteoporotic virtual physiological human project (VPHOP FP7-ICT2008-223865) is gratefully acknowledged.

References

[1] R. Huiskes, R. Ruimerman, G. H. van Lenthe, and J. D. Janssen. Effects of mechanical forces on maintenance and adaptation of form in trabecular bone. *Nature*, 405(6787):704–706, 2000.

[2] A. G. Robling, A. B. Castillo, and C. H. Turner. Biomechanical and molecular regulation of bone remodeling. *Annu Rev Biomed Eng*, 8:455–98, 2006.

[3] D. Taylor, J. G. Hazenberg, and T. C. Lee. Living with cracks: damage and repair in human bone. *Nat Mater*, 6(4):263–8, 2007.

[4] R. B. Martin. Fatigue microdamage as an essential element of bone mechanics and biology. *Calcif Tissue Int*, 73(2):101–7, 2003.

[5] A. M. Parfitt. Osteonal and hemi-osteonal remodeling: the spatial and temporal framework for signal traffic in adult human bone. *J Cell Biochem*, 55(3):273–86, 1994.

[6] T. Sugiyama, J. S. Price, and L. E. Lanyon. Functional adaptation to mechanical loading in both cortical and cancellous bone is controlled locally and is confined to the loaded bones. *Bone*, 46(2):314–21, 2010.

[7] F. M. Lambers, G. Kuhn, F. A. Gerhard, and R. Müller. In vivo micro computed tomography allows monitoring of load induced microstructural bone adaptation. *Bone*, 44(S2):300, 2009.

[8] M. Mullender, A. J. El Haj, Y. Yang, M. A. van Duin, E. H. Burger, and J. Klein-Nulend. Mechanotransduction of bone cells in vitro: mechanobiology of bone tissue. *Med Biol Eng Comput*, 42(1):14–21, 2004.

[9] T. Adachi, Y. Aonuma, S. Ito, M. Tanaka, M. Hojo, T. Takano-Yamamoto, and H. Kamioka. Osteocyte calcium signaling response to bone matrix deformation. *J Biomech*, 42(15):2507–12, 2009.

[10] F. A. Schulte, F. M. Lambers, G. Kuhn, and R. Müller. In vivo micro-computed tomography allows direct three-dimensional quantification of both bone formation and bone resorption parameters using time-lapsed imaging. *Bone*, 48(3):433–442, 2011.

[11] D. J. Webster, P. L. Morley, G. H. van Lenthe, and R. Müller. A novel in vivo mouse model for mechanically stimulated bone adaptation - a combined experimental and computational validation study. *Comput Methods Biomech Biomed Engin*, 11(5):435–441, 2008.

[12] D. R. Carter. Mechanical loading histories and cortical bone remodeling. *Calcif Tissue Int*, 36 Suppl 1:S19–24, 1984.

[13] D. R. Carter. Mechanical loading history and skeletal biology. *J Biomech*, 20(11-12):1095–109, 1987.

[14] P. Fratzl. Bone fracture: When the cracks begin to show. *Nat Mater*, 7(8):610–2, 2008.

[15] Wilhelm Roux. *Der Kampf der Theile im Organismus.* Wilhelm Engelman, Leipzig, 1881.

[16] J. Wolff. *Das Gesetz der Transformation der Knochen (The Law of Bone Remodelling).* Springer-Verlag, Berlin, Germany, 1892.

[17] H. M. Frost. The mechanostat: a proposed pathogenic mechanism of osteoporoses and the bone mass effects of mechanical and nonmechanical agents. *Bone Miner*, 2(2):73–85, 1987.

[18] H. M. Frost. Bone's mechanostat: a 2003 update. *Anat Rec A Discov Mol Cell Evol Biol*, 275(2):1081–101, 2003.

[19] C. H. Turner, M. P. Akhter, D. M. Raab, D. B. Kimmel, and R. R. Recker. A noninvasive, in vivo model for studying strain adaptive bone modeling. *Bone*, 12(2):73–9, 1991.

[20] R. Weinkamer, M. A. Hartmann, Y. Brechet, and P. Fratzl. Stochastic lattice model for bone remodeling and aging. *Phys Rev Lett*, 93(22):228102, 2004.

[21] R. Ruimerman, P. Hilbers, B. van Rietbergen, and R. Huiskes. A theoretical framework for strain-related trabecular bone maintenance and adaptation. *J Biomech*, 38(4):931–41, 2005.

[22] T. Adachi, K. Tsubota, Y. Tomita, and S. J. Hollister. Trabecular surface remodeling simulation for cancellous bone using microstructural voxel finite element models. *J Biomech Eng*, 123(5):403–9, 2001.

[23] J. W. Dunlop, M. A. Hartmann, Y. J. Brechet, P. Fratzl, and R. Weinkamer. New suggestions for the mechanical control of bone remodeling. *Calcif Tissue Int*, 85(1):45–54, 2009.

[24] F. M. Lambers, K. Koch, F. Schulte, G. Kuhn, and R. Müller. Ovariectomy increases bone formation rate as well as bone resorption rate in mouse tail vertebra. *Bone*, 47(Supplement 1):S165–S165, 2010. 8756-3282 doi: DOI: 10.1016/j.bone.2010.04.383.

[25] P. Arbenz, G. H. van Lenthe, U. Mennel, R. Müller, and M. Sala. A scalable multi-level preconditioner for matrix-free μ-finite element analysis of human bone structures. *Int. J. for Numerical Methods in Engineering*, 73(7):927–947, 2008.

[26] R Development Core Team. *R: A language and environment for statistical computing*. R Foundation for Statistical Computing, Vienna, Austria, 2007.

[27] A. M. Parfitt. Misconceptions (2): turnover is always higher in cancellous than in cortical bone. *Bone*, 30(6):807–809, 2002.

[28] D. B. Burr. Targeted and nontargeted remodeling. *Bone*, 30(1):2–4, 2002.

Chapter 5

In silico bone biology

5.1 *In vivo* validation of a computational bone adaptation model using open-loop control and time-lapsed micro-computed tomography

Friederike A. Schulte[1], Floor M. Lambers[1], Duncan J. Webster[1], Gisela Kuhn[1] and Ralph Müller[1]

[1]Institute for Biomechanics, ETH Zurich, Zurich, Switzerland

Abstract:

Cyclic mechanical loading augments trabecular bone mass, mainly by increasing trabecular thickness. For this reason, we hypothesized that an *in silico* thickening algorithm using open-loop control would be sufficient to reliably predict the response of trabecular bone to cyclic mechanical loading. This would also mean that trabecular bone adaptation could be modeled as a system responding to an input signal at the onset of the process in a predefined manner, without feedback from the outputs. Here, time-lapsed *in vivo* micro-computed tomography scans of mice cyclically loaded at the sixth caudal vertebra were used to validate the *in silico* model. When comparing *in silico* and *in vivo* data sets after a period of four weeks, a maximum prediction error of 2.4% in bone volume fraction and 5.4% in other bone morphometric indices was calculated. Superimposition of sequentially acquired experimental images and simulated structures revealed that *in silico* simulations deposited thin and homogeneous layers of bone whilst the experiment was characterized by local areas of strong thickening, as well as considerable volumes of bone resorption. From the results, we concluded that the proposed computational algorithm predicted changes in bone volume fraction and global parameters of bone structure very well over a period of four weeks while it was unable to reproduce accurate spatial patterns of local bone formation and resorption. This study demonstrates the importance of validation of computational models through the use of experimental *in vivo* data, including the local comparison of simulated and experimental remodeling sites. It is assumed that the ability to accurately predict changes in bone micro-architecture will facilitate a deeper understanding of the

cellular mechanisms underlying bone remodeling and adaptation due to mechanical loading.

Keywords:
in silico modeling; simulation; validation; mechanical loading; *in vivo* micro-computed tomography; dynamic bone morphometry

5.1.1 Introduction

Bone has a complex trabecular microstructure consisting of many interconnected struts and plates. This architecture is constantly changed over time by bone forming and resorbing cells which respond to a variety of biophysical and biochemical stimuli. For example, cyclic mechanical loading leads to increased bone mass whereas aging and disease processes diminish bone tissue. The ability to simulate these time dependent changes in bone micro-architecture would facilitate a deeper understanding of the cellular mechanisms underlying bone remodeling and bone adaptation. Such *in silico* approaches may eventually allow a better prediction of individual fracture risk in osteoporotic patients or improved implant design and performance in orthopaedic applications.

A variety of models have been established which attempt to simulate the bone modeling and remodeling process in response to various stimuli. A number of these models act on image voxels constituting three-dimensional (3D) bone structures, which may in turn have been acquired using high-resolution imaging methods such as micro-computed tomography (micro-CT). For example Ruimerman et al. [1] and Adachi et al. [2] propose algorithms which are capable of simulating both the anabolic and catabolic activity of bone by making use of a mechanical feedback-loop control. These approaches couple osteoblast and osteoclast activity with mechanical strain and remove or add image voxels according to the local mechanical environment as determined by micro-finite element (μFE) models. However, owing to the large computational overhead associated with μFE they have only been applied to either artificial grids or small 3D volumes of trabecular bone. Furthermore, these simulations lack quantitative validation using controlled experimental data. Müller et al. [3–5] previously introduced an algorithm called Simulated Bone Atrophy (SIBA) to simulate the catabolic activity of bone associated with menopause. This algo-

rithm used open-loop control to predict changes in the bone micro-architecture over time, which would mean that bone can be described as a system responding to a control signal (estrogen depletion) in a pre-defined way (by thinning) without incorporating feedback from the outputs generated along the path of the simulation. Using the attributes of a simple Gaussian filter to model the activity of bone multi-cellular units (BMU) with a net formation deficit, the algorithm was able to uniformly thin trabecular structures and transform normal bone micro-architectures to osteopenic states using a realistic underlying time line. This approach yielded structures similar in appearance as well as in structural behaviour when compared to a post-menopausal group of women.

In the study presented here, we extend SIBA and investigate the feasibility of modeling anabolic activity in bone using an open-loop control. Furthermore, we validate our approach by longitudinal experimental data from a recently established mouse model which permits the study of load regulated bone adaptation *in vivo*. In a previous study, the 6^{th} caudal vertebrae of C57BL/6 mice were mechanically stimulated according to a repetitive dynamic loading regime. Using time-lapsed *in vivo* micro-CT to quantify the resultant morphological changes in each loaded mouse, trabecular bone mass was shown to significantly increase via the thickening of pre-existing trabeculae [6]. For the purpose of this study, we hypothesize that the anabolic response of trabecular bone in mechanically loaded C57BL/6 mouse caudal vertebrae can be modeled by redefining the model parameters of SIBA to enlarge pre-existing bone structures. To our knowledge this is the first time that an *in silico* model for bone adaptation has been validated using longitudinal *in vivo* data sets.

5.1.2 Materials and Methods

Materials

All experimental *in vivo* data were taken from a published experimental study [7]. Briefly, anabolic bone adaptation was induced in 15-week-old, female C57BL/6 mice (n=9; RCC; Füllinsdorf, Switzerland) by subjecting their 6^{th} caudal vertebra to a cyclic mechanical loading regime (amplitude: 8 N, frequency: 10 Hz, number of cycles: 3000) three times per week for four weeks *in vivo* [8]. All vertebrae were scanned weekly with *in vivo* micro-computed tomography (vivaCT 40, Scanco Medical, Brüttisellen, Switzerland) at an isotropic voxel resolution of 10.5 μm. After four weeks, loading resulted in a significant net gain in trabecular bone volume

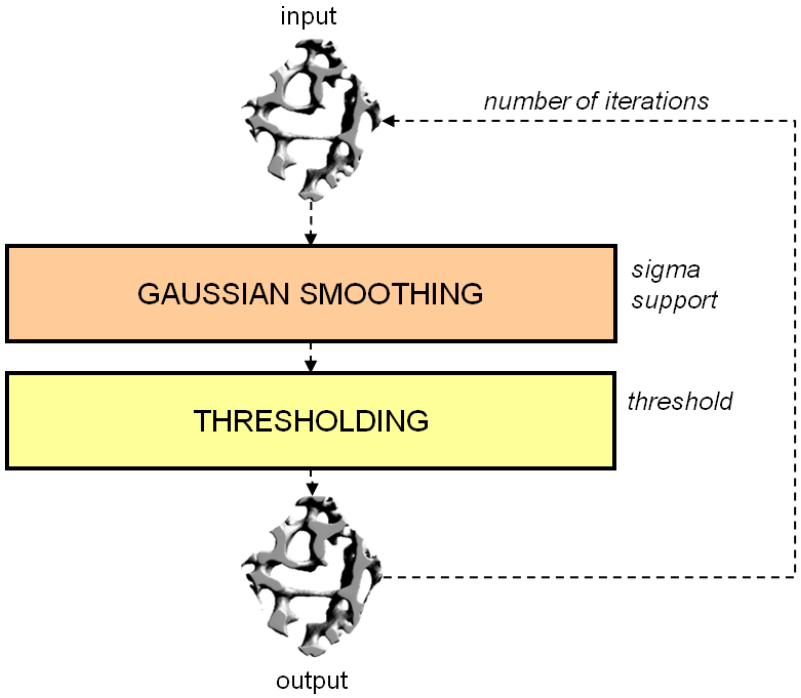

Figure 5.1: Schematic representation of the computational algorithm to predict bone changes (SIBA). The algorithm expects a thresholded image as input structure. A Gaussian filter is applied to the thresholded image. In this step, the free variables are the Gaussian filter width (sigma) and the Gaussian filter support. In a second step, the image is re-binarized with a global threshold. The resulting output image serves as the input image of the next iteration.

fraction of 21.6% compared to the basal scan. Trabecular thickness was significantly increased while trabecular number was not significantly changed [6].

In silico thickening algorithm

Previously, Müller [3] introduced an algorithm (SIBA) that simulates post-menopausal bone loss by uniform iterative thinning of the bone microstructure, which was, for our purposes, slightly modified to model an anabolic bone response. Our approach was based on the assumption that during increased mechanical loading, the balance between osteoclastic and osteoblastic activity is shifted such that osteoblastic activity predominates.

Figure 5.1 displays a schematic representation of the *in silico* algorithm. The input structure is a binary image of the trabecular compartment. In a next step, a Gaussian filter is applied, blurring the surfaces of the trabecular structures. Finally,

the blurred image is binarized at a global threshold and the resulting output image serves as input for the next iteration.

The model parameters that can be varied in order to achieve a net gain or loss in bone mass are the Gaussian filter width (sigma) and Gaussian filter support, the threshold and the number of iterations. Previously Müller [3] related all model parameters to biological variables, measurable and quantifiable from human data. For example, the number of iterations described the activation frequency, the Gaussian sigma defined the osteoclast penetration depth, whilst the threshold was seen as the biological efficiency level of the osteoblasts to refill empty cavities. Here, the number of iterations is defined as the activation frequency in the mouse, whilst the Gaussian sigma and threshold level describe the thickness of osteoid which can be formed by mouse osteoblasts along with their level of efficiency. To define these parameters we chose a combination of values which matched the increase in bone volume fraction from the first to the second micro-CT scan (see Table 5.1).

In particular, a combination of sigma, support and number of iterations was chosen so that the amount of bone gain per day was consistent with values found in the literature. The rate of bone gain per day is usually described by the mineral apposition rate (MAR) and typical values in loaded C57BL/6 mice are reported to be up to 2.39 μm/d [9, 10]. This ensured that osteoblasts could maximally deposit 21 μm bone per week, which corresponds to a MAR of 3 μm/d. Furthermore, in our approach, the Gaussian sigma is represented by three values for the three orthogonal directions instead of one scalar value so as to compress the Gaussian kernel along the main axis of loading, thereby enabling the algorithm to emulate the experimentally observed phenomenon that trabeculae align in direction of the main axis of loading [11–13].

Table 5.1: Model parameters, their associated biological correspondence and the value assigned to them in the present implementation

Parameter	Biological meaning (unit)	Value (in biological terms)
Gaussian sigma $[\sigma_x, \sigma_y, \sigma_z]$	Osteoid thickness (μm)	[2 voxel, 1 voxel, 1 voxel]
Gaussian support	Constraint of osteoid thickness (μm)	1 voxel (10.5 μm)
Threshold	Efficiency level (%, 0.5=100%)	0.4 (120%)
Number of iterations	Activation frequency (1/d)	8 (1/3.5 d)

Finally, the threshold was varied until a good match in bone volume fraction was found between experiment and simulation after one week. Matching was performed for each animal. This gave an array of percent differences between simulation and experiment, from which the mean value was calculated. The optimal mean value, i.e. the best match, was found at a threshold value of 0.4 which corresponds to an osteoblastic efficiency level of 120%. This value was then used for all simulations and all animals.

Model assessment / validation

In a first step, the binary trabecular structures were converted into *in silico* structures by running one iteration of the simulation algorithm with parameters sigma=1, support=1, threshold=0.5. This initial iteration constitutes a pre-processing step to remove very thin spikes at the edge between trabecular and cortical shell. The resulting binary models were used as input structures for the *in silico* thickening algorithm and four weeks of treatment were simulated.

Simulated bone morphometric indices were calculated at each simulation step and were compared to the experimental indices at the corresponding measurement point using repeated measurements ANOVA. The calculated morphometric indices were bone volume fraction (BV/TV), bone volume-to-surface ratio (BS/BV), trabecular thickness (Tb.Th), trabecular number (Tb.N) and trabecular separation (Tb.Sp) according to the guidelines for assessment of bone microstructure in rodents using micro-CT [14]. In addition, bone morphometric indices were plotted as percentage change to the basal scan (ΔBV/TV, ΔBS/BV, ΔTb.Th, ΔTb.Sp and ΔTb.N). Again, the changes in simulated bone morphometric indices were compared to the changes in experimental indices over time using repeated measurements ANOVA. Furthermore, at the last point in time (week 4), a linear regression analysis between the simulated and experimental BV/TV was performed to find out if the predicted BV/TV was still most similar to the BV/TV of the experimental structure it belonged to.

To permit identification of the local sites of bone formation and resorption, the first and last binarized experimental scans were superimposed in each vertebra using rigid image registration [15]. Similarly first and last simulated structures were registered. This procedure allowed a direct visual comparison of experimental and simulated formation and resorption sites. Using these superimposed images, dynamic mor-

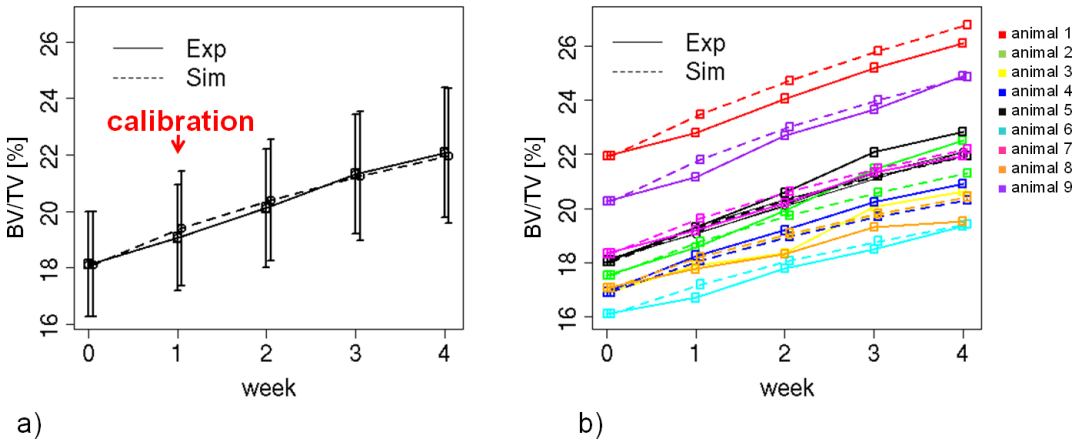

Figure 5.2: a) Time course of bone volume fraction (BV/TV). The solid line denotes the experiment and the dashed line the simulation. b) Same information as in a), but all animals are plotted separately. It is evident that the high standard deviation in a) is not caused by the simulation but by the wide range of BV/TV associated with the individual animals.

phometric indices were quantified for the 4 week loading period [7]. These indices included parameters such as bone formation rate (BFR), mineral apposition rate (MAR), mineralizing surface (MS) as well as bone resorption rate (BRR), mineral resorption rate (MRR) and eroded surface (ES) [7]. A paired Student's t-test was performed between simulated and experimental overlays of week 0 and week 4 to detect significances in dynamic bone morphometry parameters. All statistical tests were performed using R [16] and p-values < 0.05 were considered significant.

5.1.3 Results

In the present study, the response of bone to increased mechanical loading was simulated over a period of four weeks, using two iterations per week. The input structures were *in vivo* micro-CT scans of the trabecular compartments of the 6^{th} caudal vertebrae of 9 C57BL/6 mice. For experimental validation, the vertebrae were subjected to a cyclic *in vivo* loading protocol for four weeks. After completion of the experiment, the simulated and experimental curves of bone morphology were compared. The simulated structures were calibrated so that the simulated BV/TV of the second measurement matched the experimental BV/TV at that time point. Weeks 2, 3, and 4 were then used to determine the prediction error of the

Table 5.2: Error (in %) between simulated and experimental bone morphometric indices at every week in the *in vivo* setup. The simulation errors at week 0 result from the fact that the input structures were in a first step converted into a model by one initial iteration of the Gaussian simulation algorithm with homeostatic parameters. ($p < 0.05$ considered significant with repeated measures ANOVA, n.s. = not significant)

Parameter	Error w0	Error w1	Error w2	Error w3	Error w4	p-value
BV/TV	0.0%	1.9%	2.1%	2.3%	2.4%	n.s.
BS/BV	0.0%	4.1%	5.3%	4.6%	5.0%	0.01
Tb.Th	1.5%	2.0%	3.7%	4.0%	5.4%	0.02
Tb.Sp	1.8%	1.1%	1.0%	2.4%	2.4%	n.s.
Tb.N	2.6%	3.6%	2.8%	4.3%	4.6%	n.s.

computational model.

Figure 5.2a illustrates the course of BV/TV over time for both experiment and simulation, showing the mean and standard deviation averaged over all animals at the different time points. The prediction error at weeks 1, 2, 3, and 4 amounted to 1.9%, 2.1%, 2.3%, and 2.4% respectively. The dissimilarities detected between simulation and experiment were not significant. Figure 5.2b contains the same information as Figure 5.2a, but experimental measurements and *in silico* simulations are shown for each animal individually. As can be seen in Figure 5.2b, the high standard deviation in Figure 5.2a is not caused by the simulation but by the wide range of BV/TV between the animals. Linear regression analysis between simulated and experimental BV/TV values at the last time point resulted in R^2=0.92, indicating that even after four weeks, the simulated and experimental structures of each animal were closely matched.

A comparison of other structural indices revealed that simulation and experiment deviated significantly in BS/BV and Tb.Th at the endpoint of the study ($p<0.05$, see Fig. 5.3a and b) although the differences were still relatively small (5.3% and 5.4% respectively). In contrast, trabecular number agreed very well in both experiment and simulation (Fig. 5.3c). Table 5.2 summarizes the absolute mean deviation between simulation and experiment for all morphometric indices at all time points. Morphometric indices showed a maximum deviation of 5.4% over the weeks. In Ta-

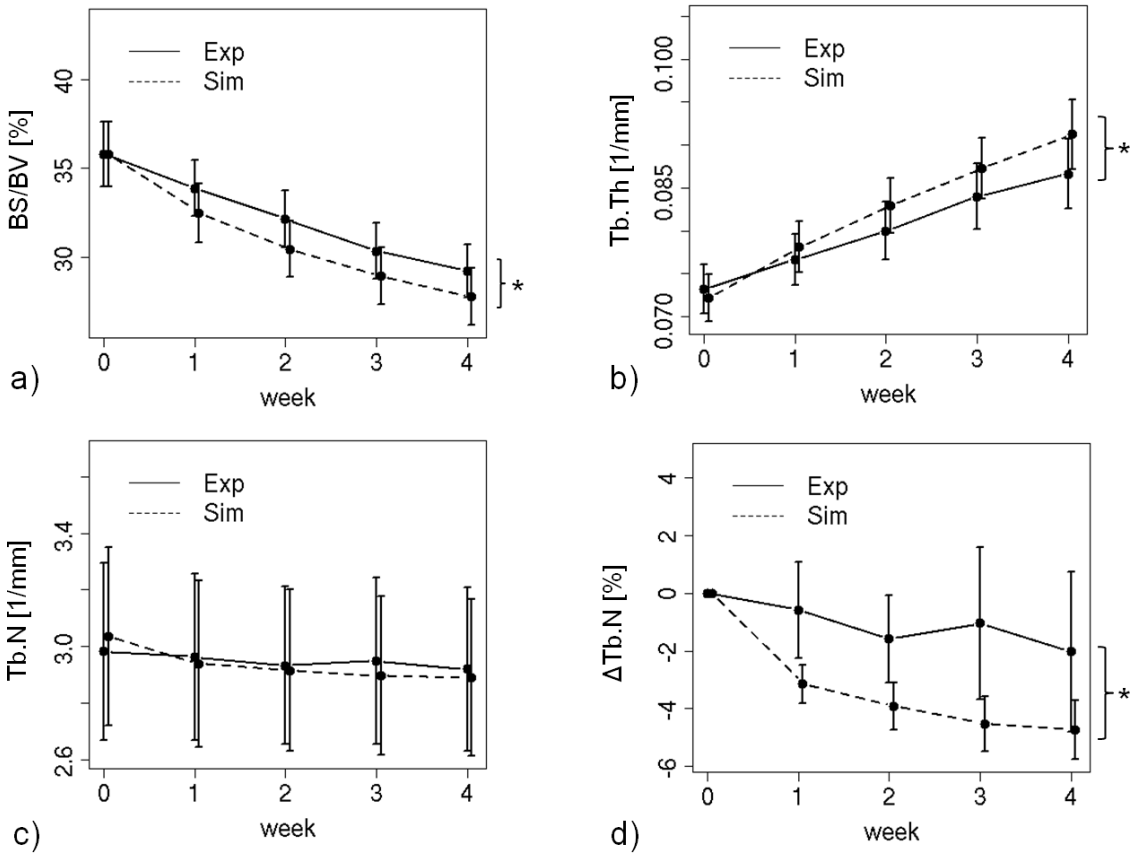

Figure 5.3: Time course of bone morphometric indices over four weeks. The dashed line denotes the simulation and the solid line the experiment. The curves are presented by the mean and standard deviation at each week. a) BS/BV b) Tb.Th c) Tb.N d) ΔTb.N.

Table 5.3: Error (in %) between simulated and experimental percentage changes of bone morphometric indices at every week in the *in vivo* setup. All values were normalized with respect to their value at the starting point of the experiment. ($p < 0.05$ considered significant with repeated measures ANOVA, n.s. = not significant)

Parameter	Error w0	Error w1	Error w2	Error w3	Error w4	p-value
ΔBV/TV	0.0%	44.1%	23.9%	15.3%	14.0%	n.s.
ΔBS/BV	0.0%	-80.3%	-49.3%	-28.2%	-24.6%	0.05
ΔTb.Th	0.0%	85.8%	64.5%	46.3%	48.3%	0.01
ΔTb.Sp	0.0%	-91.5%	-155.2%	-527.4%	-11.1%	<0.0001
ΔTb.N	0.0%	136.6%	-50.4%	0.24%	-47.6%	0.04

ble 5.3, the deviation between simulation and experiment in normalized structural indices ΔBV/TV, ΔBS/BV, ΔTb.Th, ΔTb.Sp and ΔTb.N is presented. With percentage errors in about the same range but more significant dissimilarities between groups, normalized morphometric indices are even more sensitive to differences between model and experiment (see also Fig. 5.3d, ΔTb.N).

Figure 5.4 shows a detail of the trabecular microstructure displaying the changes over the 4-week experiment (Fig. 5.4a) and simulation (Fig. 5.4b). The encircled area highlights a trabecular structure which becomes thicker over the weeks for both experiment and simulation. Nevertheless, the simulated structure does not reproduce all changes in the bone microstructure as in the experiment. The hole in the rectangle, for example, is closed in the experiment after 4 weeks, but not in the simulation.

Superimposition of *in vivo* and *in silico* images between week 0 and 4 showed distinct differences in the local patterns of bone formation and resorption. In the simulated structure in Figure 5.5 (left), we find almost exclusively sites of bone formation, illustrated in yellow. A few small resorption spots occur at very thin tissue walls, indicating that tiny connections are smoothed out by the simulation algorithm. In contrast, the experiment (middle) shows considerable amounts of bone resorption. These resorption volumes are compensated locally with even more and thicker bone formation packets. The image on the right of Figure 5.5 depicts the disagreement between simulation and experiment. Areas that were formed, but not

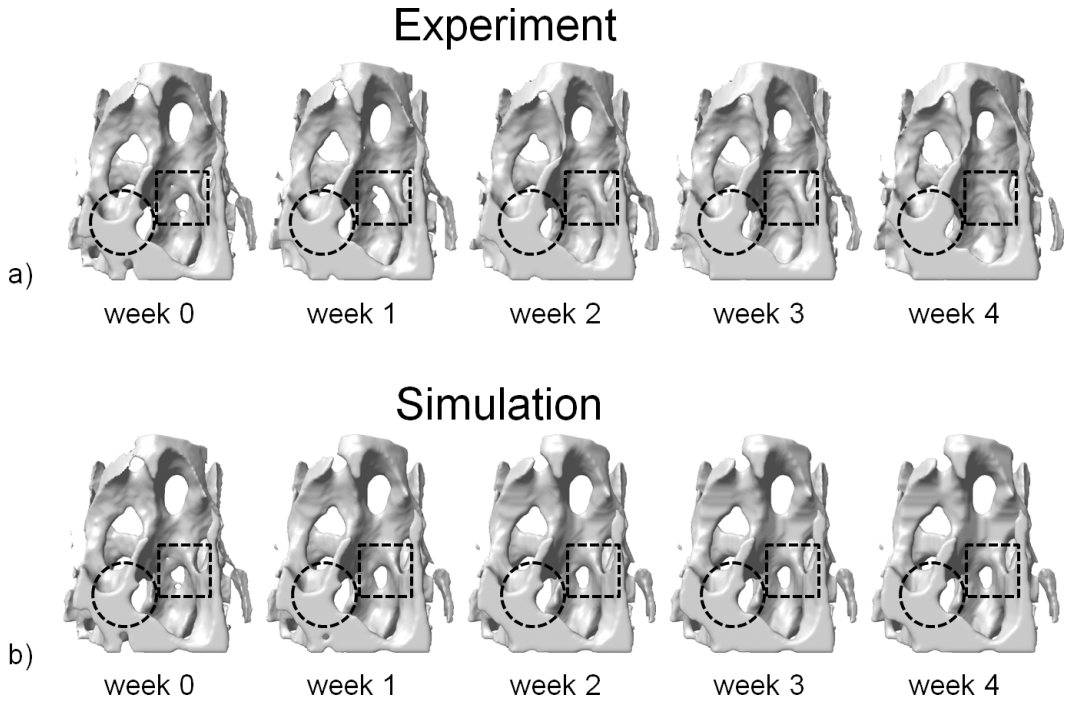

Figure 5.4: Changing experimental and simulated bone microstructure over time. a) Detail of an experimental trabecular microstructure which changes over the duration of the experiment. The encircled area highlights a trabecula which became thicker over the weeks. At the same time, holes were filled in (indicated by the rectangle). b) Same detail over the course of the simulation. Simulated trabeculae became thicker (circle) similar to the experiment. Nevertheless, not all local changes occurring in the experiment could be reproduced by the simulation. The hole in the rectangle, for example, was not closed after 4 weeks.

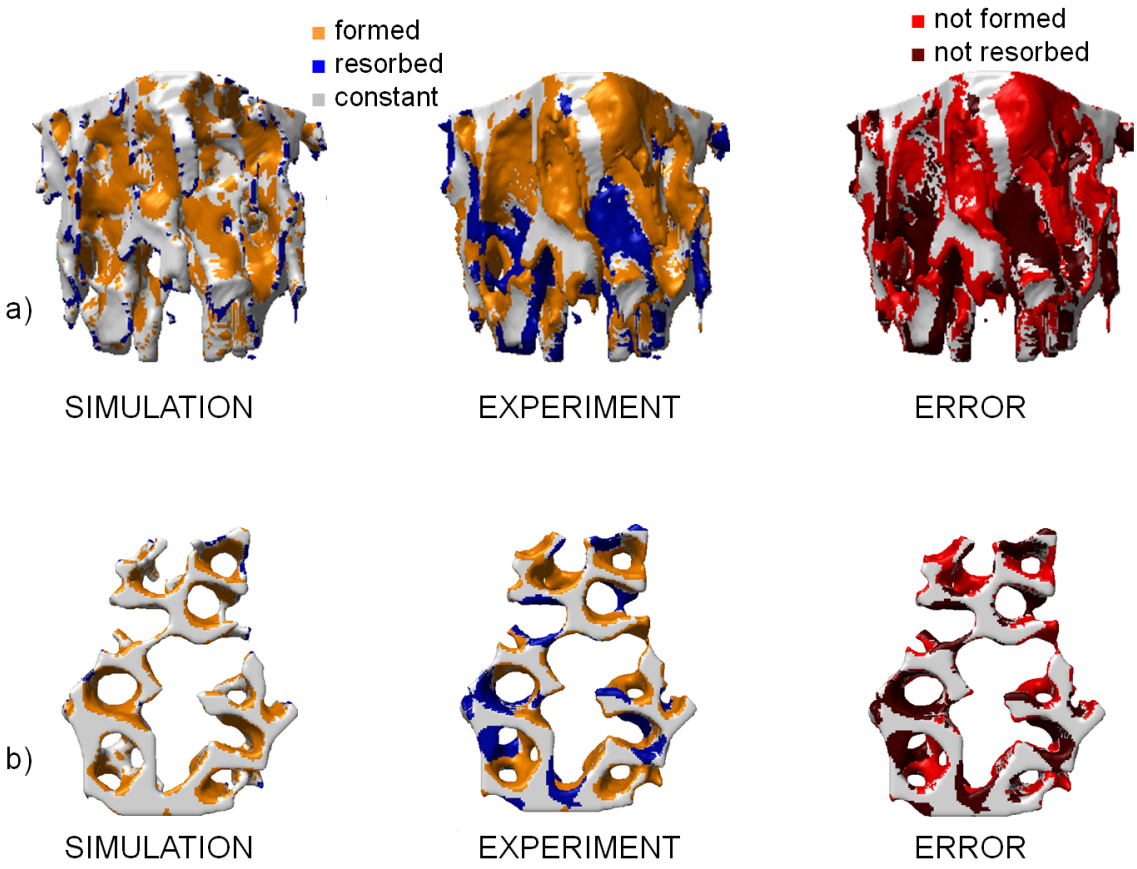

Figure 5.5: Visualization of the bone formation and resorption sites in a simulated animal (left) and an experimental structure (middle). Yellow sites denote bone formation and blue sites bone resorption. The simulated structure is characterized by large but thin layers of formation. In contrast, the experiment features thick and compact formation volumes but also considerable volumes of bone resorption in a more localized fashion. The "error"-image (right) displays bone formation which was not formed by the simulation in light red, and the bone resorption which was not resorbed by the simulation in dark red.

Table 5.4: Experimental and simulated dynamic bone morphometry parameters (mean ± standard deviation) for simulation and experiment

Parameter	Experiment	Simulation	p-value
BFR^*_{BV} [%/d]	1.05 ± 0.21	0.56 ± 0.03	0.0003
BRR^*_{BV} [%/d]	0.404 ± 0.1156	0.002 ± 0.0003	<0.0001
MAR* [μm/d]	0.74 ± 0.08	0.55 ± 0.02	0.0027
MRR* [μm/d]	1.09 ± 0.16	0.38 ± 0.00	<0.0001
MS* [%]	62.55 ± 2.87	66.96 ± 1.91	0.0002
ES* [%]	18.14 ± 1.86	0.79 ± 0.08	<0.0001

predicted as such by the simulation, are visualized in light red whereas areas that were erroneously not resorbed in the simulation are coloured in dark red.

Table 5.4 lists the dynamic bone formation and resorption rates. As already indicated in Figure 5.5, all simulated resorption rates were predicted to be close to zero and deviated significantly from the experimental bone resorption rates ($p<0.001$). At the same time, simulated formation rates BFR and MAR were significantly lower than in the experiment ($p<0.01$), whereas simulated MS was close to but significantly higher than the value found in the experiment ($p<0.001$). These results showed that the simulation deposited bone on most surfaces in very thin layers, whilst hardly any bone was resorbed. In contrast, the formed bone volumes in the experiment were thicker and more compact, furthermore considerable volumes of bone resorption were found in the experiment.

5.1.4 Discussion

In this study we adapted an *in silico* model capable of simulating post-menopausal bone loss to simulate the anabolic process associated with cyclic mechanical loading. By using an open-loop control, realized by a Gaussian filter, we showed that we were able to successfully predict the changes in bone volume fraction and other bone morphometric indices with less than 5.4% error when compared to longitudinal experimental data. This is the first time an *in silico* algorithm for bone adaptation has been quantitatively validated against actual *in vivo* data from a controlled loading experiment also demonstrating the ability to accurately predict the quantity and

structure of newly formed bone.

Comparison of theoretical and experimental patterns of bone formation showed that the proposed algorithm was unable to replicate spatially varying osteoblastic and osteoclastic activity. In our model bone was hardly resorbed, whereas in the experiment the large amount of bone formation was accompanied by relatively high amounts of bone resorption. This discrepancy is explained by the model design. The algorithm was generated to produce net formation by combining both bone formation and resorption into one process. Thus, any visible bone resorption must be considered an artifact. More specifically, small exposed spikes were removed by the Gaussian filter averaging out voxels that were connected to very few neighbors. These voxels were then lost in the subsequent thresholding step.

The criterion which determines where bone is formed in the simulation is the curvature of the bone surface. In general, areas of concave curvature are preferentially filled while convex areas will most likely remain unchanged. Whilst this phenomenon has been observed in a recent *in vitro* experiment [17], the inability of the algorithm to simulate spatial patterns of bone resorption and formation indicates the absence of a local feedback mechanism which determines, on site, if bone is formed or resorbed. A mechanical feedback mechanism has been incorporated into algorithms proposed by Ruimerman et al. [1] and Adachi et al. [2]. These models couple both osteoblast and osteoclast activity with mechanical strain and remove or add image voxels according to the local mechanical environment as determined by μFE models. For example Ruimerman et al. [1] assumed random osteoclast activity which is superseded by osteoblast activity in areas of high mechanical deformation. This approach has been shown to approximate growth-related increase in trabecular bone volume fraction in pigs; however it is not clear if such models are able to predict spatial patterns of bone formation and resorption throughout life and disease. With this in mind, when developing the presented algorithm further, and in addition to incorporating a mechanical feedback mechanism, future studies should also focus in characterizing the spatial relationship between the local mechanical environment and regions of bone formation and resorption.

A limitation of the proposed model is that values describing cellular activity are not entirely based on actual biological values, i.e the best parameter set is derived by matching increases in BV/TV for the first week. Furthermore these model parameters are assumed to be constant over time. This is sufficient to capture the

linear response observed experimentally throughout the 4-week time-frame of the experiment, however, studies have shown the anabolic response of bone due to loading to reach a saturation point [18–20]. This would not be captured by the current algorithm unless parameters were updated. Future development of the algorithm may therefore be required to link model parameters to transient variations in cellular activity which would require much more validation. Nevertheless it is also possible that saturation can be achieved with the inclusion of a mechanical feedback mechanism.

To our knowledge this is the first time a bone remodeling algorithm has been validated against controlled experimental data acquired *in vivo*. In doing so we have shown that by uniform Gauss filtration of 3D images of trabecular bone we were able to predict increases in BV/TV due to mechanical loading in the caudal vertebra of C57BL/6 mice. Furthermore, the inability of this algorithm to reproduce spatial patterns of bone formation and resorption highlighted the importance of incorporating local feedback mechanisms when attempting to simulate load-induced adaptation. To improve the modeling of bone adaption, future studies should evaluate existing theoretical frameworks which incorporate mechanical feedback mechanisms by also taking the local patterns of bone formation and resorption into consideration. The ability to predict changes in bone micro-architecture accurately is assumed to facilitate a deeper understanding of the cellular mechanisms underlying bone remodeling and bone adaptation due to mechanical loading. Furthermore, in the future, *in silico* bone remodeling approaches may eventually lead to a better prediction of individual fracture risk in osteoporotic patients or improved implant design and performance in orthopaedic applications.

Acknowledgements

Funding from the European Union for the osteoporotic virtual physiological human project (VPHOP FP7-ICT2008-223865) is gratefully acknowledged.

References

[1] R. Ruimerman, P. Hilbers, B. van Rietbergen, and R. Huiskes. A theoretical framework for strain-related trabecular bone maintenance and adaptation. *J Biomech*, 38(4):931–41, 2005.

[2] T. Adachi, K. Tsubota, Y. Tomita, and S. J. Hollister. Trabecular surface remodeling simulation for cancellous bone using microstructural voxel finite element models. *J Biomech Eng*, 123(5):403–9, 2001.

[3] R. Müller. Long-term prediction of three-dimensional bone architecture in simulations of pre-, peri- and post-menopausal microstructural bone remodeling. *Osteoporos Int*, 16 Suppl 2:S25–35, 2005.

[4] R. Müller, T. Hildebrand, H. J. Häuselmann, and P. Rüegsegger. In vivo reproducibility of three-dimensional structural properties of noninvasive bone biopsies using 3D-pQCT. *J Bone Miner Res*, 11(11):1745–1750, 1996.

[5] R. Müller and P. Rüegsegger. Micro-tomographic imaging for the nondestructive evaluation of trabecular bone architecture. *Stud Health Technol Inform*, 40:61–79, 1997.

[6] F. M. Lambers, G. Kuhn, F. A. Gerhard, and R. Müller. In vivo micro computed tomography allows monitoring of load induced microstructural bone adaptation. *Bone*, 44(S2):300, 2009.

[7] F. A. Schulte, F. M. Lambers, G. Kuhn, and R. Müller. In vivo micro-computed tomography allows direct three-dimensional quantification of both bone formation and bone resorption parameters using time-lapsed imaging. *Bone*, 48(3):433–442, 2011.

[8] D. J. Webster, P. L. Morley, G. H. van Lenthe, and R. Müller. A novel in vivo mouse model for mechanically stimulated bone adaptation - a combined experimental and computational validation study. *Comput Methods Biomech Biomed Engin*, 11(5):435–441, 2008.

[9] J. C. Fritton, E. R. Myers, T. M. Wright, and M. C. van der Meulen. Bone mass is preserved and cancellous architecture altered due to cyclic loading of the mouse tibia after orchidectomy. *J Bone Miner Res*, 23(5):663–71, 2008.

[10] D. Webster, E. Wasserman, M. Ehrbar, F. Weber, I. Bab, and R. Müller. Mechanical loading of mouse caudal vertebrae increases trabecular and cortical bone mass-dependence on dose and genotype. *Biomech Model Mechanobiol*, 9(6):737–47, 2010.

[11] J. Wolff. *Das Gesetz der Transformation der Knochen (The Law of Bone Remodelling)*. Springer-Verlag, Berlin, Germany, 1892.

[12] E. Tanck, J. Homminga, G. H. van Lenthe, and R. Huiskes. Increase in bone volume fraction precedes architectural adaptation in growing bone. *Bone*, 28(6):650–654, 2001.

[13] J. Homminga, B. Van-Rietbergen, E.M. Lochmüller, H. Weinans, F. Eckstein, and R. Huiskes. The osteoporotic vertebral structure is well adapted to the loads of daily life, but not to infrequent "error" loads. *Bone*, 34(3):510–516, 2004.

[14] M. L. Bouxsein, S. K. Boyd, B. A. Christiansen, R. E. Guldberg, K. J. Jepsen, and R. Müller. Guidelines for assessment of bone microstructure in rodents using micro-computed tomography. *J Bone Miner Res*, 25(7):1468–86, 2010.

[15] P. Thevenaz, U. E. Ruttimann, and M. Unser. A pyramid approach to subpixel registration based on intensity. *IEEE Trans Image Process*, 7(1):27–41, 1998.

[16] R Development Core Team. *R: A language and environment for statistical computing*. R Foundation for Statistical Computing, Vienna, Austria, 2007.

[17] M. Rumpler, A. Woesz, J. W. Dunlop, J. T. van Dongen, and P. Fratzl. The effect of geometry on three-dimensional tissue growth. *J R Soc Interface*, 5(27):1173–80, 2008.

[18] J. C. Fritton, E. R. Myers, T. M. Wright, and M. C. H. van der Meulen. Loading induces site-specific increases in mineral content assessed by microcomputed tomography of the mouse tibia. *Bone*, 36(6):1030–1038, 2005.

[19] L. K. Saxon, A. G. Robling, I. Alam, and C. H. Turner. Mechanosensitivity of the rat skeleton decreases after a long period of loading, but is improved with time off. *Bone*, 36(3):454–64, 2005.

[20] D. M. Cullen, R. T. Smith, and M. P. Akhter. Time course for bone formation with long-term external mechanical loading. *J Appl Physiol*, 88(6):1943–8, 2000.

5.2 Strain-adaptive *in silico* modeling of bone adaptation - a computer simulation validated by *in vivo* micro-computed tomography data

Friederike A. Schulte[1], Alexander Zwahlen[1], Floor M. Lambers[1], Gisela Kuhn[1], Duncan J. Webster[1] and Ralph Müller[1]

[1]Institute for Biomechanics, ETH Zurich, Zurich, Switzerland

Abstract:

Computational models are an invaluable tool to test different mechanobiological theories and, if validated properly, for predicting changes in individuals over time. Concise validation of computational models, however, has been a bottleneck in the past due to a lack of appropriate reference data. Here, we present a strain-adaptive *in silico* algorithm which is validated by means of experimental *in vivo* loading data as well as by an *in vivo* ovariectomy experiment in the mouse. The maximum prediction error following four weeks of loading resulted in 2.4% in bone volume fraction and 8.4% in other bone structural parameters. The extent of formation and resorption rates was not significantly different between simulation and experiment (BFR, BRR, $p>0.05$). Ovariectomy was simulated with a maximum prediction error of 12.1% in BV/TV and other bone morphometric indices, including a saturation level after a few weeks. In the osteoporotic case dynamic rates were more difficult to be accurately predicted by the simulation, showing evidence by significant differences between simulation and experiment ($p<0.05$). In conclusion, we propose a computational model which is validated by means of experimental *in vivo* data. Such evaluation can assess the validity of a computational model and determine its prediction error. This information may become of major significance if computational models will be applied in clinics for a better fracture risk prediction and the effect of a potential pharmaceutical therapy.

Keywords:

in silico simulation; validation; mechanical loading; ovariectomy; *in vivo* micro-

computed tomography

5.2.1 Introduction

Bone is an organ which is able to continuously change its internal microstructure to adapt to mechanical and metabolic demands. Bone remodeling is executed by bone forming and resorbing cells. It is known that bone mass and morphology are adapted to the influence of external forces. Physical exercise increases bone mass [1] while inactivity reduces it [2]. During post-menopausal osteoporosis, the regulatory mechanisms are obviously disturbed by a systemic lack of the hormone estrogen. This leads to a deterioration of bone mass and structure and an increased fracture risk.

The extraction of a common regulatory mechanism, which would combine all above phenomena and would be able to transfer these onto the cellular level, is a matter of computational models these days. On one hand, computational models can be used to test different mechanobiological theories and on the other hand, - if validated properly - they can be used for the prediction of changes in bone. This would be useful in osteoporotic patients to predict the individual fracture risk and select the optimal treatment. Concise validation of computational models, however, has presented a difficulty in the past due to a lack of appropriate experimental reference data.

In an earlier study we have proposed to use experimental *in vivo* data for the validation of a predictive computational algorithm using open-loop control (see Section 5.1). When validating this *in silico* model, it was found that bone volume fraction could be predicted with 2.4% deviation after 4 weeks of experiment. The spatial patterns of bone formation and resorption however were not replicated by the computational algorithm. For this reason, it was proposed that a local control mechanism guiding bone formation and resorption is required as was already suggested by other researchers in more hypothetical simulation frameworks [3,4].

Here, we implemented a local feedback mechanism following the so-called mechanostat theory [5] into our computational model and validated the model's predictive value by means of experimental *in vivo* loading as well as *in vivo* ovariectomy data. The aim was to investigate whether the morphometric bone properties and the spatial patterns of bone formation and resorption could be predicted by the simulation model. Furthermore, we aimed at investigating which discrepancies

could arise between simulation and experiment. With this information, we hoped to gain a better understanding of the impact of a mechanical feedback loop on bone remodeling with loading or disease.

5.2.2 Materials and Methods

Experimental *in vivo* data

The experimental data serving as reference measurements for the proposed simulation algorithm were taken from two published *in vivo* studies [6, 7]. Briefly, in the first study, *in vivo* bone adaptation was induced in nine 15 week old, female C57BL/6 mice (RCC; Füllinsdorf, Switzerland) by subjecting the 6^{th} caudal vertebra to mechanical loading at 8 N for 3000 cycles at 10 Hz, 3 times per week for 4 weeks, following an established loading protocol [8]. The 6^{th} caudal vertebra was scanned weekly with *in vivo* micro-computed tomography (vivaCT 40, Scanco Medical, Brüttisellen, Switzerland) at an isotropic voxel resolution of 10.5 μm.

In the second *in vivo* data set, trabecular bone loss was evoked in nine 15-week-old female C57BL/6 mice (RCC Ltd, Füllinsdorf, Switzerland) by ovariectomy (OVX). The 6^{th} caudal vertebra was scanned on the day of ovariectomy and every two weeks after with *in vivo* micro-computed tomography, over a period of 12 weeks. All animal procedures were performed under isoflurane anaesthesia (2-2.5%, 0.4 L/min) delivered through a nose mask and were approved by the local animal ethics committee (Kantonales Veterinäramt Zürich, Zürich, Switzerland).

Computational algorithm

The computational algorithm was based on the idea that the initial bone surface was moved as a function of the local mechanical stimulus. In order to relate bone gain or loss at a particular location with the mechanical signal, we implemented a function M similar to the mechanostat theory proposed by Frost [5] with

$$M(x) = \begin{cases} -umax, & x < P_{lower} - \frac{umax}{\tau} \\ -(P_{lower} * \tau) + \tau * x, & P_{lower} - \frac{umax}{\tau} < x < P_{lower} \\ 0, & P_{lower} < x < P_{upper} \\ (P_{upper} * \tau) + \tau * x, & P_{upper} < x < P_{upper} + \frac{umax}{\tau} \\ umax, & P_{upper} + \frac{umax}{\tau} < x \end{cases} \tag{5.1}$$

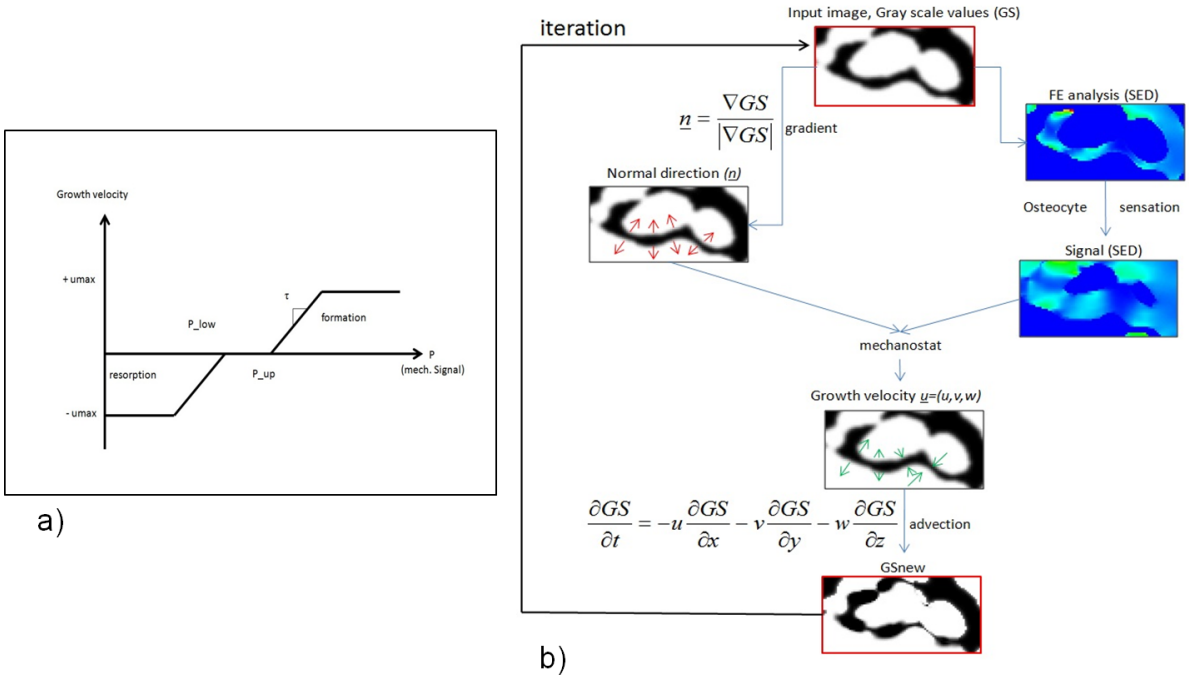

Figure 5.6: a) Function M relating bone formation and resorption to the mechanical signal SED. This function is defined following the mechanostat theory proposed by Frost [5]. b) Schematic workflow representation of the *in silico* model. The binary input is blurred to extract the surface normal. After thresholding, finite element analysis is performed to derive the prevailing local SED-environment. Mechanical signal and the direction normal are used to determine the growth velocity and direction. The non-linear advection equation to determine the surface growth is solved, a new blurred image is derived and the process starts with the second iteration.

A graphical representation of the function M is displayed in Figure 5.6a. The function M is defined by the slope τ (measure for how fast bone formation and resorption rates reach their maximum velocity), by two thresholds (P_{lower} and P_{upper}) below and above which bone resorption and formation would occur, respectively, and a maximum velocity for bone formation and resorption (umax). In the current implementation, it was assumed that the mechanical strains would not reach the range in which micro-damage usually occurs.

The algorithmic design is schematically outlined in Figure 5.6b. Micro-Finite Element Analysis (μFEA) was applied in order to estimate the mechanical signal in the bone which was in this case defined to be the strain energy density (SED) distribution. Similar to other studies, it was assumed that an osteocyte senses a

mechanical load and sends signals in all directions activating osteoblasts and osteoclasts [3, 4, 9]. Consequently a single osteoblast or osteoclast receives more signals from a close osteocyte and less from a distant one. The influence of all osteocytes summed up each with a distance $(x - x_i)$ from an osteoblast or osteoclast and was described with the following function:

$$P(x) = \sum e^{-\frac{(x-x_i)^2}{2\sigma^2}} \, SED * x_i \tag{5.2}$$

where P is the sum of the signals from all osteocytes in the neighborhood of a voxel and σ represents the sensing distance of the signals. This definition is similar to the equation proposed by Huiskes and co-workers [3, 9, 10]. A difference compared to the proposal of these authors is that here a second-order decay was used instead of a first order decay. The reason for choosing a decay of second order was because it could then be implemented as a Gaussian filter which is an optimal lowpass filter and therefore preferred over a first order filter.

Function M represents the mathematical formulation how the extent of the growth velocity is determined. The actual surface growth or loss of bone at a particular location was realized as follows: In a first step, the binary input image was blurred by a Gaussian filter in a first step. By changing from a binary image to a blurred grayscale image (GS), the bone surface is not clearly defined anymore. Therefore, a non-linear advection equation was used to expand or shrink bone at a particular location. The advection equation

$$\frac{\delta GS(x)}{\delta t} = -u(x) * \frac{\delta GS(x)}{\delta x} - v(x) * \frac{\delta GS(x)}{\delta y} - w(x) * \frac{\delta GS(x)}{\delta z} \tag{5.3}$$

becomes non-linear when the velocities u, v and w in x, y and z direction are defined so that the velocity always shows in the direction of the steepest decent:

$$(u(x), v(x), w(x)) = -M(P(x)) * \frac{\nabla GS(x)}{|\nabla GS(x)|}, mm/week \tag{5.4}$$

This non-linear equation was solved in an iterative process; first $P(x)$ was calculated from the μFEA results, and then the advection equation with the velocity field was solved. For the calculation of the advection equation, an FTCS (Forward Time Central Space) scheme was applied. In a second iteration, a new μFEA calculation was run on the new geometry and $P(x)$ was calculated again. To solve the advection equation and to fulfill stable numerical calculation, the maximum absolute velocity

Table 5.5: Model parameters

Parameter	Variable name	Unit	Value Loading	Value OVX
Bone formation/resorption rate per SED	τ	(mm/week)/(J/mm^3)	0.5	1.25
Resorption threshold	P_{upper}	J/mm3	0.01	0.010426
Formation threshold	P_{lower}	J/mm3	0.0163	0.030426
Saturation level	umax	mm/week	0.005	0.0175
Osteocyte influence distance [12]	σ	μm	26.25	26.25
Support for osteocyte influence distance	voxel		5	5
preSIBA blur	sigma	voxel	1	1
Support preSIBA	blur	voxel	2	2
Force FE calculation	N		9	9
Youngs modulus [13]	E	MPa	5300	5300
Poisson's ratio [13]	ν	-	0.3	0.3
Integration timestep	dt	weeks	0.5	0.5
FE calculation timestep	Dt	weeks	2	2

umax was introduced.

micro-FE-analysis

The mechanical environment was determined from μFEA. In a first step, simplified disks were added on both sides of the 6^{th} vertebra to allow homogeneous loading conditions. Segmented image data were converted into three-dimensional FE-models by converting all voxels to 8 node brick elements, with each model consisting of approximately 1,800,000 elements. A Young's Modulus of 5.3 GPa, and a poisson's ratio of 0.3 were assigned as material properties and a force of 9 N (8 N loading + 1 N preload) was applied. The models were solved using ParFE, a parallel solver for large scale linear elastic FE systems running on 128 CPUs at the Swiss National Supercomputing Centre (CSCS, Manno, Switzerland) [11].

Parameter selection

In contrast to assigning all model parameters values from the literature, as has become an established approach, it was refrained from in the present implementation. A reason for this decision was that the availability of a number of biological indices is constrained to human data or other animal species but does not necessarily apply to mouse C57BL/6 data. Instead, a reasonable choice of parameters was used and where applicable, values were chosen from the literature. The amount of bone gain or loss in the present implementation depends on the variables of the function P, i.e. the location of the two setpoints (P_{lower}, P_{upper}) and the amount of bone formed

or resorbed (τ) per SED value. Each iteration represents a time frame of one week in the mechanical loading and two weeks in the ovariectomy study, with internal incremental steps of 0.25 and 0.5 weeks for solving the advection equation. For the mechanosensory system, the osteocyte density was assumed to be $1/(10.5\ \mu\text{m})^3$ (1 per voxel) and the influencing distance was 26.25 μm by definition. Table 5.5 lists all model parameters used and the values assigned to them in the present implementation for the different scenarios.

The amount of bone gain or loss (bone volume fraction) itself was approximated to the bone gain or loss (bone volume fraction) between the first and second measurement in the experiment. Matching was performed by changing the two setpoints, the slope τ, or umax. The bone volume fraction (BV/TV) of the simulated structures at the time of the second micro-CT measurement was matched by design to the BV/TV of the corresponding experimental structure. For simplicity reasons, the same model parameters were chosen for all animals (returning the least mean of the differences of each simulation/experiment-pair).

Validation by means of *in vivo* micro-computed tomography

The input to the computational algorithm were the binary micro-CT images of the baseline structures which were re-aligned along their main axis to ensure best possible loading preconditions. For this purpose, the unfiltered baseline scans of the *in vivo* micro-computed tomography measurements were re-aligned in a preprocessing step, Gaussian filtered (sigma 1.2, support 1) and segmented at a global threshold (22% of the maximum gray-scale value). The input structures of the loading experiment were the scans at start of loading (1^{st} micro-CT scan) and the input structures of the OVX experiment were the scans at week 4 after surgery (3^{rd} micro-CT scan) when the phase of high bone loss began [7]. For both loading and ovariectomy data, a trabecular mask was defined in the baseline scans following an established protocol [14]. In the algorithmic design, remodeling was only allowed in the trabecular compartment which means that the cortical shell remained unchanged over the course of the simulation.

The curves of five trabecular bone morphometric indices between simulation and experiment were compared using repeated measurements ANOVA and the statistical software package R [15]. The morphometric indices which were compared were bone volume fraction (BV/TV), specific bone surface (BS/BV), trabecular thickness

(Tb.Th), trabecular number (Tb.N) and trabecular separation (Tb.Sp).

Furthermore, dynamic bone morphometry was calculated in the simulation and the experiment from the overlay of the input to the simulation and the final output structure (week 0-4 for loading and 4-12 for OVX, respectively) [16]. In particular, three-dimensional trabecular bone formation rate (BFR), mineral apposition rate (MAR), mineralizing surface (MS), as well as resorption measures bone resorption rate (BRR), mineral resorption rate (MRR) and eroded surface (ES) were compared. A paired Student's t-test was used to detect differences between simulation and experiment. P-values < 0.05 were considered significant.

5.2.3 Results

Figure 5.7 shows the course of experiment and simulation in the bone morphometric indices in response to mechanical loading. The match between simulation and experiment at the second measurement (week 1) was by design while the subsequent points in time demonstrate the predictive potential of the algorithm. All values assigned to the model parameters can be found in Table 5.5.

The percent errors calculated as the difference between simulated and experimental mean of all bone morphometric indices at all time points are listed in Table 5.6. The simulation errors at week 0 result from the fact that the input structures were in a first step converted into a model by one initial iteration of the Gaussian simulation algorithm with homeostatic parameters. The computational model captured the trend in all bone morphometric indices with a prediction error ranging between 2.39% (BV/TV) and 8.44% (Tb.Sp). The deviation between simulation and experiment was significant in BS/BV, Tb.Th, Tb.Sp and Tb.N ($p<0.05$).

Ovariectomy led to an experimental decrease of 32% in BV/TV, with the highest phase of bone loss between weeks 4 and 8 after ovariectomy and a subsequent course into saturation until week 12. The simulation followed this trend by a slight (non-significant) overestimation of BV/TV (Figure 5.8a), including the saturation at a lower bone mass. Figure 5.8b-d show the curves of simulation and experiment of BS/BV, Tb.Th and Tb.N. The trends were always captured, with a maximum prediction error of 12.1% in BV/TV while the maximum error for other structural indices amounted to 4.6% (Tb.N) with none of the differences being significant between simulation and experiment.

Visual comparison of the spatial patterns of bone formation and resorption fol-

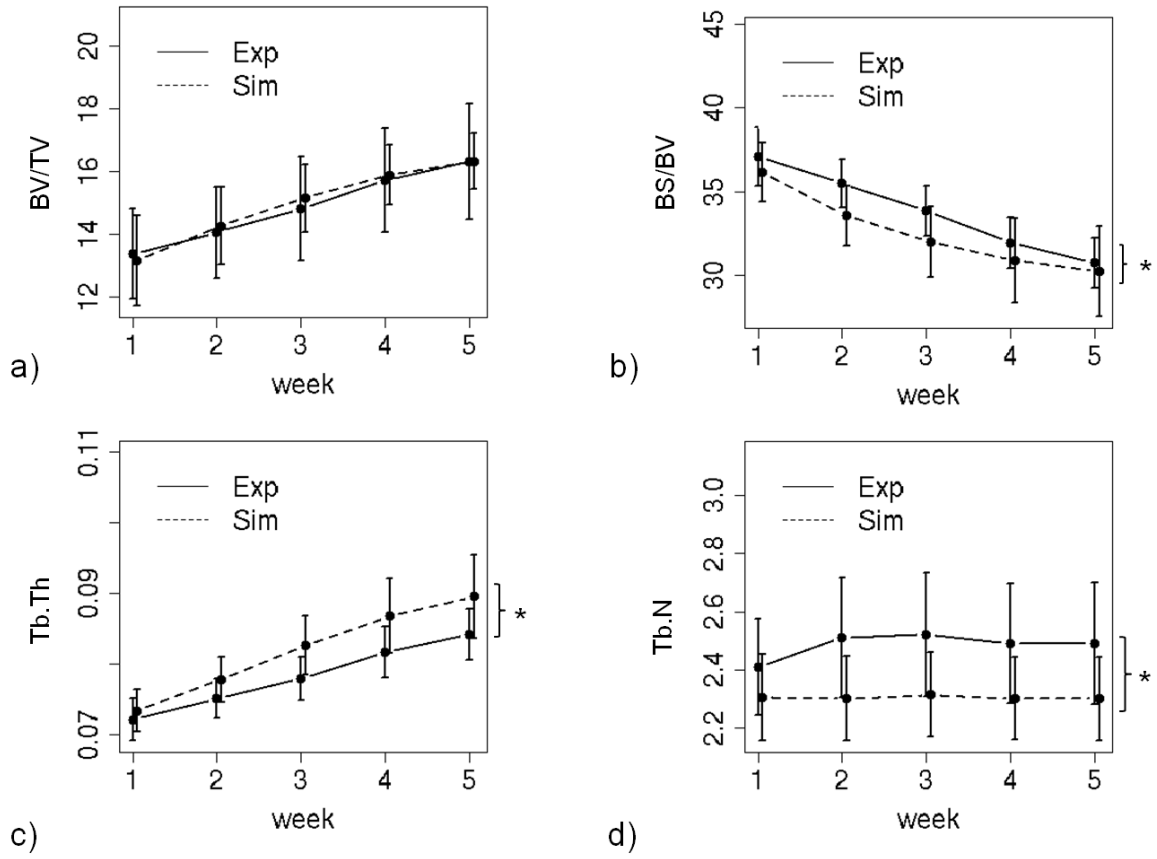

Figure 5.7: Mechanical loading: Course of bone morphometric indices over time. The solid line denotes the experiment and the dashed line the simulation. a) BV/TV, b) BS/BV, c) Tb.Th, d) Tb.N, $*p<0.05$

lowing mechanical loading is presented in Figure 5.9. Figure 5.9a visualizes the simulated and 5.9b the experimental overlay of week 0 and 4. Yellow sites denote formed bone and blue sites resorbed bone. The prediction of the bone response to mechanical loading shows a very similar spatial pattern as the experiment. This pattern is characterized by increased formation sites accompanied by a few resorption areas in both the experiment and simulation.

For ovariectomy-related bone loss, the overlaid images from the simulation and experiment are shown in Figure 5.10. The simulated spatial pattern of bone formation and resorption is characterized by less resorption and less formation sites than the corresponding experimental structure. This means that the simulated structure arrives at the same lower bone volume fraction after eight weeks with comparatively less bone remodeling. Quantitative comparison of bone formation and resorption

Table 5.6: Mechanical loading: Error (in %) between simulated and experimental mean bone morphometric indices at every week in the *in vivo* setup. P-values < 0.05 from a repeated measures ANOVA are considered significant.

Parameter	Error w0	Error w1	Error w2	Error w3	Error w4	p-value
BV/TV	-1.54%	1.47%	2.39%	1.07%	0.08%	n.s.
BS/BV	-2.52%	-5.45%	-5.55%	-3.39%	-1.65%	0.0075
Tb.Th	1.70%	3.59%	6.03%	6.18%	6.37%	0.0002
Tb.Sp	1.57%	7.37%	7.77%	8.44%	7.84%	0.0005
Tb.N	-4.30%	-8.29 %	-8.17%	-7.59%	-7.57%	<0.0001

Table 5.7: Ovariectomy: Error (in %) between simulated and experimental bone morphometric indices at every week in the *in vivo* setup. P-values < 0.05 from a repeated measures ANOVA are considered significant.

Parameter	Error w0	Error w1	Error w2	Error w3	Error w4	p-value
BV/TV	-1.28%	-0.43%	5.78%	12.10%	12.03%	n.s.
BS/BV	-2.26%	-1.61%	-3.15%	-4.33%	-3.21%	n.s.
Tb.Th	1.42%	0.08%	1.94%	2.41%	2.07%	n.s.
Tb.Sp	2.42%	3.36%	2.33%	0.25%	-1.41%	n.s.
Tb.N	-4.61%	-3.75%	-2.53%	-0.41%	2.12%	n.s.

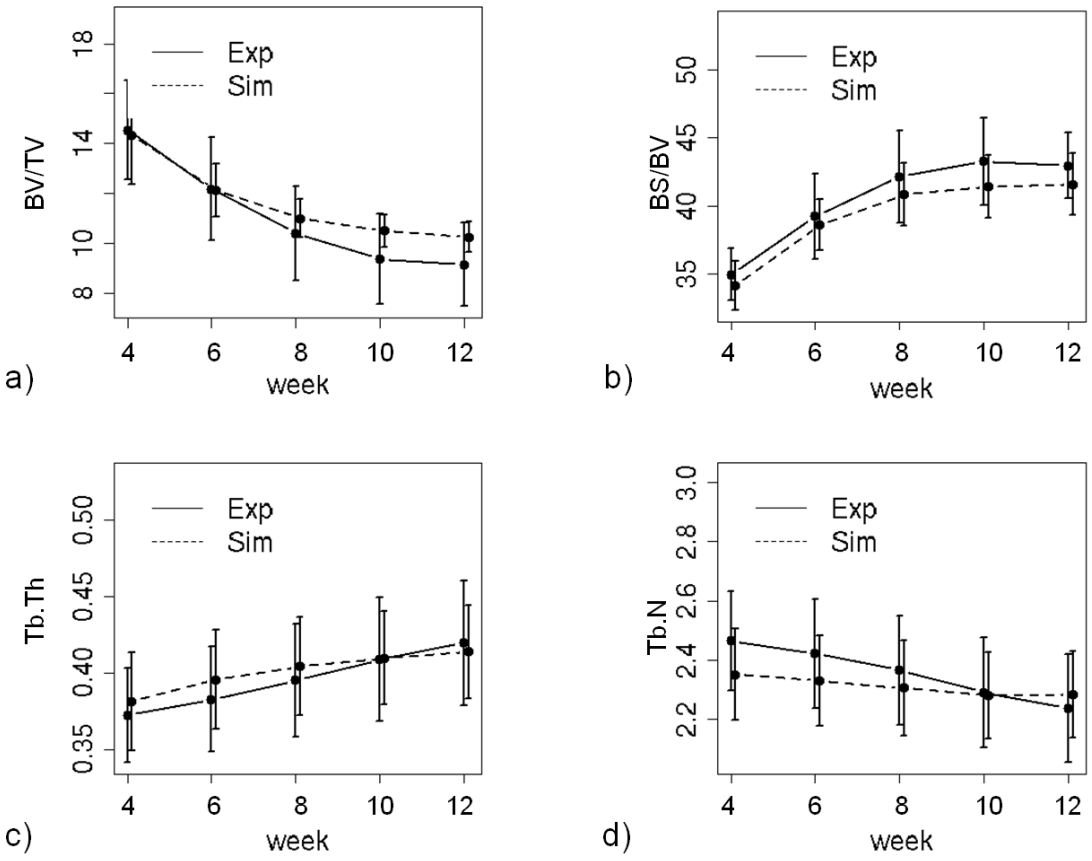

Figure 5.8: Ovariectomy: Course of bone morphometric indices over time. The solid line denotes the experiment and the dashed line the simulation. a) BV/TV, b) BS/BV, c) Tb.Th, d) Tb.N, $*p<0.05$

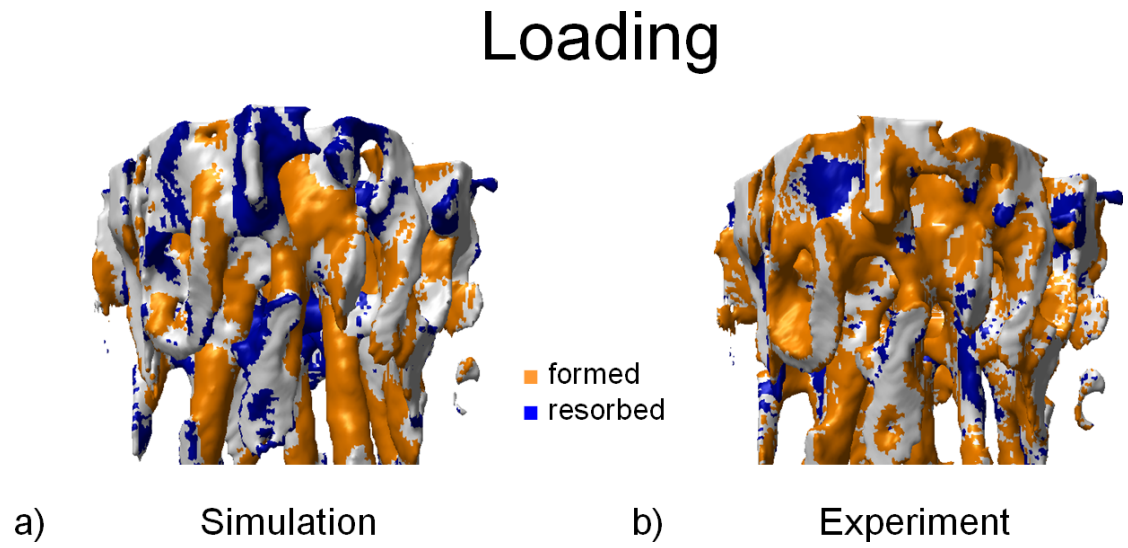

Figure 5.9: Mechanical loading: Visual comparison of spatial patterns of bone formation and resorption gained from overlay between week 0 and week 4. (a) simulation and b) experiment).

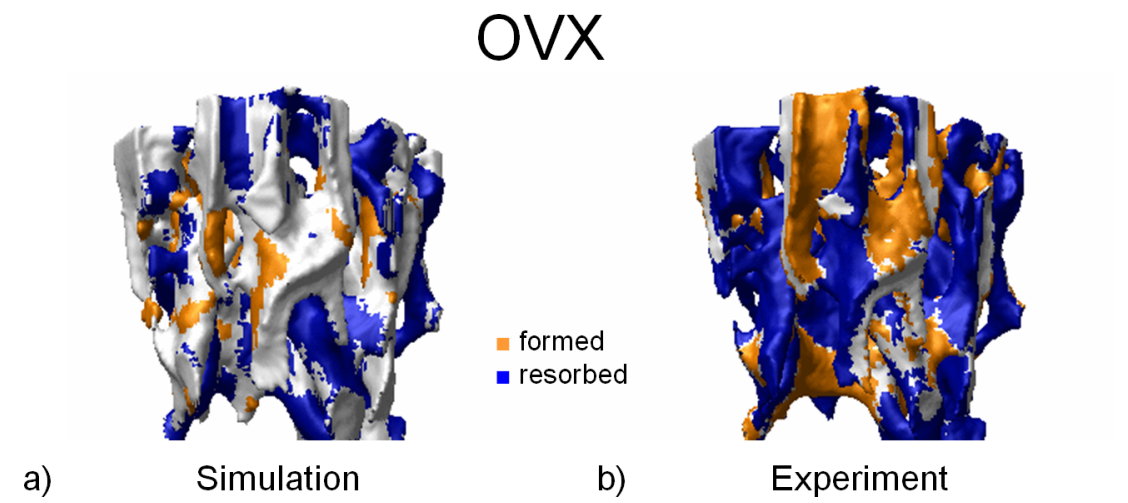

Figure 5.10: Ovariectomy: Visual comparison of spatial patterns of bone formation and resorption gained from overlay between week 4 and 12 (a) simulation and b) experiment).

Table 5.8: Mechanical loading: Mean and standard deviation of three-dimensional dynamic bone morphometry in the experiment compared to the simulation. ($p < 0.05$ considered significant, n.s. = not significant)

Parameter	Experiment	Simulation	p-value
BFR^*_{BV} [%/d]	1.05 ± 0.21	1.12 ± 0.24	n.s.
BRR^*_{BV} [%/d]	0.40 ± 0.12	0.29 ± 0.08	n.s.
MAR* [μm/d]	0.74 ± 0.09	0.81 ± 0.02	0.0362
MRR* [μm/d]	1.09 ± 0.16	0.66 ± 0.05	<0.0001
MS* [%]	62.71 ± 2.98	49.32 ± 7.98	0.0041
ES* [%]	18.16 ± 1.87	17.56 ± 5.32	n.s.

rates confirmed the visual impression. Table 5.8 lists the mean and standard deviation of BFR, BRR, MAR, MRR, MS and ES as assessed after four weeks of mechanical loading. BFR and BRR are not significantly different in simulation and experiment, indicating that the total amounts of bone formation and resorption are well captured. Differences exist in MAR and MS ($p<0.05$), which reflects that the simulation forms slightly thicker but less bone packets than the experiment while at the same time, simulated bone resorption packets are thinner (MRR <0.0001). As already indicated in Figure 5.10, simulated ovariectomy led to significantly lower bone formation rates (BFR, MS, $p<0.05$) as well as significantly lower bone resorption rates (BRR, MRR, $p<0.0001$) compared to the experiment.

5.2.4 Discussion

In this paper, we presented a strain-adaptive *in silico* algorithm which was validated by means of *in vivo* micro-CT data from an anabolic loading experiment and a catabolic ovariectomy experiment in the mouse. The advantage of a validation by means of experimental *in vivo* data is that the predictive value of a computational model can be determined.

With respect to the simulation of mechanical loading, even though structural parameters showed prediction errors of 8.4%, the volumes of formation and resorption as well as their location were accurately predicted. The agreement in remodeling sites imposes a large advantage of the current implementation and is accounted for

Table 5.9: Ovariectomy: Mean and standard deviation of three-dimensional dynamic bone morphometry in the experiment compared to the simulation. ($p < 0.05$ considered significant, n.s. = not significant)

Parameter	Experiment	Simulation	p-value
BFR^*_{BV} [%/d]	0.47 ± 0.18	0.09 ± 0.08	<0.0001
BRR^*_{BV} [%/d]	1.77 ± 0.32	0.98 ± 0.25	<0.0001
MAR* [μm/d]	0.89 ± 0.23	0.80 ± 0.07	n.s.
MRR* [μm/d]	1.74 ± 0.15	1.17 ± 0.07	<0.0001
MS* [%]	25.27 ± 3.57	4.15 ± 3.35	<0.0001
ES* [%]	35.58 ± 3.36	34.29 ± 5.30	n.s.

by the mechanical feedback loop.

Ovariectomy-related bone loss and subsequent stabilization of bone mass at a lower level were captured with a maximum prediction error of 12.1% (BV/TV) in bone structural indices. The experimental plateau that was reached after a few weeks at a lower bone mass was in the simulation reflected, too. This fact suggests that the stagnation of the bone loss after a certain time may be explained by a mechanical feedback-control. This means that once the bone structure has reached a critical mass, the local strain environment signals a need for increased bone formation (i.e. more SED values fall above the upper set point), which would compensate the pathologically increased bone resorption rates. An experimental delayed increase of bone formation rates compared to bone resorption rates was observed by Lambers et al. [7].

A limitation of the proposed computational algorithm at the current stage is that in response to mechanical loading, simulated morphometric parameters other than BV/TV show a systematic bias towards slightly thicker but less trabeculae. Following the simulated changes in response to ovariectomy, systematically less remodeling is going on compared to the experiment. This leads to a bias in the prediction of these specific morphometric indices. The apparent discrepancy might be related to the fact that the present implementation bases on a deterministic, purely mechanically motivated feedback-loop. In this model, two set points define the ranges in which bone resorption, no changes, or bone formation takes place. This implies that

bone resorption can by definition not occur at high strain signals and the other way round. This constraint is surely the most straight-forward and fastest way to achieve a mechanically optimal structure. Biology however may not stick to this demand. It is known that untargeted remodeling (e.g. regulation of the calcium or phosphate storage), other biological and biochemical signals or the repair of occurring micro-cracks also evoke bone remodeling at sites which may sometimes not be mechanically meaningful. This fact could explain why simulated ovariectomy-related bone loss leads to the same decrease in bone mass as in the experiment with significantly less bone formation and resorption volumes. The detected bone remodeling sites in the simulation probably represent the sites necessary to be adapted from a mechanical point of view while other stimuli are disregarded. With respect to mechanical loading where bone formation and resorption volumes match but morphometric indices don't, it seems as if primarily the thickness but not total volume of the simulated bone formation and resorption packets differs from the experiment, which entails changes in the bone morphometric properties. These discrepancies between simulation and experiment implicate that additional consideration of stimuli other than of mechanical origin may lead to more accurate predictions in future implementations of computational remodeling models.

Furthermore, the predictive setup and determination of the prediction error is assumed to become of major importance when computational algorithms make it into clinics and are applied to real patient data. In particular, computational models are presumed to provide an enhanced fracture risk prediction and thus assist diagnosis and potential pharmaceutical treatment. In this case, however, a certain measure of reliability needs to be reported to the patient. Therefore, appropriate validation techniques for the computational models must be available beforehand. The current validation setup uses the same set of model parameters for all animals by disregard of variations in the behavior of different mice. Instead, an approach fitting the model parameters to each person individually instead of taking the average of a global population would be preferential for a final application in the clinics, especially in the face of personalized medicine.

In conclusion, we presented a predictive strain-adaptive computational model which was validated by means of experimental *in vivo* loading data as well as an ovariectomy experiment. The prediction error was determined as well as the potential to predict local changes in the bone micro-structure. With the current findings,

it is proposed that future *in silico* models and experiments should not exclusively be compared for structural but also for dynamic parameters. Apart from this, the presented validation approach revealed that experimental computer simulations can be improved through validation by *in vivo* data. With this, it is assumed that a better understanding of the biological processes involved during bone remodeling is gained.

Acknowledgements

Funding from the European Union for the osteoporotic virtual physiological human project (VPHOP FP7-ICT2008-223865) is gratefully acknowledged.

References

[1] B. Cohen, P. J. Millett, B. Mist, M. A. Laskey, and N. Rushton. Effect of exercise training programme on bone mineral density in novice college rowers. *Br J Sports Med*, 29(2):85–8, 1995.

[2] A. D. Leblanc, V. S. Schneider, H. J. Evans, D. A. Engelbretson, and J. M. Krebs. Bone-mineral loss and recovery after 17 weeks of bed rest. *Journal of Bone and Mineral Research*, 5(8):843–850, 1990.

[3] R. Ruimerman, P. Hilbers, B. van Rietbergen, and R. Huiskes. A theoretical framework for strain-related trabecular bone maintenance and adaptation. *J Biomech*, 38(4):931–41, 2005.

[4] T. Adachi, K. Tsubota, Y. Tomita, and S. J. Hollister. Trabecular surface remodeling simulation for cancellous bone using microstructural voxel finite element models. *J Biomech Eng*, 123(5):403–9, 2001.

[5] H. M. Frost. The mechanostat: a proposed pathogenic mechanism of osteoporoses and the bone mass effects of mechanical and nonmechanical agents. *Bone Miner*, 2(2):73–85, 1987.

[6] F. M. Lambers, G. Kuhn, F. A. Gerhard, and R. Müller. In vivo micro computed tomography allows monitoring of load induced microstructural bone adaptation. *Bone*, 44(S2):300, 2009.

[7] F. M. Lambers, K. Koch, F. Schulte, G. Kuhn, and R. Müller. Ovariectomy increases bone formation rate as well as bone resorption rate in mouse tail vertebra. *Bone*, 47(Supplement 1):S165–S165, 2010. 8756-3282 doi: DOI: 10.1016/j.bone.2010.04.383.

[8] D. J. Webster, P. L. Morley, G. H. van Lenthe, and R. Müller. A novel in vivo mouse model for mechanically stimulated bone adaptation - a combined experimental and computational validation study. *Comput Methods Biomech Biomed Engin*, 11(5):435–441, 2008.

[9] R. Huiskes, R. Ruimerman, G. H. van Lenthe, and J. D. Janssen. Effects of mechanical forces on maintenance and adaptation of form in trabecular bone. *Nature*, 405(6787):704–706, 2000.

[10] R. Huiskes, H. Weinans, H. J. Grootenboer, M. Dalstra, B. Fudala, and T. J. Slooff. Adaptive bone-remodeling theory applied to prosthetic-design analysis. *J Biomech*, 20(11-12):1135–50, 1987.

[11] P. Arbenz, G. H. van Lenthe, U. Mennel, R. Müller, and M. Sala. A scalable multi-level preconditioner for matrix-free μ-finite element analysis of human bone structures. *Int. J. for Numerical Methods in Engineering*, 73(7):927–947, 2008.

[12] M. G. Mullender and R. Huiskes. Proposal for the regulatory mechanism of wolff's law. *J Orthop Res*, 13(4):503–12, 1995.

[13] B. Van Rietbergen, A. Odgaard, J. Kabel, and R. Huiskes. Direct mechanics assessment of elastic symmetries and properties of trabecular bone architecture. *J Biomech*, 29(12):1653–1657, 1996.

[14] T. Kohler, M. Stauber, L. R. Donahue, and R. Müller. Automated compartmental analysis for high-throughput skeletal phenotyping in femora of genetic mouse models. *Bone*, 41(4):659–667, 2007.

[15] R Development Core Team. *R: A language and environment for statistical computing*. R Foundation for Statistical Computing, Vienna, Austria, 2007.

[16] F. A. Schulte, F. M. Lambers, G. Kuhn, and R. Müller. In vivo micro-computed tomography allows direct three-dimensional quantification of both bone formation and bone resorption parameters using time-lapsed imaging. *Bone*, 48(3):433–442, 2011.

Chapter 6

Synthesis

Bone research is often focused on a better understanding of the most common bone disease: osteoporosis. Osteoporosis is characterized by an excessive loss of bone mass and a related increased risk of fracture. This results from a shift in the remodeling balance with bone resorption exceeding bone formation. The pathological mechanism disturbing this balance is a topic of major interest because it is postulated that its specification will lead to a safer and more efficient treatment of osteoporosis.

In the search for the defective mechanism, it can be of great help to have a good understanding of the laws that apply to bone remodeling in healthy states. Under physiological conditions, it is well established that mechanical loading is a key regulator of bone in homeostasis. How the mechanical stimuli are translated into biochemical signals evoking bone formation and resorption is however still poorly understood. Lacking access to experimental measures of dynamic bone formation and resorption rates *in vivo*, the investigation of the interplay between bone forming and resorbing cells and a potential mechanical signal has to date mostly been reserved for *in silico* simulation models.

Computational models are an invaluable tool to investigate questions related to bone remodeling. Besides their potential in clinical settings to assist diagnosis and monitoring of treatment, they also allow the exploration of mechanobiological remodeling theories that to date have been unrealizable for experimental studies. Such theories reach back to more than 100 years ago when bone adaptation was associated with mechanical loads for the first time [1, 2]. A further advantage of *in silico* models is that they do not require a long planning and design period to implement and test various theories. Thus, *in silico* algorithms can support new hypotheses and therefore also have the potential to guide experimental research.

On the other hand, computer simulations can only be as good as their validation and thus they require appropriate experimental data for validation. This interdependency results in the requirement for a sensitive balance between computational modeling and experimental studies in the long term, where one can inform the other and vice versa. The lack of appropriate *in vivo* data in the last decades has led to an abundance of implementations of remodeling theories without appropriate tools to strengthen or rule out any of these hypotheses.

With the advent of *in vivo* micro-computed tomography it is now possible to provide access to essential experimental data by which computational models can be validated. Especially the ability to quantify and monitor local bone changes in the experiment is considered a major enhancement for the validation of *in silico* models. Furthermore, appropriate analysis of *in vivo* data might allow questions to be answered by experiments that to date had been reserved for *in silico* simulations. Lastly, experimental *in vivo* micro-CT data potentially provide access to experimental measures of dynamic bone remodeling rates *in vivo*.

Along those lines of investigation, the final aim of this thesis was to develop and validate a computational model for bone adaptation by experimental *in vivo* data and by making use of the information provided from the experimental analysis. Firstly, three-dimensional bone remodeling rates were quantified from *in vivo* micro-CT. Secondly, these rates were compared to the prevalent mechanical environment, and thirdly, a computational model was developed taking into account the experimental dynamic rates as well as a mechanical signaling pathway.

Novel methods for dynamic bone morphometry

The major achievement of Chapter 3 was the establishment of a three-dimensional technique to measure bone formation and resorption rates from follow-up *in vivo* micro-CT scans. This technique was based on rigid image registration of time-lapsed gray-scale images.

However, since interpolation is required for registration and can affect the image quality, and therefore the inherent measured structural properties, the error coming from interpolation was investigated in the first part of this chapter. The impact of this interpolation error on the quantification of the bone structure was unknown up to now. Therefore, the purpose of this study was to elaborate the interpolation error on bone morphometric indices by using three different interpolator schemes: near-

est neighbor, tri-linear and B-spline interpolation. B-spline approximation (BSP) showed, in contrast to the other two interpolation techniques, no significant deviations in bone morphometric indices between the untransformed and registered scans. Because the interpolation errors were in the same range as the reproducibility reported in earlier *in vivo* studies, the evaluation of trabecular bone morphometric indices on transformed images using B-spline interpolation was considered legitimate, at least in combination with BSP used as interpolator during the registration itself.

With this prerequisite fulfilled, the second part of the chapter was concerned with the extraction of dynamic bone formation and resorption rates from *in vivo* micro-computed tomography scans. Bone formation rates are well-established two-dimensional histomorphometric indices. In the present thesis, three-dimensional mineralizing surface (MS), mineral apposition rate (MAR), and bone formation rate (BFR) were introduced in accordance to the current nomenclature of dynamic histomorphometry. Furthermore, three-dimensional resorption parameters such as eroded surface (ES) as well as newly defined indices such as mineral resorption rate (MRR) and bone resorption rate (BRR) were introduced. To establish the accuracy of the new technique, linear regression analysis of newly developed dynamic formation parameters and the traditional quantitative measures of histomorphometry was performed. This analysis resulted in $R=0.68$ and $R=0.78$ for MAR and MS respectively ($p<0.05$). Reproducibility was assessed in 8 samples that were scanned 5 times *ex vivo* with precision errors ranging from 0.9% (MRR) to 6.6% (BRR). The sensitivity was shown by applying the method to a murine *in vivo* loading model. The new technique detected significantly increased trabecular bone formation (BFR and MS, $p<0.01$) and decreased bone resorption (ES, $p<0.01$) after four weeks of loading compared to the control group which agreed with earlier findings in the literature based on dynamic histomorphometry [3–5]. With these results, it was concluded that the newly developed method is reproducible, accurate and sensitive and thus well-suited for the calculation of dynamic bone morphometry indices from time-lapsed *in vivo* micro-CT images. Compared to histomorphometry, the new technique is non-invasive, non-destructive, three-dimensional and fully-automated. Furthermore, direct assessment of time-dependent bone resorption rates becomes accessible. It is assumed that the quantification of dynamic bone resorption rates over time will open new perspectives for measuring dynamic changes in a wide range of

treatments and will especially be advantageous in studies where bone loss is a dominant factor such as in osteoporosis; something that so far was difficult to investigate using quantitative analysis of bone resorption.

New findings in mechanobiology

The major finding of Chapter 4 was the proof and quantitative description of a local mechano-regulatory mechanism controlling both bone formation and resorption. This finding was gained by comparison of the local bone formation and resorption sites following mechanical loading of the 6^{th} caudal vertebra of mice and the prevailing local mechanical milieu in these regions. This study was motivated by the fact that a number of existing computational models were based on the assumption that local bone formation is a direct result of increased mechanical strains while for bone resorption, controversial remodeling theories exist. Some implementations used random bone resorption [6] while others related low strains with local bone loss [7]. The proposed experimental *in vivo* setup in combination with newly extracted bone remodeling sites and finite element analysis allowed this question to be properly investigated for both formation and resorption sites. Results showed that mean SED at formation sites was significantly higher than mean SED at constant sites while mean SED at resorption sites was significantly lower than mean SED at constant sites ($p<0.0001$, $p<0.0001$). Such differences in SED between subsequent bone formation and bone resorption sites were shown to exist both in response to mechanical loading as well as in controls and ovariectomized mice ($p<0.001$). Thus this relation was considered to be a general rule in a variety of physiological and pathological situations. Furthermore, a strong correlation between increasing strain-energy-density-values and subsequent probability for bone formation was found ($R=0.995$) as well as a strong reciprocal correlation between increasing SED-values and subsequent probability for bone resorption ($R=0.995$). The combination of experimental three-dimensional dynamic remodeling rates and finite element simulation was the first time a mechano-regulation mechanism was demonstrated to exist at the local level in trabecular bone.

Determination of the predictive value of *in silico* models

The major achievement of Chapter 5 was the development of a computational model of bone adaptation and its validation by means of experimental *in vivo* data.

First, a predictive validation setup using experimental *in vivo* data was developed to determine the prediction error of a computational model. In this section, a simple thickening algorithm was implemented to predict the bone response to increased mechanical loading. While morphometric indices were accurately predicted after four weeks of experiment, spatial patterns of formation and resorption could not be replicated by the *in silico* model. This finding underlined the importance of using a local feedback mechanism, deciding on-site whether bone should be formed or resorbed. Thus, in a second step, a mechanical feedback loop was implemented in the *in silico* model. Results showed that after four weeks of mechanical loading, an agreement between morphometric as well as dynamic remodeling rates was achieved (prediction error 8.4% in bone morphometric indices). Bone loss after ovariectomy was as well successfully simulated, including the prediction of a saturation level at a lower bone mass after a few weeks, however still showing discrepancies in spatial patterns of bone remodeling (prediction error 12.1% in bone morphometric indices).

With these results, it was shown that continued validation by means of experimental *in vivo* data is able to guide the development of the *in silico* model and simultaneously gain novel insights into the biological interrelationships involved during bone adaptation.

Limitations and future research

A general limitation of the presented method in Chapter 3 is its dependency on the image resolution of *in vivo* micro-CT scanners. In conventional histomorphometry, short time periods (days) can be addressed giving insight into the activity of particular bone cells; this is not possible with the micro-CT technique. Here, the minimum time interval is dependent on the voxel size of the imaging system. For the underlying mechanical loading data, however, the authors found a time interval of 7 days to be sufficient for a voxel size of 10.5 μm. This was verified by the good correlation between dynamic histomorphometry and micro-CT morphometry.

A limitation of the proposed setup in Chapter 4 was that only SED values on the surface were considered for the comparison, disregarding the thickness of remodeling packets. The surface voxels, however, are most at risk if it comes to registration errors, partial volumes effects, or artifacts from the finite element calculations. Thus, it is likely that any relationship between groups is weakened by these noise factors. As an outlook, the impact of this limitation might be investigated further. Apart

from this, the proposed setup allows testing different remodeling theories by means of experimental data without the need to fall back on a number of additional assumptions as is typically the case in *in silico* modeling. This opens wide possibilities to the field of *in silico* algorithms as a validation for existing hypotheses of bone adaptation.

A limitation of the proposed validation technique presented in Chapter 5 was that not all model parameters were taken from the literature but some parameters were chosen to match experimental increase or decrease of bone mass. Furthermore, the same set of model parameters was used for all animals, disregarding variations in the phenotypic behavior of the mice. For a final application in the clinics, an approach fitting the model parameters to each person individually instead of taking the average of a global population would be preferential.

Using local mechanical regulation for the *in silico* model, there still existed differences between simulation and experiment. An explanation for these discrepancies is that the theory behind the implementation of the *in silico* algorithm was purely based on a mechanical decision rule. In biology, however, this mechanistic regulation mechanism may be one out of a number of mechanisms controlling the local interplay between formation and resorption. Biological interferences with the mechanical trigger might result from non-targeted remodelling and other influences, e.g. by hormones or cytokines. This implies that *in silico* modeling might, in the future, consider moving away from a purely deterministic view towards a more probabilistic implementation of bone remodeling which would also go in line with the findings gained in Chapter 4.

Conclusions

The present thesis has described three novel main findings or approaches: First, a non-invasive three-dimensional and fully-automated technique to assess both bone formation and resorption rates from *in vivo* micro-computed tomography data was presented. Second, this work established a relationship between the prevailing local mechanical milieu and subsequent bone formation and resorption as well as a functional form of the underlying local mechano-regulatory mechanism for bone adaptation. Third, it was shown that the combination of predictive computational modeling and step-wise validation by means of *in vivo* micro-computed tomography data builds a powerful unit to guide the development of predictive *in silico* mod-

els and gain novel insights into the biological interrelationships involved in bone remodeling and adaptation.

References

[1] J. Wolff. *Das Gesetz der Transformation der Knochen (The Law of Bone Remodelling)*. Springer-Verlag, Berlin, Germany, 1892.

[2] Wilhelm Roux. *Der Kampf der Theile im Organismus*. Wilhelm Engelman, Leipzig, 1881.

[3] R. A. Hillam and T. M. Skerry. Inhibition of bone resorption and stimulation of formation by mechanical loading of the modeling rat ulna in vivo. *J Bone Miner Res*, 10(5):683–9, 1995.

[4] D. Webster, E. Wasserman, M. Ehrbar, F. Weber, I. Bab, and R. Müller. Mechanical loading of mouse caudal vertebrae increases trabecular and cortical bone mass-dependence on dose and genotype. *Biomech Model Mechanobiol*, 9(6):737–47, 2010.

[5] T. J. Chambers, M. Evans, T. N. Gardner, A. Turner-Smith, and J. W. Chow. Induction of bone formation in rat tail vertebrae by mechanical loading. *Bone Miner*, 20(2):167–78, 1993.

[6] R. Ruimerman, P. Hilbers, B. van Rietbergen, and R. Huiskes. A theoretical framework for strain-related trabecular bone maintenance and adaptation. *J Biomech*, 38(4):931–41, 2005.

[7] T. Adachi, K. Tsubota, Y. Tomita, and S. J. Hollister. Trabecular surface remodeling simulation for cancellous bone using microstructural voxel finite element models. *J Biomech Eng*, 123(5):403–9, 2001.

Curriculum Vitae

Friederike A. Schulte

nee Gerhard
Born 4^{th} July, 1981, in Nürnberg, Germany

Education

2006 – 2011	Ph.D. studies (Dr. sc. ETH), Institute for Biomechanics, ETH Zurich, Switzerland, under the supervision of Prof. Dr. Ralph Müller
2006	Diploma thesis, Institute for Computer Vision, ETH Zurich, Switzerland, under the supervision of Dr. Mireille Reeff and Prof. Dr. Gabor Szekely
2000 – 2006	Studies of Computer Science, FAU Erlangen-Nürnberg, Germany, with graduation Dipl.-Inf.
1991 – 2000	Scientific high school, Ansbach, Germany, with graduation Abitur
1987 – 1991	Primary school, Ansbach, Germany

Awards and honors

2010	ESB Student Award, European Society of Biomechanics (ESB), Edinburgh, Scotland
2010	ECTS New Investigator Award, European Calcified Tissue Society (ECTS), Glasgow, Scotland
2009	ECTS Travel Award, European Calcified Tissue Society (ECTS), Vienna, Austria

Publications

2011 F. A. Schulte, F. M. Lambers, G. Kuhn, and R. Müller. *In vivo micro-computed tomography allows direct three-dimensional quantification of both bone formation and bone resorption parameters using time-lapsed imaging.* Bone, 48:433-442, 2011.

2011 F. M. Lambers, F. A. Schulte, G. Kuhn, D. J. Webster, and R. Müller. *Mouse tail vertebrae adapt to mechanical loading by increasing bone formation rate and decreasing bone resorption rate, leading to an overall increased strength.* Bone, 2011, submitted.

2011 F. A. Schulte, F. M. Lambers, D. J. Webster, G. Kuhn, and R. Müller. *In vivo validation of a computational bone adaptation model using open-loop control and time-lapsed micro-computed tomography.* Bone, 2011, submitted.

2011 F. A. Schulte, F. M. Lambers, T. L. Mueller, M. Stauber, and R. Müller. *Quantitative outcomes after image registration of micro-computed tomography scans critically depend on interpolation technique.* Computer Methods in Biomechanics and Biomedical Engineering, 2011, submitted.

2011 F. A. Schulte, D. Ruffoni, F. M. Lambers, G. Kuhn, D. Christen, D. J. Webster, and R. Müller. *Local mechanical environment regulates osteoblast and osteoclast activity.* in preparation, 2011.

2011 F. A. Schulte, A. Zwahlen, F. M. Lambers, G. Kuhn, D. J. Webster, and R. Müller. *Predictive model for bone adaptation using local load-adaptive feedback control.* in preparation, 2011.

2011 F. M. Lambers, G. Kuhn, F. A. Schulte, K. Koch, and R. Müller. *Transient bone morphometry in a mouse tail model of postmenopausal osteoporosis.* in preparation, 2011.

2011 F. M. Lambers, G. Kuhn, C. Weigt, K. Koch, F. A. Schulte, and R. Müller. *Bone strength but not microstructure is retained in aging mice.* in preparation, 2011.

2011 F. M. Lambers, C. Weigt, K. Koch, F. A. Schulte, G. Kuhn, and R. Müller. *Caudal vertebrae of mice remain mechanosensitive with age after cyclic loading.* in preparation, 2011.

2011 F. M. Lambers, F. Stuker, C. Weigt, G. Kuhn, K. Koch, F. A. Schulte, J. Ripoll, M. Rudin, and R. Müller. *Multimodality imaging of load-induced bone adaptation.* in preparation, 2011.

2011 F. M. Lambers, K. Koch, G. Kuhn, C. Weigt, F. A. Schulte, and R. Müller. *Longitudinal effect on bone strength and dynamic morphometry during 14 weeks of cyclic loading in a mouse model of bone adaptation.* in preparation, 2011.

2009 F. A. Gerhard, D. J. Webster, G. H. van Lenthe, and R. Müller. *In silico biology of modelling and remodelling: adaptation.* Phil. Trans. R. Soc. A, 367:2011-2030, 2009.

2006 M. Reeff, F. Gerhard, P. Cattin, and G. Szekély. *Mosaicing of Endoscopic Placenta Images.* Informatik 2006. Informatik für Menschen, P-93:467-474, 2006.

2006 J. G. Snedeker, G. Pelled, Y. Zilberman, F. Gerhard, R. Müller, and D. Gazit. *Endoscopic Cellular Microscopy for In Vivo Biomechanical Assessment of Tendon Function.* Journal of Biomedical Optics, 11:06040-10, 2006.